

BELINDA ELINE FLEM

NEI-NO--791

NO9705222

PELTIER HEATS IN CRYOLITE MELTS  
WITH ALUMINA

RECEIVED

JUL 21 1997

OSTI



**NTH**

UNIVERSITETET I TRONDHEIM  
NORGES TEKNISKE HØGSKOLE

DOKTOR INGENIØRAVHANDLING 1996:10  
INSTITUTT FOR FYSIKALSK KJEMI  
TRONDHEIM

IFK-rapport 1996:48

# **Peltier Heats in Cryolite Melts with Alumina**

by

**Belinda Eline Flem**

Thesis submitted in partial fulfillment  
of the requirements for the degree of  
Doktor Ingeniør

# **MASTER**

**DISTRIBUTION OF THIS DOCUMENT IS UNLIMITED**

*RB*

**DISCLAIMER**

**Portions of this document may be illegible in electronic image products. Images are produced from the best available original document.**

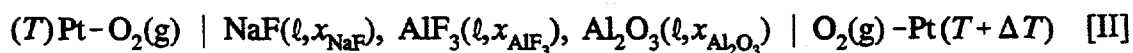
## ABSTRACT

This thesis presents measurements of the Seebeck coefficient, or the thermoelectric power, of the aluminium and the oxygen electrode. The measurements help to determine whether there is reversible cooling or heating of the aluminium electrode and decide the magnitude of the Peltier effects of both the aluminium and the carbon electrode. The theory of irreversible thermodynamics describes interacting transport processes, and is most suited to analyse local heat effects such as Peltier heats. Central quantities in the theory of irreversible thermodynamics are explained and defined.

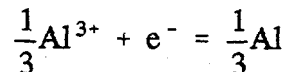
A thermodynamic description of the Peltier heat at the aluminium and the oxygen electrode is given for the system NaF-AlF<sub>3</sub>-Al<sub>2</sub>O<sub>3</sub>, for all compositions of alumina and any NaF/AlF<sub>3</sub> molar ratio. The thermoelectric power in melts with NaF/AlF<sub>3</sub> molar ratios equal to 1.8, 1.2 and 1.0, saturated with alumina, are measured and carefully investigated for the thermocells:



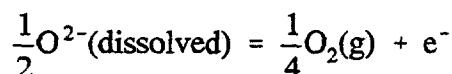
and



where  $x_{\text{Al}_2\text{O}_3}$  is the mole fraction of alumina at saturation. The electrode reaction on the right-hand side in thermocell [I] is given by:



The left-hand side electrode reaction of thermocell [II] may be written:



A lot of time and effort was used to design suitable experimental cells for thermoelectric power measurements in thermocell [I] and [II]. In designing thermocells, special attention has to be put on the design of the electrodes and the temperature measurement. A full account of material choices, experimental design and procedures is reported. The aluminium electrodes, in thermocell [I], were found to be stable for at least 13 hours. With a proper design, thermocells can also be used for determination of diffusion coefficients. A suggestion for an experimental cell for measuring thermoelectric powers under stationary state conditions is given. The only modification that is necessary for measuring thermoelectric powers in melts without alumina, or in melts that is not saturated with alumina, is to exchange the parts that consist of alumina with boron nitride.

The Seebeck coefficient was measured for cells with electrolytes of molten mixtures of cryolite and aluminium fluoride, saturated with alumina. The electrodes were either a pair of oxygen electrodes or a pair of aluminium electrodes. For the molar ratios NaF/AlF<sub>3</sub> 1.8, 1.2 and 1.0, the Seebeck coefficients  $-1.80 \pm 0.03 \text{ mV K}^{-1}$  at 971 °C,  $-1.63 \pm 0.03 \text{ mV K}^{-1}$  at 813.6 °C and  $-0.583 \pm 0.008 \text{ mV K}^{-1}$  at 758 °C were respectively obtained, for the oxygen electrode. The large variation in the Seebeck coefficient, between NaF/AlF<sub>3</sub> molar ratio 1.2 and 1.0, is due to lack of participation from the heat of transfer to the Seebeck coefficient at molar ratio NaF/AlF<sub>3</sub> 1.0. For the aluminium electrode, the Seebeck coefficient  $-1.23 \pm 0.04 \text{ mV K}^{-1}$  at 962 °C was obtained at molar ratio NaF/AlF<sub>3</sub> equal to 1.8. When the molar ratio

NaF/AlF<sub>3</sub> is changed to 1.0, the reversible heat effect at the aluminium electrode approaches zero.

The thesis suggests that there is substantial reversible heat consumption at the oxygen anode during aluminium electrolysis and large reversible heat production at the aluminium cathode. The highest temperature in the Hall-Héroult cell may then be closer to the cathode than the anode. Any final conclusions on the magnitude of the reversible heat effect at the electrodes in the Hall-Héroult process cannot however be drawn from the present work. Experiments have to be carried out in melts of industrial composition. This start of a more detailed mapping of the heat consumption due to the anodic reaction and the heat production due to the cathodic reaction may give new information to the heat balance model of the aluminium electrolysis cell.

The transported entropy of Al<sup>3+</sup> and O<sup>2-</sup> was calculated to be  $77 \pm 2 \text{ J mol}^{-1} \text{ K}^{-1}$  and  $10 \pm 2 \text{ J mol}^{-1} \text{ K}^{-1}$ , respectively, at molar ratio NaF/AlF<sub>3</sub> equal to 1.0. The transported entropy of oxygen ions, O<sup>2-</sup>, at the carbon electrode was calculated to be equal to the transported entropy of O<sup>2-</sup> at the oxygen electrode. At NaF/AlF<sub>3</sub> molar ratios equal to 1.8 and 1.2, the transported entropy of sodium ions,  $S_{\text{Na}^+}^*$ , were calculated to  $238 \pm 4 \text{ J mol}^{-1} \text{ K}^{-1}$  and  $244 \pm 4 \text{ J mol}^{-1} \text{ K}^{-1}$ , respectively. This result allows for a correction of the estimate of the transported entropy of sodium ions in cryolite melt given in the literature.

Measurements showed that stationary state was obtained in about 30 minutes. It should therefore be possible to obtain the thermoelectric power at stationary state during the time of stability of the electrodes. The measurements made a rough estimate of the inter diffusion coefficient in NaF-AlF<sub>3</sub> melts possible. At molar ratio NaF/AlF<sub>3</sub> equal to 4.0, the inter diffusion coefficient was estimated to be  $1.5 \times 10^{-3} \text{ cm}^2 \text{ s}^{-1}$ .

In this work, reproduction of the measurements has been emphasized more than getting measurements for a wide range of compositions. A theoretical description of the system NaF-AlF<sub>3</sub>-Al<sub>2</sub>O<sub>3</sub> and the method for thermoelectric power measurements at initial- and stationary

state conditions has been established and is described in detail. More work in the field can therefore concentrate on obtaining the concentration variations of the thermoelectric power.

## ACKNOWLEDGEMENTS

First, I wish to thank Professor Signe Kjelstrup Ratkje, my supervisor, at the Norwegian University of Science and Technology for stimulating discussions and encouragement during the study. I especially want to thank her for believing in the project and in me, even when the experimental difficulties were larger than what was easy to cope with. I particularly thank Åsmund Sterten, if it was not for his assistance in the experimental work during the last year, this thesis would not be finished yet.

During this project, I had the pleasure of spending two weeks at Hydro Aluminium in Årdal in 1993 and two days in 1992. In Årdal my gratitude goes to Kåre Vee and Trygve Foosnes. I would also thank Gjerterud Rian and Halvor Kvande for being my contacts in the aluminium industry. I will also thank the Research Council of Norway and the Norwegian aluminium industry for financial support through the EXPOMAT research program.

Furthermore, I wish to thank everybody at Department of Physical Chemistry at the Norwegian University of Science and Technology for helping me through this 4-year period of my life. I would also like to thank Edvard Sivertsen for carrying out the experiments where the stability of the AlN/Al composite material was tested and Tommy Førland for invaluable discussions during the study. I also wish to express my sincere gratitude to Geir Martin Haarberg, at Department of Electrochemistry at the Norwegian University of Science and Technology, for helpful discussions and for offering time to make a critical reading of this thesis. I am grateful to Stewart Clark from the International office, at the Norwegian University of Science and Technology, who edited the English in this thesis.

I want to thank my parents, Karsten and Solfrid Flem, for always supporting my choices and inspiring me to work even harder. I also thank them for financial support and for being there when I needed someone to talk to. Last, but certainly not least, I wish to thank Andreas Grimstvedt for his love, support and care.



# CONTENTS

	Page
ABSTRACT .....	-3-
ACKNOWLEDGEMENTS .....	-7-
CONTENTS .....	-9-
NOMENCLATURE .....	-13-
1. INTRODUCTION .....	-15-
1.1 BACKGROUND AND PURPOSE OF THE PRESENT WORK .....	-15-
1.2 THE HALL-HÉROULT PROCESS .....	-19-
1.3 ENERGY AND HEAT BALANCE OF THE ALUMINA REDUCTION CELL .....	-23-
REFERENCES, CHAPTER 1 .....	-25-
2. THEORY .....	-27-
2.1 THERMOCELL: $(T) \text{Al}(\ell)   \text{NaF}, \text{AlF}_3   \text{Al}(\ell) (T+\Delta T)$ .....	-27-
2.1.1 The Dissipation Function .....	-29-
2.1.2 Forces and Fluxes .....	-34-
2.1.3 Local Mass and Entropy Balances .....	-36-
2.1.4 The Seebeck Coefficient and The Peltier Heat .....	-41-
2.2 TEMPERATURE DEPENDENCY OF THE THERMOELECTRIC POWER .....	-47-
2.3 THE SYSTEM $\text{AlF}_3\text{-NaF-Al}_2\text{O}_3$ .....	-51-
2.3.1 Thermocell: $(T)\text{Al}(\ell)   \text{NaF}, \text{AlF}_3, \text{Al}_2\text{O}_3   \text{Al}(\ell)(T+\Delta T)$ .....	-51-
2.3.2 Thermocell: $(T)\text{Pt-O}_2(\text{g})   \text{NaF}, \text{AlF}_3, \text{Al}_2\text{O}_3   \text{O}_2(\text{g})\text{-Pt}(T+\Delta T)$ .....	-55-
2.4 CONSISTENCY CONTROL .....	-58-
2.5 RELEVANCE TO THE HALL - HÉROULT CELL .....	-59-
2.6 OTHER SYSTEMS, TRENDS .....	-61-
REFERENCES, CHAPTER 2 .....	-65-
3. EXPERIMENTAL .....	-69-
3.1 EXPERIMENTAL EQUIPMENT .....	-69-
3.2 ALUMINIUM AND OXYGEN ELECTRODES IN CRYOLITE MELTS .....	-73-
3.2.1 General Criteria .....	-73-
3.2.2 Stability of Aluminium Electrodes .....	-74-
3.2.3 Limited Extension of the Aluminium Electrode .....	-79-
3.2.4 The Oxygen Electrode .....	-80-
3.3 EXPERIMENTAL CELLS, INITIAL STATE .....	-82-
3.3.1 The thermocell $(T)\text{Al}(\ell)   \text{NaF}, \text{AlF}_3, \text{Al}_2\text{O}_3   \text{Al}(\ell)(T+\Delta T)$ .....	-82-

---

3.3.2	The thermocell $(T)\text{Pt-O}_2(\text{g}) \mid \text{NaF, AlF}_3, \text{Al}_2\text{O}_3 \mid \text{O}_2\text{-Pt}(T+\Delta T)$ . . . . .	-83-
3.4	EXPERIMENTAL CELL, STATIONARY STATE . . . . .	-85-
3.5	MATERIALS AND CHEMICALS USED . . . . .	-88-
3.6	EXPERIMENTAL PROCEDURE . . . . .	-89-
	REFERENCES, CHAPTER 3 . . . . .	-90-
<b>4.</b>	<b>RESULTS</b> . . . . .	<b>-93-</b>
4.1	THERMOELECTRIC POWER IN CRYOLITE MELT WITH $n_{\text{NaF}}/n_{\text{AlF}_3}=1.8$ . . . . .	-93-
4.1.1	Consistency Control, $n_{\text{NaF}}/n_{\text{AlF}_3} = 1.8$ . . . . .	-99-
4.2	THERMOELECTRIC POWER IN CRYOLITE MELT WITH $n_{\text{NaF}}/n_{\text{AlF}_3}=1.2$ . . . . .	-100-
4.3	THERMOELECTRIC POWER IN CRYOLITE MELT WITH $n_{\text{NaF}}/n_{\text{AlF}_3}=1.0$ . . . . .	-102-
4.4	TRANSPORTED ENTROPIES IN CRYOLITE MELTS . . . . .	-104-
4.5	RELEVANCE TO THE HALL-HÉROULT CELL . . . . .	-107-
4.6	THERMOELECTRIC POWER AT STATIONARY STATE CONDITIONS . . . . .	-108-
4.7	SOURCES OF EXPERIMENTAL ERRORS . . . . .	-111-
	REFERENCES, CHAPTER 4 . . . . .	-114-
<b>5.</b>	<b>LOCAL HEAT EFFECTS IN HALL-HÉROULT CELLS</b> . . . . .	<b>-117-</b>
5.1	JOULE HEAT . . . . .	-117-
5.1.1	Electrolyte . . . . .	-117-
5.1.2	Anode . . . . .	-120-
5.1.3	Cathode . . . . .	-121-
5.2	OVERVOLTAGE . . . . .	-122-
5.2.1	Anode . . . . .	-122-
5.2.2	Cathode . . . . .	-124-
5.3	BUBBLE LAYER RESISTANCE . . . . .	-124-
5.4	REVERSIBLE HEAT PRODUCTION AT THE ELECTRODES . . . . .	-125-
	REFERENCES, CHAPTER 5 . . . . .	-127-
<b>6.</b>	<b>DISCUSSION AND CONCLUSIONS</b> . . . . .	<b>-129-</b>
6.1	SEEBECK COEFFICIENTS AND PELTIER HEATS . . . . .	-129-
6.2	OTHER METHODS OF FINDING THE PELTIER EFFECT . . . . .	-133-
6.3	ELECTRONIC CONDUCTION . . . . .	-136-
6.4	TRANSPORTED ENTROPIES IN CRYOLITE MELTS . . . . .	-142-
6.5	COMPARISON WITH OTHER LOCAL HEAT EFFECTS IN THE HALL-HÉROULT CELL . . . . .	-145-
6.6	INDUSTRIAL SCALE MEASUREMENTS AND TECHNICAL CONSEQUENCES . . . . .	-148-
6.7	THE THEORY OF IRREVERSIBLE THERMODYNAMICS . . . . .	-151-
6.8	FINAL CONCLUSIONS AND PERSPECTIVES . . . . .	-153-

---

6.8.1	Thermoelectric Power at Initial State Conditions	-153-
6.8.2	Thermoelectric Power at Stationary State Conditions	-155-
6.8.3	Diffusion Coefficients	-156-
REFERENCES, CHAPTER 6		-158-
APPENDICES		-163-
APPENDIX A	The Relation Between $I_{ij}$ and $r_{ij}$	-165-
APPENDIX B	Mass and Entropy Balance at the Oxygen Electrode	-169-
APPENDIX C	Temperature Gradient of the Vertical Tube Furnace.	-171-
APPENDIX D	Flow Diagram for the Apparatus	-173-
APPENDIX E	Materials and Chemicals Used in the Experiments	-175-
APPENDIX F	Statistics	-177-
F.1	INDICATOR VARIABLES	-177-
F.2	TEST ON COMMON SLOPE IN EXPERIMENTS A, B AND C, TABLE 4.2-	185-
F.3	TEST ON INDIVIDUAL REGRESSION COEFFICIENTS	-187-



## NOMENCLATURE

$A$	The electrode areal [ $\text{m}^2$ ]
$a_i$	The activity of $i$
$c$	Concentration [ $\text{mol m}^{-3}$ ]
$C_{p,i}$	Molar heat capacity at constant pressure of component $i$ [ $\text{J K}^{-1} \text{mol}^{-1}$ ]
$C$	Number of components, the phase rule
$D_{12}$	Fick's diffusion coefficient [ $\text{m}^2 \text{s}^{-1}$ ]
$E$	Observed cell potential [V]
$E^{\text{rev}}$	Reversible cell potential [V]
$F_0$	Fisher distributed test statistic
$F$	Faraday constant
$h$	Height [m]
$I$	Current [A]
$i$	Current density [ $\text{A m}^{-2}$ ]
$j$	Current density, $i / F$ [ $\text{mol m}^{-2} \text{s}^{-1}$ ]
$J_q$	Measurable heat flux [ $\text{J m}^{-2} \text{s}^{-1}$ ]
$J_i$	Mass flux, flux of the neutral component $i$ or flux of the ion $i$ [ $\text{mol m}^{-2} \text{s}^{-1}$ ]
$L_{ij}$	Phenomenological coefficients
$l_{ij}$	Phenomenological diffusion coefficients
$l$	The distance between the electrodes [m]
$M_{w,i}$	Molar weight of component $i$ [ $\text{kg mol}^{-1}$ ]
$n$	Number of observations
$n$	Number of components
$n_i$	Amount of component $i$ [mol]
$\Delta n_i$	The number of moles of component $i$ transferred [ $\text{mol m}^{-2}$ ]
$\nabla p$	Gradient in pressure [ $\text{N m}^{-3}$ ]
$P$	Number of phases
$dq/dt$	Reversible heat production [ $\text{J m}^{-2} \text{s}^{-1}$ ]
$Q_i^*$	Heat of transfer, component $i$ [ $\text{J mol}^{-1}$ ]
$\Delta Q$	Quantity of electricity transferred [ $\text{mol m}^{-2}$ ]
$R$	Resistance [ $\Omega$ ]
$r_{ij}$	Phenomenological diffusion coefficients
$S_i^*$	Entropy transported by ion $i$ or entropy transported through a conductor $i$ [ $\text{J mol}^{-1} \text{K}^{-1}$ ]
$S_i$	The molar entropy or the partial molar entropy of component $i$ [ $\text{J mol}^{-1} \text{K}^{-1}$ ]
$T$	Absolute temperature [K]
$T\theta$	Dissipation function [ $\text{J m}^{-3} \text{s}^{-1}$ ]
$t_i$	Transference number of the ion $i$ or transference coefficient of the neutral component $i$
$t$	Time [s]

$V_i$	Partial molar volume of component $i$ [ $\text{m}^3 \text{mol}^{-1}$ ]
$X_i$	Indicator variable
$x$	Distance in the $x$ -direction [m]
$x_i$	Mole fraction of component $i$
$z_i$	Charge of the ion $i$

### Greek Letters

$\beta_i$	Regression coefficient
$\gamma$	Degrees of freedom, statistic
$\varepsilon$	Error, statistic
$\varepsilon_0$	Seebeck coefficient at initial state conditions [ $\text{V K}^{-1}$ ]
$\varepsilon_t$	Seebeck coefficient at any time [ $\text{V K}^{-1}$ ]
$\varepsilon_\infty$	Seebeck coefficient at stationary state conditions [ $\text{V K}^{-1}$ ]
$\Theta$	Characteristic time [s]
$\theta$	Entropy production [ $\text{J m}^{-3} \text{K}^{-1} \text{s}^{-1}$ ]
$\kappa$	Electric conductivity of the electrolyte [ $\text{A V}^{-1} \text{m}^{-1}$ ]
$\nabla\mu_i$	Gradient in chemical potential of component $i$ [ $\text{J mol}^{-1} \text{m}^{-1}$ ]
$\nabla\mu_{i,T}$	Gradient in chemical potential at constant temperature of component $i$ [ $\text{J mol}^{-1} \text{m}^{-1}$ ]
$\nabla\mu_{i(c)}$	Gradient in chemical potential caused by gradient in concentration only [ $\text{J mol}^{-1} \text{m}^{-1}$ ]
$\pi$	Peltier heat [ $\text{J mol}^{-1}$ ]
$\pi/T$	Peltier effect [ $\text{J mol}^{-1} \text{K}^{-1}$ ]
$\rho_i$	Density [ $\text{kg m}^{-3}$ ]
$\tau_i$	Thomson coefficient of component $i$ [ $\text{J K}^{-1} \text{mol}^{-1}$ ]
$\Phi$	The number of degrees of freedom
$\Delta\varphi$	Electric potential, $E \cdot F$ [ $\text{J mol}^{-1}$ ]
$\nabla\varphi$	Gradient in electric potential [ $\text{J mol}^{-1} \text{m}^{-1}$ ]
$\nabla\varphi^{\text{obs}}$	Observed gradient in electric potential [ $\text{J mol}^{-1} \text{m}^{-1}$ ]
$\Delta\varphi/\Delta T$	Thermoelectric power [ $\text{J mol}^{-1} \text{K}^{-1}$ ]
$\nabla$	$d/dx$

## 1. INTRODUCTION

In this chapter, the background and purpose of the thesis are outlined in Section 1.1. The Hall-Héroult process and its energy and heat balance are briefly discussed in Sections 1.2 and 1.3.

### 1.1 BACKGROUND AND PURPOSE OF THE PRESENT WORK

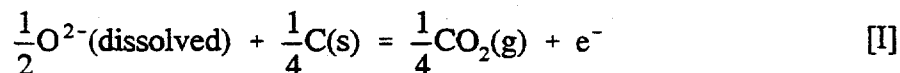
The transport processes occurring in an alumina reduction cell are complicated, but so far only Fick's and Fourier's laws have been used to describe mass diffusion and heat conduction. Extended equations which describe the coupling of mass and heat fluxes, given by irreversible thermodynamics have so far not been used, mainly because of lack of data. In particular there has been a lack of information which describes the coupling coefficients in the flux equations for heat and mass. These coefficients are the so-called Peltier or Seebeck coefficients, Førland et al. (1988), de Groot (1966). In 1834, Peltier discovered that when a current flows through an isothermal junction of a thermocouple, heating or cooling occurs. Such heat evolution at the junction between metallic conductors caused by a gradient in electric potential is called the Peltier effect. The opposite effect, is the flux of electric charge caused by a temperature gradient, and is called the Seebeck effect. Knowledge of local heat production or consumption at the electrodes, may give new understanding of the temperature distribution in electrochemical systems. These effects however, depend upon the transported entropy,  $S^*$ , among other variables. Therefore, knowledge about transported entropies is necessary in calculating local heat effects in electrochemical systems. Few values of transported entropies are reported in the literature, and the transported entropies are poorly understood. The rigorous treatment of such complicated phenomena as thermal diffusion and cell potentials of thermocells has been made possible by, for example, the development of the

methods of thermodynamics of irreversible processes, Haase (1990).

The Hall-Hèroult cell may be written:



Carbon dioxide,  $\text{CO}_2$ , is formed at the carbon anode. The anodic reaction can be written as:



where  $\text{O}^{2-}$  is an Al-O-F complex anion. At the cathode, aluminium is formed from anionic complexes such as  $\text{AlF}_6^{3-}$ ,  $\text{AlF}_5^{2-}$  and  $\text{AlF}_4^-$ . The cathode reaction may be written as:



Peltier cooling of the anode due to the gas reaction, Equation [I], was first proposed by Mozhaev et al. (1972), Mozhaev and Polyakov (1980) and Polyakov et al. (1973). Measurements were performed with two aluminium electrodes in cryolite with varying contents of alumina. The temperature difference and the electric potential were measured as a function of time. Mozhaev and Polyakov (1980) reported a Seebeck coefficient of  $100 \mu\text{V K}^{-1}$  with a relative error of 13% at  $1000^\circ\text{C}$  for reaction [II]. The corresponding effect for the anode, reaction [I], was calculated from these results and the entropy of reaction  $\Delta S$ , divided by Faraday's constant, to be  $-619 \mu\text{V K}^{-1}$ .

Ratkje (1991) used the results of Mozhaev and Polyakov (1980) to find the transported

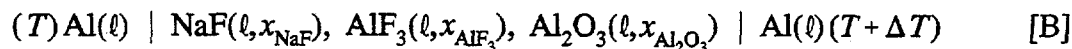
entropy of  $\text{Na}^+$ , and estimated the reversible heat effects at the electrodes during electrolysis in a cryolite-alumina melt of uniform composition. The reversible heat consumption calculated for the anode reaction was larger than the heat production caused by the anodic overvoltage, and a net cooling effect was estimated. At the cathode a net heating effect was estimated, due to the electrode reaction [II].

Ødegård et al. (1991, 1991) estimated the entropy changes at the electrodes from equilibrium thermodynamics and used the results to explain industrial-scale anode temperature measurements. They found a Peltier cooling effect of the anode surface due to reaction [I] that seemed to be somewhat larger than the heat produced by the overvoltage. At the cathode they found a positive reversible heat production, which was in agreement with Mozhaev and Polyakov (1980) and Ratkje (1991). When they took the entropy of mixing in the cryolite system into account, they concluded that the heat evolution due to the anodic overvoltage compensated for the reversible heat consumption at the carbon anode. The inclusion of the entropy of mixing resulted in a negative heat production for the aluminium cathode.

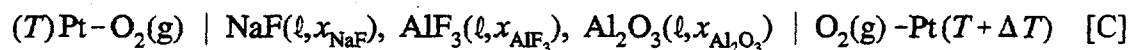
Grimstvedt (1992) illustrated the application of the theory of irreversible thermodynamics to the Hall-Héroult process. Ratkje (1991), Ødegård et al. (1991, 1991) and Grimstvedt (1992) agreed that more experimental work is needed to determine the local reversible heat effects in the cryolite system.

The main purpose of the thesis was to measure Seebeck coefficients, or thermoelectric powers, in order to settle the question of reversible cooling or heating of the aluminium electrode, and decide the magnitude of the reversible Peltier effect of both the aluminium and carbon electrode. Central quantities in the theory of irreversible thermodynamics, quantities which are needed to obtain the local reversible heat changes of the aluminium electrolysis cell will be explained and defined. The technical implications of the findings will be given special attention. The methodology of the thermocell potential measurements of fluoride melts is complicated and is discussed in detail. A full account of material choices, experimental design and procedures will be reported.

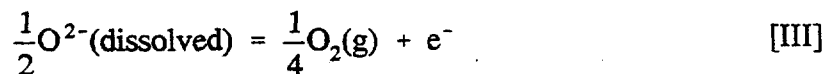
Two thermocells will be investigated:



and



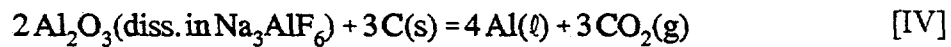
where  $x_{Al_2O_3}$  is the mole fraction of alumina at saturation. The electrode reaction on the right-hand side in thermocell [B] is given by Equation [II]. The left-hand side electrode reaction of thermocell [C] may be written:



The aluminium industries have a relatively detailed mapping of how much heat is dissipated from their cells and from where it dissipates to (see eg. Grjotheim et al. (1982)). The results from thermocell experiments can contribute to make their heat balance model even more sophisticated. Thermal effects, like the fact that the bath does not freeze out at the cathode even when the liquidus temperature for the melt at the cathode is higher than the bath temperature, may be better understood from the measurements of the thermoelectric power.

## 1.2 THE HALL-HÉROULT PROCESS

In 1886, Paul Héroult and Charles Martin Hall independently, patented a process for aluminium production based on electrochemical decomposition of alumina,  $\text{Al}_2\text{O}_3$ , dissolved in liquid cryolite,  $\text{Na}_3\text{AlF}_6$ , and with consumable carbon anodes. Aluminium is today exclusively produced after this process named after its two inventors, the Hall-Héroult Process. The primary reaction for the process is:



For several reasons it is found that it is an advantage to have an excess of aluminium fluoride,  $\text{AlF}_3$ , in the electrolyte, relative to the cryolite composition, Grjotheim et al. (1982). When an excess of  $\text{AlF}_3$  is used, then the melt is called acidic. If the composition of the electrolyte is on the left-hand side of the cryolite composition in the phase diagram, Figure 1.1, the melt is called basic.

A typical industrial electrolyte composition is:

1.5-6 wt%  $\text{Al}_2\text{O}_3$   
4-8 wt%  $\text{CaF}_2$   
5-13 wt%  $\text{AlF}_3$   
the rest mainly cryolite

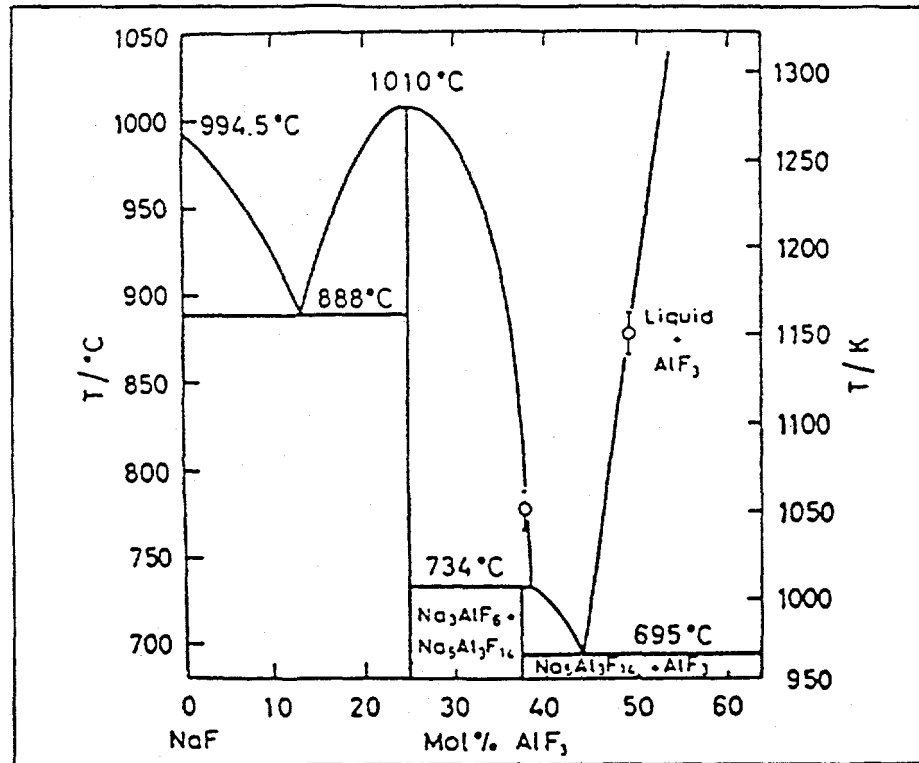


Figure 1.1 Phase diagram of the system NaF - AlF<sub>3</sub>, Holm (1973)

When alumina, Al<sub>2</sub>O<sub>3</sub>, is added to the melt, the melting point is reduced, Sterten et al. (1982). The phase diagram for the system Na<sub>3</sub>AlF<sub>6</sub>- AlF<sub>3</sub>-Al<sub>2</sub>O<sub>3</sub> is given in Figure 1.2 after Skybakmoen et al. (1990).

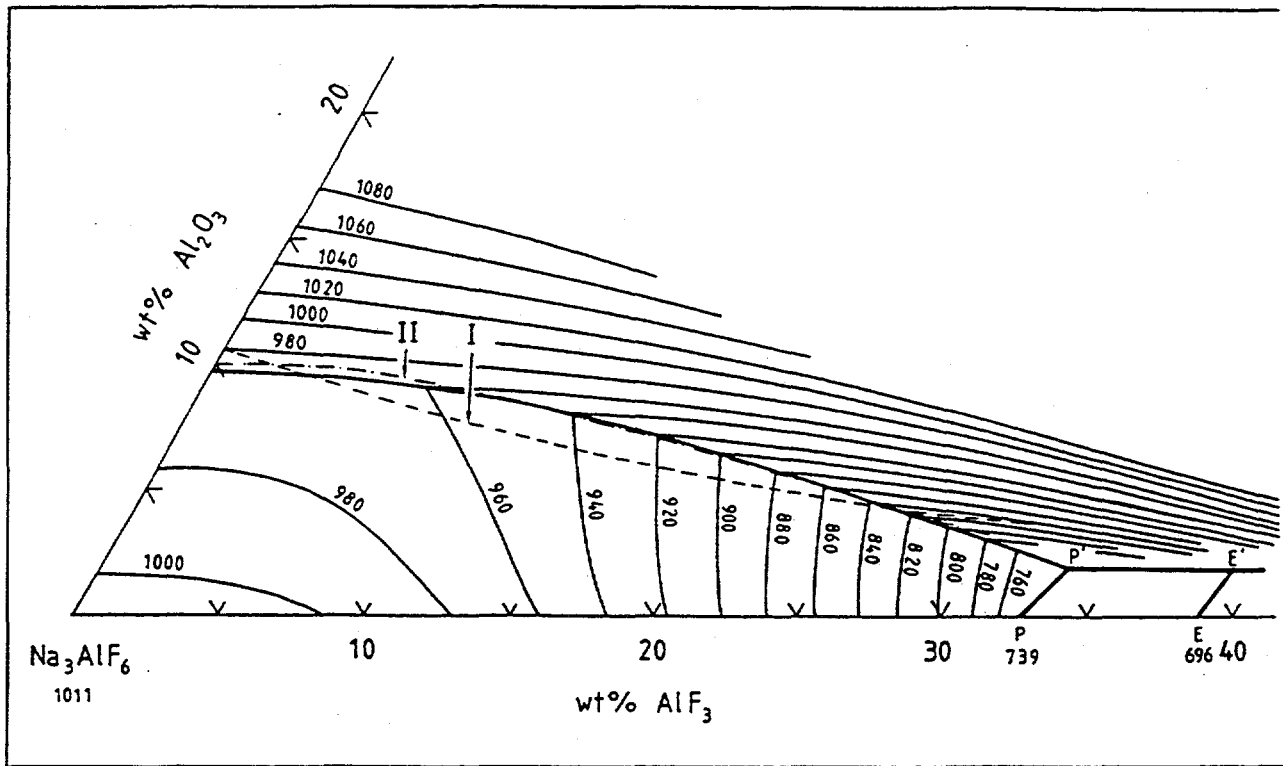


Figure 1.2 Liquidus isotherms in the system  $\text{Na}_3\text{AlF}_6\text{-AlF}_3\text{-Al}_2\text{O}_3$ . The lines marked I and II represent the  $\text{Na}_3\text{AlF}_6\text{-Al}_2\text{O}_3$  univariant line according to Foster (1975) and Phillips et al. (1955), respectively, Skybakmoen et al. (1990).

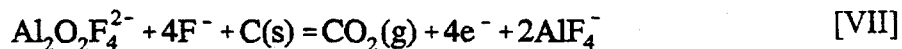
The only cation present in cryolite-alumina melts is  $\text{Na}^+$ . There is no evidence that  $\text{Al}^{3+}$  ions are present, all the aluminium in the melt is bound in different anionic complexes. The most probable cathode reactions involve  $\text{AlF}_6^{3-}$ ,  $\text{AlF}_5^{2-}$  or  $\text{AlF}_4^-$ . Aluminium is the thermodynamically preferred product. The overall cathode reactions may then be written, Grjotheim and Kvande (1986):



or



At the anode  $\text{CO}_2$  gas is the primary product. The oxygen is transported to the anode in form of Al-O-F complex anions. It seems to be established that the main anodic electrode reaction at normal industrial conditions is:



Several other Al-O-F complexes have been proposed. At "low" alumina concentrations, species like  $\text{Al}_2\text{O}_x\text{F}_x^{(4-x)}$  with a single oxygen ion eg.  $\text{Al}_2\text{OF}_8^{4-}$ ,  $\text{Al}_2\text{OF}_6^{2-}$ , have been suggested. At "high" alumina concentrations, species of the type  $\text{Al}_2\text{O}_2\text{F}_x^{(2-x)}$  have been suggested. Grjotheim and Kvande (1986).

### 1.3 ENERGY AND HEAT BALANCE OF THE ALUMINA REDUCTION CELL

The effort to improve the energy conversion efficiency and the current efficiency of the aluminium electrolysis has been considerable over the last decades, Grjotheim and Welch (1988). The energy flow through the reactor is central in this context. On an overall perspective, electric energy and heat are converted to chemical energy in the aluminium electrolysis; since the entropy of reaction is positive. The local energy balance equation, may be different, however, since the entropy change is very different for the two electrodes. When heat is not supplied to the electrodes, when an endothermic process takes place, more electrical energy is needed for the chemical reaction. If heat is supplied to the electrodes, when an exothermic process takes place, less electrical energy is needed for the chemical reaction. The local heat balance is thus important for the energy efficiency.

The Hall-Héroult cells are usually run between 930-1000°C, depending on the molar ratio of NaF/AlF<sub>3</sub>. Heat is mainly generated by ohmic voltage drops and overvoltages. Besides the heat loss to the surroundings through the sidewalls, bottom and the top of the cell, heat is consumed by heating the reactants, alumina and carbon, up to bath temperature, by alumina dissolution and by the net cell reaction, Eq.[IV]. While the irreversible heat effects have become increasingly more specified, the reversible Peltier effects have received little attention so far. The aluminium cells are insulated and operated in order to maintain frozen a ledge on the side walls and a frozen crust over the bath. By their very nature, all electrolysis processes are energy intensive. It is necessary to have an energy input to bring about a reaction that is normally unfavourable. Continuous attempts to reduce the electrical energy requirements have led to a halving of the necessary electrical energy input since the turn of the century, Fig. 1.3, Grjotheim and Welch (1988). The present trend towards slightly lower current densities and lower cell voltages will probably allow energy consumption values close to, or even below 12.0 kWh/kg Al to be reached in the near future, Kvande (1991).

Low energy requiring cells are characterized by proper thermal design, correct voltage

adjustments by computer programs, efficient alumina feeding, small variations in  $\text{AlF}_3$  concentration and bath temperature and good operational practice, Grjotheim and Kvande (1986). Flem et al. (1994) calculated the reversible Peltier effect at the electrodes in the aluminium electrolysis cell and found it to be in the same order of magnitude as the main irreversible effects. The calculations were, however, based on several assumptions and experiments are needed to verify the calculations. More information on the different heat contributions to the heat balance may help to explain thermal effects in the alumina reduction cell; eg. so-called negative superheat.

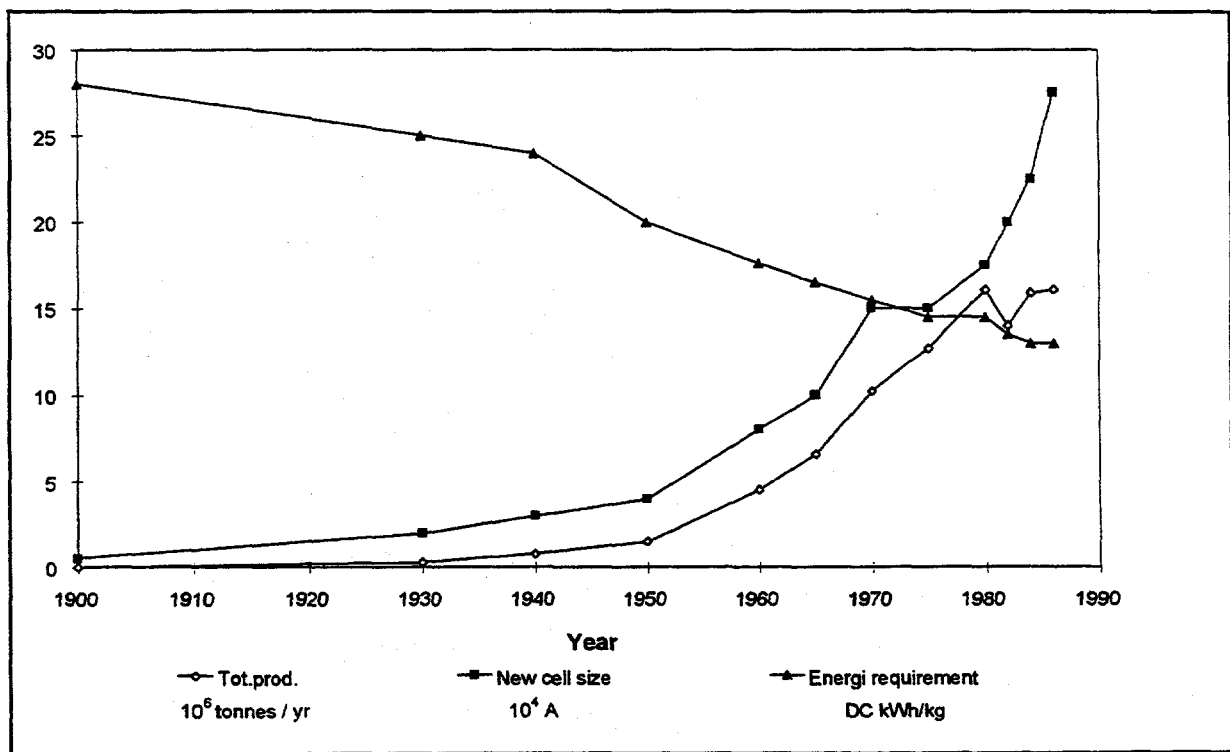


Figure 1.3 World - wide trends in aluminium production. Data adapted from Grjotheim and Welch (1988)

---

**REFERENCES, CHAPTER 1**

B. E. Flem, S. K. Ratkje and A. Grimstvedt, Ninth Australasian Electrochemistry Conference, Wollongong, Australia, Poster Presentation, P59, February 6-10, 1994.

P. A. Foster, Jr., *J. Amer. Ceram. Soc.*, **58**, p. 288, 1975

K. S. Førland, T. Førland and S. K. Ratkje, *Irreversible Thermodynamics-Theory and Applications*, (John Wiley & Sons, 1988)

A. Grimstvedt, *Thermocell Studies of Sulphate Mixtures and Melts Relevant for Aluminium Electrolysis*, Dr.Ing. Thesis, The Norwegian Institute of Technology, University of Trondheim, (1992)

S. R. de Groot, *Thermodynamics of Irreversible Processes*, (North-Holland Publishing Company, Amsterdam, 1966)

K. Grjotheim, C. Krohn, M. Malinovský, K. Matiašovský and J. Thonstad, *Aluminium Electrolysis*, 2nd ed., (Aluminium-Verlag GmbH, Düsseldorf, 1982)

K. Grjotheim and H. Kvande, *Understanding the Hall-Héroult Process for Production of Aluminium*, (Aluminium-Verlag GmbH, Düsseldorf, 1986)

K. Grjotheim and B. J. Welch, *Aluminium Smelter Technology*, 2nd ed., (Aluminium-Verlag GmbH, Düsseldorf, 1988)

R. Haase, *Thermodynamics of Irreversible Processes*, (Dover Publications, Inc, New York, 1990) p. 390

J. L. Holm, *Acta Chem.Scand.*, **27**, p. 1410, 1973

H. Kvande, *Light Metals*, p. 421, 1991

V. M. Mozhaev, P. V. Polyakov and L. M. Afans'eva, *Tsvet.Met.Sov.J. Non Ferrous Met.*, **13** (9), p. 28, 1972

V. M. Mozhaev and P. V. Polyakov, *Izv. Vyssk. Uchebn.Zav.Tsvet.Met.*, **23** (5), p. 37, 1980

N. W. F. Phillips, R. H. Singleton and E. A. Hollingshead, *J. Electrochem. Soc.*, **102**, p. 690, 1955

P. V. Polyakov, V. M. Mozhaev and L. M. Afanas'eva, *Tsvet.Met.Sov.J. Non Ferrous Met.*, **14** (3), p.32, 1973

S. K. Ratkje, *Electrochem. Acta*, **36**, p. 661, 1991

E. Skybakmoen, A. Solheim and Å. Sterten, *Light Metals*, p. 317, 1990

Å. Sterten, K. Hamberg and I. Mæland, *Acta Chem.Scand.*, **A36**, p. 329, 1982

R. Ødegård, S. Julsrud, A. Solheim and K. Thovsen, *Light Metals*, p. 307, 1991

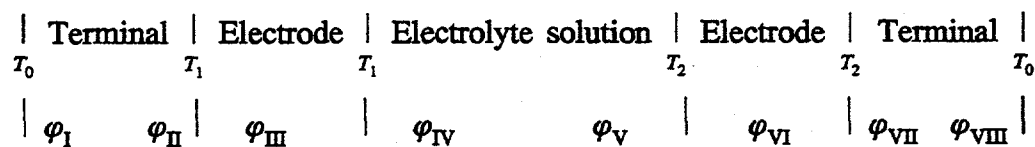
R. Ødegård, S. Julsrud, A. Solheim and K. Thovsen, *Met. Trans. B.*, **22B**, p. 831, 1991

## 2. THEORY

In this chapter, the central ideas and quantities in the thermodynamic treatment of thermocells will be explained and defined. Thermocells are non-isothermal electrochemical cells, where the electrodes are at different temperatures. A thermocell, with the binary system  $\text{AlF}_3\text{-NaF}$  and aluminium electrodes, is treated in Section 2.1. The temperature dependence of the thermoelectric power is given in Section 2.2. The binary system  $\text{AlF}_3\text{-NaF}$  is extended by adding aluminium oxide,  $\text{Al}_2\text{O}_3$ , to the molten electrolyte, in Section 2.3. Both thermocells with aluminium electrodes and oxygen electrodes are treated. Section 2.4 points out the possibilities for consistency control of thermocell measurements. The relevance of the thermocell measurements to the Hall-Héroult cell is given in Section 2.5. An overview of trends in other thermocell systems is given in Section 2.6.

### 2.1 THERMOCELL: $(T) \text{Al}(\ell) \mid \text{NaF, AlF}_3 \mid \text{Al}(\ell) (T+\Delta T)$

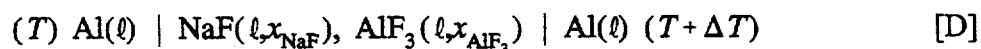
Thermocells are non-isothermal electrochemical cells with the electrodes kept at different temperatures. A thermocell can be represented by the diagram:



Here  $T_0$  is the temperature of the measuring instrument,  $T_1$  or  $T_2$  the temperature of the first or second electrode with the directly adjoining layer of the electrolyte solution. In the solution

between the electrodes, in the most general case, there are concentration and temperature gradients. The solution can consist of any substances (electrolytes and non-electrolytes), but should always contain the ionic species for which the electrodes are reversible, eg.  $\text{Ag}^+$  ions in the case of Ag electrodes or  $\text{Cl}^-$  ions in the case of Ag/AgCl electrodes. The Seebeck effect is the *emf* caused by a temperature difference across the cell. The temperature difference may also cause a flux of matter (Soret effect). The *emf* divided by  $T_2 - T_1$ , the Seebeck coefficient, is related to the heat change which occurs when an electric current passes through the cell, the Peltier heat.

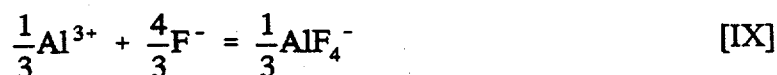
In this section, thermocell [D] will be described by means of irreversible thermodynamics:



The potential differences ( $\varphi_{\text{II}} - \varphi_{\text{I}}$ ) and ( $\varphi_{\text{VIII}} - \varphi_{\text{VII}}$ ) due to transport of charge in the metallic leads, platinum or copper wires, will be neglected here (Peltier heat of metals is small). The left hand-side electrode reaction in thermocell [D] may be written:



The aluminium ions will react with fluoride ions, in the melt, and form anionic complexes such as  $\text{AlF}_4^-$  or  $\text{AlF}_6^{3-}$ . Also  $\text{AlF}_5^{2-}$  has been suggested, Gilbert et al. (1995):



### 2.1.1 The Dissipation Function

The electrolyte, of thermocell [D], consists of two *thermodynamic components*,  $\text{AlF}_3$  and  $\text{NaF}$ . The thermodynamic components are the neutral chemical species that are needed to describe the system, and therefore, the chemical species  $\text{AlF}_3$  and  $\text{NaF}$  need not be stable or really exist. The choice of the thermodynamic components is not unique, see eg. Barrow (1988). For example, the system in thermocell [D] may also be described by  $\text{AlF}_3$  and  $\text{Na}_3\text{AlF}_6$  or by  $\text{NaAlF}_4$  and  $\text{NaF}$ .

Five forces exist in this system,  $-\nabla \ln T$ ,  $-\nabla \mu_{\text{NaF},T}$ ,  $-\nabla \mu_{\text{AlF}_3,T}$ ,  $-\nabla \mu_{\text{Al},T}$  and  $-\nabla \varphi^{\text{obs}}$ . For simplicity all transport will be assumed to occur in one direction only, the  $x$ -direction, and  $\nabla$  means  $d/dx$ . The gradient in electric potential of the cell is  $\nabla \varphi^{\text{obs}} = \lim (\Delta \varphi^{\text{obs}}/\Delta x)$  for  $\Delta x \rightarrow 0$ . The unit of  $\nabla \varphi^{\text{obs}}$  is  $\text{J mol}^{-1} \text{m}^{-1}$  and is equal to the gradient in the observed cell potential,  $\nabla E$ , with the unit  $\text{V m}^{-1}$  multiplied by Faraday constant,  $F$ . Here,  $T$  is the absolute temperature and  $\nabla \mu_{i,T}$  is the chemical potential gradient of component  $i$  at constant temperature, with the unit  $\text{J mol}^{-1} \text{m}^{-1}$ . The corresponding fluxes to the forces are  $J_q$  (heat flux),  $J_{\text{NaF}}$ ,  $J_{\text{AlF}_3}$ ,  $J_{\text{Al}}$  (mass fluxes) and  $j$  (flux of electric current density,  $i/F$ ). The unit of the heat flux is  $\text{J m}^{-2} \text{s}^{-1}$ , for the mass fluxes  $\text{mol m}^{-2} \text{s}^{-1}$ , and the unit of the flux of electric current density is  $\text{mol m}^{-2} \text{s}^{-1}$ . According to irreversible thermodynamics, Førlund et al. (1988), the dissipation function,  $T\theta$ , is defined as the sum of the force-flux products and can be expressed by:

$$T\theta = -J_q \nabla \ln T - J_{\text{NaF}} \nabla \mu_{\text{NaF},T} - J_{\text{AlF}_3} \nabla \mu_{\text{AlF}_3,T} - J_{\text{Al}} \nabla \mu_{\text{Al},T} - j \nabla \varphi^{\text{obs}} \quad [2.1]$$

where  $\theta$  is the entropy production per unit volume and unit time.

One of the mass fluxes,  $J_{\text{NaF}}$  or  $J_{\text{AlF}_3}$ , in Eq.[2.1] can be eliminated from the dissipation function by introducing one of the components or one of the ions as the frame of reference

for the movements in the system. The different frames of references of transference numbers and transference coefficients are well explained by Rajabu et al. (1992) and Ratkje et al. (1993). The *transference number* of the ion  $i$ ,  $t_i$ , is defined as the fraction of the electric current density,  $j$ , carried by the ion in a solution of uniform composition ie.  $\Delta c = 0$ :

$$t_i = \left| \frac{z_i J_i}{j} \right|_{\Delta c=0} \quad [2.2]$$

where  $z_i$  is the charge of the ion  $i$  and  $J_i$  is the mass flux of component  $i$ . The *transference coefficient* for a neutral component  $i$  is defined as the number of moles of  $i$ ,  $\Delta n_i$ , transferred, divided by the number of moles of electric charge,  $\Delta Q$ , passing the cell of uniform composition, in the limit  $\Delta Q \rightarrow 0$ :

$$t_i^H = \lim_{\Delta Q \rightarrow 0} \left( \frac{\Delta n_i}{\Delta Q} \right) \quad [2.3]$$

Superscript H means Hittorf type experiments. When the Hittorf method is used  $\Delta n_i$ , and hence  $t_i^H$  is referred to a fixed amount of a compound or ion. A modification of the Hittorf transference coefficient is obtained by using one of the ions in the electrolyte, eg.  $F^-$ , as a fixed frame of reference. This is then a quasi lattice of immobile  $F^-$  ions. Then the transport of all other ions will be considered with respect to the  $F^-$  ions. The transference coefficient for a component  $i$  is then defined as:

$$t_i^{L,F^-} = \left( \frac{J_i}{j} \right)_{\Delta c=0} \quad [2.4]$$

where  $J_i$  expresses the transfer of the neutral component  $i$  from left to right. Superscript L means such a quasi-lattice reference.

A quasi lattice of fluoride ions will be chosen as the frame of reference for thermocell [D]. This means, from Eqs.[2.2] and [2.4], that the transference number for fluoride ions,  $t_{F^-}$ , and the flux of fluoride ions,  $J_{F^-}$ , is equal to zero.

The demand for electroneutrality in the system makes the fluxes interdependent. In a non-moving quasi lattice of fluoride ions, the fluxes of thermocell [D] are related by:

$$J_{Na^+} + 3J_{Al^{3+}} = J_{NaF} + 3J_{AlF_3} = 0 \quad [2.5]$$

To be able to establish a temperature gradient between the two aluminium electrodes in thermocell [D] in a laboratory cell, it is in practice, necessary to have a distinct distance between them in a vertical direction. This will cause a pressure difference in the electrolyte at the two electrode surfaces. For an isothermal system, the gradient in chemical potential,  $\nabla\mu_i$ , includes concentration and pressure dependent terms:

$$\nabla\mu_i = \nabla\mu_i(c) + V_i\nabla P \quad [2.6]$$

where  $\nabla\mu_i(c)$  is a function of concentration gradients only,  $V_i$  is the partial molar volume of

component  $i$  and  $\nabla p$  is the gradient in pressure. Liquids and solids have small molar volumes compared with gases. For many purposes the pressure dependence of the free energy of liquids and solids can be neglected. In Example 1, it is shown that this is the case for aluminium, which forms a separate liquid phase in equilibrium with dissolved aluminium in the cryolite melt.

### ***Example 1 Gradient in Chemical Potential and Pressure***

*From Equation [2.6] the gradient in chemical potential of aluminium can be written:*

$$\nabla\mu_{Al} = \nabla\mu_{Al}(c) + V_{Al}\nabla p$$

*Aluminium forms a separate phase, therefore  $\nabla\mu_{Al}(c)$  must be equal to zero. The molar volume of aluminium at 1020°C is given by the density,  $\rho_{Al}$ , and the molar weight,  $M_{w, Al}$ . At 1020°C,  $\rho_{Al}$  is equal to 2282 kg/m<sup>3</sup>, Perry's (1984). The molar weight of aluminium is 27 g/mol. Then the molar volume is equal to 0.0118 m<sup>3</sup>/kmol at 1020°C. An electrolyte with molar ratio  $n_{NaF} / n_{AlF_3}$  equal to 3 has a density of 2.06 g/cm<sup>3</sup>, Grjotheim and Welch (1988). If the distance between the electrodes is 6 cm, then the pressure difference between the two aluminium electrodes will be equal to  $1.21 \cdot 10^3$  N/m<sup>2</sup>. The chemical potential difference of aluminium across the cell is then 0.0143 J/mol. The chemical potential difference of aluminium will then contribute with 0.15  $\mu$ V to the observed cell potential of cell [D]. This value is not significant compared to the potential raised by a temperature gradient, Mozhaev and Polyakov (1980).*

---

The composition of the electrolyte may be described by the mole fractions of the components,  $x_i = n_i/\sum n_i$ . The sum of the mole fractions is always equal to one. With  $n$  components in the solution, there are only  $n-1$  independent mole fractions. Correspondingly the chemical potentials are interrelated by the Gibbs-Duhem equation,  $\sum_i x_i d\mu_i = 0$ . One of the components is chosen as the frame of reference, and all changes refer to this frame. There are two components in thermocell [D], giving the Gibbs-Duhem equation for constant temperature:

$$x_{\text{NaF}} \nabla \mu_{\text{NaF},T} + x_{\text{AlF}_3} \nabla \mu_{\text{AlF}_3,T} = 0 \quad [2.7]$$

By combining Equations [2.5] and [2.7] with Equation [2.1], the mass flux of  $\text{AlF}_3$ ,  $J_{\text{AlF}_3}$ , and the gradient in chemical potential for  $\text{AlF}_3$ ,  $-\nabla \mu_{\text{AlF}_3,T}$ , can be eliminated from the dissipation function. The participation from the gradient in chemical potential of Al,  $-\nabla \mu_{\text{Al},T}$ , can be neglected, see Example 1. The dissipation function,  $T\theta$ , may then be expressed as:

$$T\theta = -J_q \nabla \ln T - J_{\text{NaF}} \left(1 + \frac{x_{\text{NaF}}}{3x_{\text{AlF}_3}}\right) \nabla \mu_{\text{NaF},T} - j \nabla \phi^{\text{obs}} \quad [2.8]$$

## 2.1.2 Forces and Fluxes

Equation [2.8] contains three independent forces  $-\nabla \ln T$ ,  $-(1 + x_{\text{NaF}}/3x_{\text{AlF}_3})\nabla \mu_{\text{NaF},T}$  and  $-\nabla \varphi^{\text{obs}}$  with the conjugate fluxes  $J_q$ ,  $J_{\text{NaF}}$  and  $j$ . Each flux,  $J_i$ , is linear, homogeneous function of the forces,  $J_i = \sum_{j=1}^k L_{ij} X_j$ , where  $i, j=1, \dots, k$ . Linear relations are approximations that are valid when there is microscopic reversibility, ie. local equilibrium, in the system, Onsager (1931). The fluxes expressed by the forces for thermocell [D] are accordingly:

$$J_q = -L_{11} \nabla \ln T - L_{12} \nabla \mu_{\text{NaF},T} \left(1 + \frac{x_{\text{NaF}}}{3x_{\text{AlF}_3}}\right) - L_{13} \nabla \varphi^{\text{obs}} \quad [2.9a]$$

$$J_{\text{NaF}} = -L_{21} \nabla \ln T - L_{22} \nabla \mu_{\text{NaF},T} \left(1 + \frac{x_{\text{NaF}}}{3x_{\text{AlF}_3}}\right) - L_{23} \nabla \varphi^{\text{obs}} \quad [2.9b]$$

$$j = -L_{31} \nabla \ln T - L_{32} \nabla \mu_{\text{NaF},T} \left(1 + \frac{x_{\text{NaF}}}{3x_{\text{AlF}_3}}\right) - L_{33} \nabla \varphi^{\text{obs}} \quad [2.9c]$$

The phenomenological coefficients  $L_{ij}$  are independent of the forces. The direct coefficients,  $L_{11}$ ,  $L_{22}$  and  $L_{33}$ , relate conjugate fluxes and forces. The coefficients,  $L_{12}$ ,  $L_{13}$ ,  $L_{21}$ ,  $L_{23}$ ,  $L_{31}$  and  $L_{32}$ , represent cross phenomena. They refer to reactions of the components to forces that are acting directly on other components. Equation [2.9c], solved with respect to  $\nabla \varphi^{\text{obs}}$ , gives:

$$\nabla \varphi^{\text{obs}} = -\frac{L_{31}}{L_{33}} \nabla \ln T - \frac{L_{32}}{L_{33}} \nabla \mu_{\text{NaF},T} \left(1 + \frac{x_{\text{NaF}}}{3x_{\text{AlF}_3}}\right) - \frac{1}{L_{33}} j \quad [2.10]$$

By introducing Equation [2.10] into Equations [2.9a] and [2.9b], the flux equations can be written as:

$$J_q = -l_{11} \nabla \ln T - l_{12} \nabla \mu_{\text{NaF},T} \left(1 + \frac{x_{\text{NaF}}}{3x_{\text{AlF}_3}}\right) + \left(\frac{L_{13}}{L_{33}}\right) j \quad [2.11a]$$

$$J_{\text{NaF}} = -l_{21} \nabla \ln T - l_{22} \nabla \mu_{\text{NaF},T} \left(1 + \frac{x_{\text{NaF}}}{3x_{\text{AlF}_3}}\right) + \left(\frac{L_{23}}{L_{33}}\right) j \quad [2.11b]$$

where  $l_{ij} = (L_{ij} - L_{3j}L_{i3}/L_{33})$  and  $l_{ij}$  are phenomenological diffusion coefficients. According to Onsager (1931) the cross coefficients are related to each other in the following way:

$$L_{ij} = L_{ji} \quad \text{ie} \quad l_{ij} = l_{ji} \quad (i, j = 1, \dots, k \quad \text{and} \quad j \neq i) \quad [2.12]$$

Equation [2.12] is called the Onsager Reciprocal Relations, ORR. For Equation [2.9a-c] the relations are  $L_{12}=L_{21}$ ,  $L_{13}=L_{31}$  and  $L_{23}=L_{32}$ .

### 2.1.3 Local Mass and Entropy Balances

The transference coefficient,  $t_i$ , was defined as the number of moles of component  $i$  transferred with one faraday electric charge, Eq.[2.4]. In a two component system there is only one *independent* transference coefficient. Equation [2.9b] combined with Equation [2.9c] gives the transference coefficient of NaF as:

$$\left( \frac{J_{\text{NaF}}}{j} \right)_{\nabla T=0, \nabla \mu_i=0} = \frac{L_{23}}{L_{33}} = t_{\text{NaF}}^{\text{L,F}^-} \quad [2.13]$$

The relation between transference coefficients and transference numbers can be obtained from a local mass balance at the aluminium electrode - electrolyte interface. The mass changes are listed in Table 2.1 and they show that the transference coefficients are equal to:

$$t_{\text{NaF}}^{\text{L,F}^-} = t_{\text{Na}^+} \quad [2.14a]$$

$$t_{\text{AlF}_3}^{\text{L,F}^-} = -\frac{1}{3}(1 - t_{\text{el}} - t_{\text{Al}^{3+}}) = -\frac{1}{3}t_{\text{Na}^+} \quad [2.14b]$$

where  $t_{\text{Na}^+}$ ,  $t_{\text{el}}$ , and  $t_{\text{Al}^{3+}}$  are the transference numbers of  $\text{Na}^+$ , of "electrons" and of  $\text{Al}^{3+}$ , respectively. The mass balance is done by separating the melt into single ions,  $\text{Al}^{3+}$ ,  $\text{Na}^+$ ,  $\text{F}^-$  and "electrons", for simplicity reasons. The transference number,  $t_{\text{Al}^{3+}}$ , is the fraction of the electric current density flux,  $j$ , carried by the sum of all aluminium containing species. The presence of aluminium in NaF- $\text{AlF}_3$  melts causes electronic conduction, Borisolebskii et al.

(1978). Model studies indicate that sodium dissolves in the electrolyte as free Na, while dissolved Al is predominantly present as the monovalent species  $\text{AlF}_2^-$ , Ødegaard et al. (1988). Any electronic conductivity is most likely associated with the Na species that may form trapped electrons (analogous to F-centres in solid crystals) and electrons in the conduction band, Haarberg et al. (1990). This means that only  $\frac{1}{3}(1-t_{\text{el}})$  mole aluminium will be transported from left to right when one faraday of positive electric charge is passing through the cell. The rest of the electric charge will pass through the electrolyte by free Na or monovalent  $\text{AlF}_2^-$ . This part of the current is represented by  $t_{\text{el}}$ .

The Peltier heat,  $\pi$ , is the flux of heat,  $J_q$ , caused by the electric current,  $j$ , in the cell and is defined for an isothermal cell with uniform composition by de Groot (1966) as:

$$\left(\frac{J_q}{j}\right)_{\nabla T=0, \nabla \mu_i=0} = \frac{L_{13}}{L_{33}} = \pi \quad [2.15]$$

The Peltier heat of an electrode/electrolyte interface can be obtained from an entropy balance for reversible changes at the interface. The change in entropy in a cell with transfer of heat, mass and electric charge,  $dS$ , can be expressed as an irreversible, time-dependent entropy change,  $dS(t)$ , and a charge dependent term,  $dS(Q)$ :

$$dS = dS(t) + dS(Q) \quad [2.16]$$

For small current densities, the last term in Equation [2.16] is zero (a condition compatible with validity of the Onsager reciprocal relations). The condition  $dS(Q)_{j \rightarrow 0} = 0$  gives the reversible entropy balance, Grimstvedt et al. (1994). The Peltier heat is defined as positive when the left-hand side electrode-electrolyte interface receives heat from the surroundings.

Each contribution to the entropy balance is listed in Table 2.2 and the changes in transported entropies are illustrated in Figure 2.1. The following expression for the Peltier effect, is given from Table 2.2, keeping in mind that  $t_{\text{Na}^+} + t_{\text{Al}^{3+}} + t_{\text{el}} = 1$ :

$$\frac{\pi}{T} = -S_{\text{Al}}^* - t_{\text{el}} S_{\text{el}}^* - \frac{1}{3}(1 - t_{\text{el}})(S_{\text{Al}} - S_{\text{Al}^{3+}}^*) + t_{\text{Na}^+} \left( S_{\text{Na}^+}^* - \frac{1}{3} S_{\text{Al}^{3+}}^* - S_{\text{NaF}} + \frac{1}{3} S_{\text{AlF}_3} \right) \quad [2.17]$$

Here  $S_i^*$  denotes the transported entropy of ion  $i$  and  $S_i$  are the partial molar entropy of the neutral component  $i$ . The total entropy transferred is independent of the chosen frame of reference for transport. The partial molar entropies,  $S_i$ , which originate from the chemical reaction, will normally give the major contribution to the Peltier heat. The entropy transported through the electrolyte,  $S_{\text{Na}^+}^*$  and  $S_{\text{Al}^{3+}}^*$ , may, however, contribute substantially, Ratkje and Sharivker (1995). The entropy transported through the metal,  $S_{\text{Al}}^*$ , is small, showing only small variations with the nature of the metal and with temperature, Borelius and Gunneson (1921), Moore and Graves (1972). The Peltier heat of thermocells is usually much larger than the Peltier heat of thermocouples, because there are no chemical reactions in a system of electronic conductors.

Table 2.1 Local mass changes in thermocell [D]

A quasi stationary lattice of fluoride ions is chosen as the frame of references for the changes at the electrode - electrolyte interface when one faraday of positive charges is transferred from left to right.

	Left-hand side electrode ( $T$ )	Right-hand side electrode ( $T+\Delta T$ )
$\text{Al}^{3+}$ :	$\frac{1}{3}(1-t_{\text{el}}-t_{\text{Al}^{3+}})$	$-\frac{1}{3}(1-t_{\text{el}}-t_{\text{Al}^{3+}})$
$\text{F}^-$ :	$t_{\text{F}^-} = 0$	$-t_{\text{F}^-} = 0$
$\text{Na}^+$ :	$-t_{\text{Na}^+}$	$t_{\text{Na}^+}$
$\text{NaF}$ :	$-t_{\text{Na}^+}$	$t_{\text{Na}^+}$
$\text{AlF}_3$ :	$\frac{1}{3}(1-t_{\text{el}}-t_{\text{Al}^{3+}})$	$-\frac{1}{3}(1-t_{\text{el}}-t_{\text{Al}^{3+}})$
$\text{Al}$ :	$-\frac{1}{3}(1-t_{\text{el}})$	$\frac{1}{3}(1-t_{\text{el}})$

Table 2.2 Reversible entropy balance at the left-hand side electrode-electrolyte interface.

The entropy received and consumed is given for the transfer of one faraday of positive electric charge passing from the left to the right electrode.

ENTROPY RECEIVED	
$\pi/T$	the interface receives entropy from the heat reservoir
$S_{\text{Al}}^*$	entropy transported through the electrode to the interface
$\frac{1}{3}(1-t_{\text{el}})S_{\text{Al}}$	the disappearance of $\frac{1}{3}(1-t_{\text{el}})$ mole Al liberates entropy
$t_{\text{Na}^+}S_{\text{NaF}}$	the disappearance of $t_{\text{Na}^+}$ mole NaF liberates entropy
$t_{\text{el}}S_{\text{el}}^*$	entropy transported through the electrolyte to the interface
ENTROPY CONSUMED	
$\frac{1}{3}(1-t_{\text{el}}-t_{\text{Al}^{3+}})S_{\text{AlF}_3}$	the formation of $\frac{1}{3}(1-t_{\text{el}}-t_{\text{Al}^{3+}})$ mole $\text{AlF}_3$ consumes entropy
$t_{\text{Na}^+}S_{\text{Na}^+}^*$	entropy transported through the electrolyte away from the interface
$\frac{1}{3}t_{\text{Al}^{3+}}S_{\text{Al}^{3+}}^*$	entropy transported through the electrolyte away from the interface

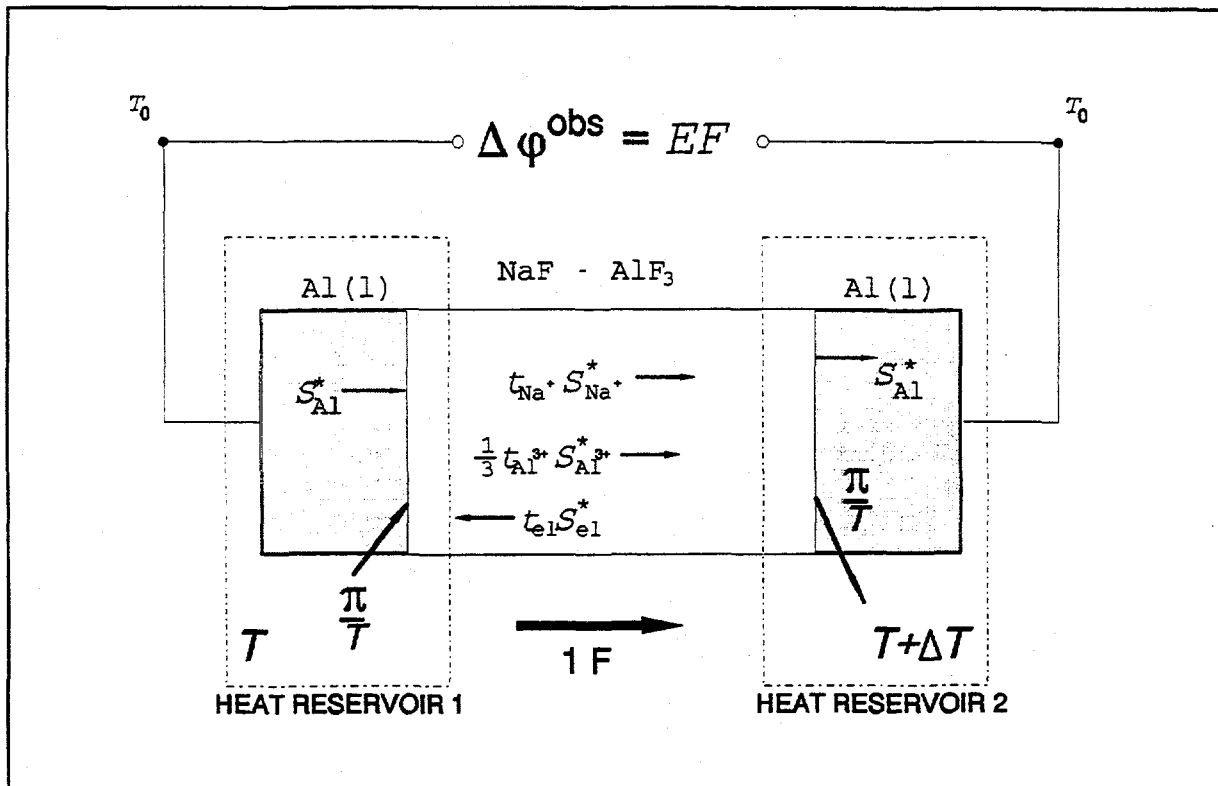


Figure 2.1 Schematic illustration of thermocell [D], The transported entropy changes and the sign of the Peltier effect are indicated.

### 2.1.4 The Seebeck Coefficient and The Peltier Heat

Introduction of the relations in Eqs.[2.12], [2.13] and [2.15] into Eq.[2.10], gives the electric potential gradient in terms of the Peltier heat and the transference coefficients:

$$\nabla\varphi^{\text{obs}} = -\pi\nabla\ln T - t_{\text{NaF}}\nabla\mu_{\text{NaF},T}\left(1 + \frac{x_{\text{NaF}}}{3x_{\text{AlF}_3}}\right) - \frac{1}{L_{33}}j \quad [2.18]$$

The initial state is defined at time equal to "zero". Then there can be a temperature gradient between the two electrodes, but no concentration gradients. The Seebeck coefficient is the electromotive force divided by the temperature difference, for small  $\Delta T$ . Onsager reciprocal relations imply that the Peltier effect is opposite and equal to the Seebeck coefficient multiplied by Faraday's constant,  $F\varepsilon_0$ , of a cell with identical electrodes and uniform composition, Førland et al. (1988).

$$F\varepsilon_0 = \left(\frac{\nabla\varphi^{\text{obs}}}{\nabla T}\right)_{j=0, i=0} = \lim_{\Delta T \rightarrow 0} \left(\frac{\Delta\varphi^{\text{obs}}}{\Delta T}\right)_{j=0, i=0} = -\frac{\pi}{T} \quad [2.19]$$

The thermoelectric power is defined as the ratio  $\Delta\varphi/\Delta T$  and the Peltier effect is equal to the negative of the thermoelectric power. This means that the Peltier effect,  $\pi/T$ , can be obtained as the slope of the curve, by plotting the observed cell potential multiplied by Faraday's constant versus  $\Delta T$ .

When Equations [2.17] and [2.19] are combined, the following expression for the

thermoelectric power at initial state conditions is obtained:

$$F \varepsilon_0 = S_{Al}^* + t_{el} S_{el}^* + \frac{1}{3}(1-t_{el})(S_{Al} - S_{Al^{3+}}^*) - t_{Na} \cdot (S_{Na}^* - \frac{1}{3}S_{Al^{3+}}^* - S_{NaF} + \frac{1}{3}S_{AlF_3}) \quad [2.20]$$

A quantity used in the description of transfer phenomena in non-isothermal systems is the heat of transfer (or heat of transport),  $Q_i^*$ . This was first introduced by Eastman (1926, 1928) and Wagner (1929, 1930). The heat of transfer is the heat transferred from left to right, coupled to the transfer of component  $i$  at zero temperature difference and in the absence of an electric current, Førlund et al. (1988). The heat of transfer,  $Q_i^*$ , depends on the frame of reference in the same way as the transport numbers.

The forces,  $-\nabla \ln T$  and  $-\nabla \mu_{NaF,T}$  can be expressed in a similar way as the fluxes, Eq.[2.11]. For a multi-component system, at  $j$  equal to zero, the force  $-\nabla \ln T$  can be written as:

$$-\nabla \ln T = r_{11} J_q + \sum_{i=2}^{k+1} r_{1i} J_i \quad [2.21]$$

By comparing Eq.[2.21] with the heat- and mass flux equations for a multi-component system, one finds the following relations between the  $l$ 's and the  $r$ 's:

$$\sum_{i=1}^{k+1} l_{1i} r_{li} = 1 \quad \text{and} \quad \sum_{i=1}^{k+1} l_{ji} r_{li} = 0 \quad (j=2,3,\dots,k+1) \quad [2.22]$$

The derivation of the relation in Eq.[2.22], which is shown in Appendix A for a two component system, is valid for a set of independent fluxes and forces. From Equation [2.21] the heat of transfer can be defined as:

$$\left( \frac{J_q}{J_i} \right)_{j=0, \nabla T=0, J_{j \neq i}=0} = -\frac{r_{1i}}{r_{11}} = Q_i^* \quad (j, i = 2, 3, \dots, k+1) \quad [2.23]$$

where j stands for all species apart from species i. Equation [2.23] will only be valid when there are no relations between the mass fluxes or when the wall is used as the frame of reference. The heat of transfer can also be given implicitly by phenomenological diffusion coefficients, from Eqs.[2.22]and [2.23], as:

$$l_{j1} = \sum_{i=2}^{k+1} l_{ji} Q_i^* \quad (j=2, 3, \dots, k+1) \quad [2.24]$$

If the frame of reference is changed from the wall to a fluoride ion lattice, Equation [2.5] can be applied. Equations [2.5] and [2.24] shows that in a fluoride lattice frame of reference only the net heat of transfer,  $Q^*$ , can be obtained, Eq.[2.25]. The heat of transfer,  $Q^*$ , can be associated with interdiffusion of NaF and  $AlF_3$ , the Dufour effect. The Dufour effect is the reciprocal of the Soret effect. Equations [2.11a] and [2.11b], which are valid in a fluoride lattice frame of reference, give the heat of transfer,  $Q^*$ , as the ratio between the heat flux,  $J_q$  and the mass flux,  $J_{NaF}$  when  $\Delta T$  and  $j$  are equal to zero:

$$\left( \frac{J_q}{J_{NaF}} \right)_{\Delta T=0, j=0} = (Q_{NaF}^* - \frac{1}{3} Q_{AlF_3}^*) = \frac{l_{12}}{l_{22}} = Q^* \quad [2.25]$$

In the fluoride ion lattice frame of reference, there is only one heat of transfer,  $Q^*$ , it is not possible to distinguish between the heat of transfers,  $Q_{NaF}^*$  and  $Q_{AlF_3}^*$ .

In a multi-component electrolyte with a temperature gradient, there may be a flux of matter leading to a partial separation of the electrolyte (Soret effect). When there is no mixing by convection, the separation process continues until the thermal force is balanced by the chemical force. The stationary state is often called the Soret equilibrium, Agar (1963). The stationary state is defined at time equal to "infinity", which is the situation where there is no mass transfer, but a non-vanishing energy transfer exists. In this situation the system only exchanges heat with the surroundings and the state variables of the system (those variables which describe the state of a system macroscopically) no longer depends on time. Variables such as pressure and temperature can however depend on the space coordinates, de Groot (1966). Then there can be both a temperature and a concentration gradient between the two electrodes. It is therefore important to have a cell with no convection when measuring the thermoelectric power at stationary state conditions,  $F\varepsilon_\infty$ .

At stationary state the mass fluxes,  $J_i$ , are zero. The entropy changes at the interface electrode - electrolyte are then the same as those caused by the transport of one faraday of positive charges through the thermocell, or by the transport of  $\frac{1}{3}(1-t_{el})$  mole of  $Al^{3+}$  and  $t_{el}$  mole of electrons in thermocell [D]:

$$\begin{aligned} \frac{1}{3}(1-t_{el})S_{Al^{3+}}^* - t_{el}S_{el}^* &= \frac{1}{3}t_{Al^{3+}}S_{Al^{3+}}^* + t_{Na^+}S_{Na^+}^* - t_{el}S_{el}^* - t_{Na^+} \frac{Q^*}{T} \\ &\quad - t_{Na^+}S_{NaF} + \frac{1}{3}(1-t_{el}-t_{Al^{3+}})S_{AlF_3} \end{aligned} \quad [2.26]$$

Rearranging Equation [2.26] with respect to the term containing the heat of transfer, gives:

$$t_{\text{Na}} \cdot \frac{Q^*}{T} = t_{\text{Na}} \cdot (S_{\text{Na}}^* - \frac{1}{3} S_{\text{Al}^{3+}}^* - S_{\text{NaF}} + \frac{1}{3} S_{\text{AlF}_3}) \quad [2.27]$$

The heat of transfer,  $Q^*$ , can be both negative and positive. All terms in Eq.[2.27] are independent of the forces, and the equation is valid whether we have stationary state or not. A combination of Eqs.[2.20] and [2.27] gives the following expression for the thermoelectric power at initial state conditions:

$$F\varepsilon_0 = -\frac{\pi}{T} = \frac{1}{3}(1-t_{\text{el}})(S_{\text{Al}} - S_{\text{Al}^{3+}}^*) + S_{\text{Al}}^* - t_{\text{NaF}} \frac{Q^*}{T} + t_{\text{el}} S_{\text{el}}^* \quad [2.28]$$

The thermoelectric power, or the Seebeck coefficient multiplied by Faraday's constant,  $F\varepsilon_\infty$ , at stationary state conditions, is defined in a similar way as the thermoelectric power at initial state,  $F\varepsilon_0$ , Eq.[2.18] and Eq. [2.19]:

$$F\varepsilon_\infty = \left( \frac{\nabla \varphi^{\text{obs}}}{\nabla T} \right)_{j=0, t \rightarrow \infty} = \lim_{\Delta T \rightarrow 0} \left( \frac{\Delta \varphi^{\text{obs}}}{\Delta T} \right)_{j=0, t \rightarrow \infty} = -\frac{\pi}{T} - t_{\text{NaF}} \left( 1 + \frac{x_{\text{NaF}}}{3x_{\text{AlF}_3}} \right) \frac{\nabla \mu_{\text{NaF}, T}}{\nabla T} \quad [2.29]$$

At stationary state conditions, the term containing  $\nabla \mu_{\text{NaF}}$  is different from zero, but this term can be eliminated from Equation [2.29] by solving the mass flux Equation [2.11b] with respect to  $\nabla \mu_{\text{NaF}, T} (1 + x_{\text{NaF}}/3x_{\text{AlF}_3})$ , when  $J_{\text{NaF}} = 0$  (at stationary state conditions):

$$\nabla \mu_{\text{NaF},T}^{t \rightarrow \infty} \left(1 + \frac{x_{\text{NaF}}}{3x_{\text{AlF}_3}}\right) = -\frac{l_{21}}{l_{22}} \frac{\nabla T}{T} + \frac{t_{\text{NaF}}}{l_{22}} j \quad [2.30]$$

where  $l_{21}/l_{22}$  is equal to the heat of transfer, Eq.[2.25]. This term will cancel the same term in the Peltier effect, Eq.[2.28]. The thermoelectric power at stationary state may then be expressed as:

$$F \varepsilon_{\infty} = \left( \frac{\nabla \varphi^{\text{obs}}}{\nabla T} \right)_{t \rightarrow \infty, j=0} = \lim_{\Delta T \rightarrow 0} \left( \frac{\Delta \varphi^{\text{obs}}}{\Delta T} \right)_{t \rightarrow \infty, j=0} = S_{\text{Al}}^* + \frac{1}{3} (1 - t_{\text{el}}) (S_{\text{Al}} - S_{\text{Al}^{3+}}^*) + t_{\text{el}} S_{\text{el}}^* \quad [2.31]$$

This means, that the total transported entropy through the melt can be obtained by measuring the thermoelectric power at stationary state conditions. The transported entropy through the metal,  $S_{\text{Al}}^*$ , is small, compared with the transported entropies in the electrolyte, and is usually neglected. When the cryolite ratio  $n_{\text{NaF}}/n_{\text{AlF}_3} < 1.8$ , the electronic conductivity approaches zero at low temperatures, Haarberg (1994), and  $t_{\text{el}}$  may be neglected. Then the total transported entropy will be equal to the transported entropy of  $\text{Al}^{3+}$ ,  $S_{\text{Al}^{3+}}^*$ , the ion to which the aluminium electrodes in cell [D] are reversible.

The observable heat of transfer,  $Q^*$ , can be obtained from a combination of the measurements at initial state and at stationary state conditions, Eq.[2.28] and Eq.[2.31]:

$$t_{\text{NaF}} \frac{Q^*}{T} = F(\varepsilon_{\infty} - \varepsilon_0) \quad [2.32]$$

The heat of transfer is independent of the electrodes, and can also be found by thermal diffusion experiments.

## 2.2 TEMPERATURE DEPENDENCY OF THE THERMOELECTRIC POWER

Thermoelectric powers are usually found from plots of electric potentials,  $\Delta\phi$ , versus  $\Delta T$ . Entropies and transported entropies are generally functions of temperature. When both the molar heat capacity,  $C_{p,i}$ , and the Thomson coefficient,  $\tau_i$ , are small,  $\Delta\phi$  will appear as a linear function of  $\Delta T$ . For large values of  $\Delta T$ , the variation with  $T$  can give second-order corrections, and must then be considered, Grimstvedt (1992), Grimstvedt et al. (1994). In this section we shall study such effects for thermocell [D] in Section 2.1. The variation in the transported entropy,  $S_i^*$ , with temperature is given by the Thomson coefficient,  $\tau_i$ , in the same way as the temperature variation in the entropy,  $S_i$ , is given by the molar heat capacity for the component  $i$ ,  $C_{p,i}$ , Haase (1990).

$$\left(\frac{\partial S_i^*}{\partial \ln T}\right)_P = \tau_i \quad [2.33]$$

where  $P$  denotes constant pressure.

The transported entropy through the electrode,  $S_{Al}^*$ , is approximately equal to zero, compared with the transported entropies in the electrolyte, Borelius and Gunneson (1921), Moore and Graves (1972), and will be neglected. Equation [2.31] may then be approximated by:

$$\Delta \phi_{t \rightarrow \infty}^{obs} = \int_{T_1}^{T_2} \left[ \frac{1}{3} (1 - t_{el}) (S_{Al} - S_{Al^{3+}}^*) + t_{el} S_{el}^* \right] dT \quad [2.34]$$

The nature of the transported entropy of electrons,  $S_{el}^*$ , in molten salts is not known. If it is comparable in size with the transported entropy of an ion, in an electrolyte, it can contribute significantly to the thermoelectric power. The transport number of electrons,  $t_{el}$ , is also a function of temperature, but this is still unknown. Within small temperature gradients it will be assumed to be constant.

For constant molar heat capacity,  $C_{p,i}$ , the molar entropy,  $S_i$ , is:

$$S_i(T) = S_i(T_1) + C_{p,i} \int_{T_1}^T \frac{dT}{T} = [S_i(T_1) - C_{p,i} \ln T_1] + C_{p,i} \ln T \quad [2.35]$$

The integration of  $S_i dT$  from  $T_1$  to  $T_2$  gives:

$$\int_{T_1}^{T_2} S_i dT = S_i(T_1) \Delta T + C_{p,i} \left[ \ln \left( \frac{T_2}{T_1} \right)^{\frac{T_2}{\Delta T}} - 1 \right] \Delta T \quad [2.36]$$

In the same way, the transported entropy,  $S_i^*$ , as a function of the temperature, can be found when the Thomson coefficient,  $\tau_i$ , is constant. By expanding the logarithm in Eq.[2.36] we get:

$$T_2 \ln \frac{T_2}{T_1} - \Delta T = \frac{1}{2} \left( \frac{\Delta T}{T_1} \right) \Delta T - \frac{1}{6} \left( \frac{\Delta T}{T_1} \right)^2 \Delta T + \dots \quad [2.37]$$

If  $\Delta T/T_1 \ll 1$  the approximation  $T_2 \ln(T_2/T_1) - \Delta T \approx \frac{1}{2} \Delta T^2/T_1$  can be introduced in Eq.[2.36]. The thermoelectric power at stationary state,  $(\Delta\varphi^{\text{obs}}/\Delta T)_{t \rightarrow \infty}$ , can now be expressed as a function of  $\Delta T$  when  $T_1$  is fixed:

$$\begin{aligned} \left( \frac{\Delta\varphi^{\text{obs}}}{\Delta T} \right)_{t \rightarrow \infty} &= \frac{1}{3}(1-t_{\text{el}})[S_{\text{Al}}(T_1) - S_{\text{Al}^{3+}}^*(T_1)] + \frac{1}{6}(1-t_{\text{el}}) \left( \frac{C_{P,\text{Al}^-} - \tau_{\text{Al}^{3+}}}{T_1} \right) \Delta T \\ &+ t_{\text{el}}(S_{\text{el}}^*(T_1) - \frac{\tau_{\text{el}}}{2T_1} \Delta T) \end{aligned} \quad [2.38]$$

The observed thermoelectric power at initial state conditions for the binary mixture electrolyte is from Equation [2.26]:

$$\left( \frac{\Delta\varphi^{\text{obs}}}{\Delta T} \right)_{t=0} = \left( \frac{\Delta\varphi^{\text{obs}}}{\Delta T} \right)_{t \rightarrow \infty} - \frac{t_{\text{NaF}}}{\Delta T} \int_{T_1}^{T_2} \frac{Q^*}{T} dT \quad [2.39]$$

It is still not established if the heat of transfer,  $Q^*$ , is a function of temperature or not. The heat of transfer is a function of entropies and transported entropies, Eq.[2.27], which are temperature functions, it may therefore be assumed that also the heat of transport is a function of temperature. By expanding the value of the integral in Equation [2.39], introducing Equation [2.38] and assuming that  $Q^*$  is constant, Eq.[2.39] can be written as:

$$\begin{aligned} \left( \frac{\Delta \varphi^{\text{obs}}}{\Delta T} \right)_{t=0} &= \frac{1}{3}(1-t_{\text{el}})[S_{\text{Al}}(T_1) - S_{\text{Al}^{3+}}^*(T_1)] + \frac{1}{6}(1-t_{\text{el}}) \left( \frac{C_{P,\text{Al}^-} - \tau_{\text{Al}^{3+}}}{T_1} \right) \Delta T \\ &+ t_{\text{el}}(S_{\text{el}}^*(T_1) - \frac{\tau_{\text{el}}}{2T_1} \Delta T) - t_{\text{NaF}} \frac{Q^*}{T_1} \left( 1 - \frac{\Delta T}{2T_1} \right) \end{aligned} \quad [2.40]$$

Second-order heat effects in Equations [2.39] and [2.40] may be small even if  $\Delta T$  is large, Grimstvedt et al. (1994).

## 2.3 THE SYSTEM $\text{AlF}_3\text{-NaF-Al}_2\text{O}_3$

In this section the binary system,  $\text{NaF-AlF}_3$  in Section 2.1, will be extended to electrolytes with aluminium oxide (alumina). A thermocell, with an electrolyte of  $\text{AlF}_3$ ,  $\text{NaF}$  and  $\text{Al}_2\text{O}_3$ , and with aluminium electrodes will be discussed in Section 2.3.1. The aluminium electrodes will be replaced by oxygen electrodes in Section 2.3.2.

### 2.3.1 Thermocell: $(T)\text{Al}(\ell) \mid \text{NaF}, \text{AlF}_3, \text{Al}_2\text{O}_3 \mid \text{Al}(\ell)(T+\Delta T)$

When the melt of thermocell [D] is saturated with alumina, we have thermocell [B]:



where  $x_{\text{Al}_2\text{O}_3}$  is the mole fraction of alumina at saturation. Alumina saturated electrolyte is chosen as the standard state for the alumina activity,  $a_{\text{Al}_2\text{O}_3}$ . Since the melt is always saturated with  $\text{Al}_2\text{O}_3$ ,  $a_{\text{Al}_2\text{O}_3}$  is always equal to unity and the gradient in chemical potential of alumina,  $\nabla\mu_{\text{Al}_2\text{O}_3, T}$ , is zero. It is also possible to choose pure solid  $\text{Al}_2\text{O}_3$  as standard state for the alumina activity, but since there is an equilibrium between the solid and the liquid alumina, the activity of alumina will still be equal to one, Ratkje et al. (1993). Hence, the mass flux of alumina,  $J_{\text{Al}_2\text{O}_3}$ , times  $\nabla\mu_{\text{Al}_2\text{O}_3, T}$  will not contribute to the dissipation function. The relation between the chemical potential gradients of  $\text{NaF}$  and  $\text{AlF}_3$  is again given by equation [2.7], keeping in mind that the chemical potential gradient of  $\text{Al}_2\text{O}_3$  is zero. As in Section 2.1, a quasi lattice of fluoride ions will be chosen as the frame of reference for the transport. Since the flux of fluoride ions,  $J_{\text{F}^-}$ , is equal to zero in this frame of reference, Equation [2.5] must still be valid. Equation [2.8] is then the expression for the dissipation function also when the

electrolyte is saturated with alumina.

Application of the phase rule to regions of one liquid phase and one solid phase gives for a three component system:

$$\Phi = C - P + 1 = 3 - 2 + 1 = 2 \quad [2.41]$$

The two degrees of freedom,  $\Phi$ , can be accounted for by the temperature and one composition variable, eg. Barrow (1988).

The Pelter effect,  $\pi/T$ , in thermocell [B] can be obtained from an entropy balance for reversible changes at the electrode - electrolyte interface, in the same way as in Section 2.1.

$$\begin{aligned} \frac{\pi}{T} = & -S_{Al}^* - \frac{1}{3}(1-t_{el})(S_{Al} - S_{Al^{3+}}^*) - t_{el}S_{el}^* + t_{Na} \cdot (S_{Na^+}^* - S_{NaF} - \frac{1}{3}S_{Al^{3+}}^* + \frac{1}{3}S_{AlF_3}) \\ & - \frac{1}{6}t_{O^{2-}}(3S_{O^{2-}}^* + 2S_{Al^{3+}}^* - S_{Al_2O_3}) \end{aligned} \quad [2.42]$$

This equation is valid also for electrolytes that are not saturated with alumina. Using the same arguments as those leading up to Equation [2.27], it is found the heat of transfer is related to the transported entropies and the partial molar entropies by:

$$S_{Na^+}^* - S_{NaF} - \frac{1}{3}S_{Al^{3+}}^* + \frac{1}{3}S_{AlF_3} = \frac{Q_{NaF}^*}{T} - \frac{Q_{AlF_3}^*}{3T} \quad [2.43]$$

and

$$3S_{O^{2-}}^* + 2S_{Al^{3+}}^* - S_{Al_2O_3} = \frac{Q_{Al_2O_3}^*}{T} \quad [2.44]$$

Oxygen in alumina will react with molten NaF and  $AlF_3$  to form large aluminium-oxygen-fluoride anions, Grjotheim et al. (1982). It is doubtful that these large anions contribute significantly to the electric current transport in the electrolyte. The transport number for oxygen ions,  $t_{O^{2-}}$ , can be neglected, if this is so. The transference number,  $t_{O^{2-}}$ , means the sum of the fraction of the electric current density,  $j$ , carried by oxygen containing species. Formation of Al-O-F complexes will reduce the other Al-F-containing species. This may cause a reduction in the transport number of the aluminium ions,  $t_{Al^{3+}}$ . The addition of alumina will also change the electrical conductivity,  $\kappa$ , of the melt, which is the direct coefficient,  $L_{33}$  multiplied by  $F^2$ , Eq.[2.9c].

When the melt is saturated with alumina the net mass flux of alumina  $J_{Al_2O_3}$  is equal to zero and the heat of transport of  $Al_2O_3$ ,  $Q_{Al_2O_3}^*$ , will not contribute to the Peltier effect. Equation [2.44] is then equal to zero. Again there is only one independent mass flux,  $J_{NaF}$ , in the system and only one heat of transfer,  $Q^* = Q_{NaF}^* - \frac{1}{3} Q_{AlF_3}^*$ . The expression for the Peltier effect for the system  $AlF_3$ -NaF- $Al_2O_3$ , when the melt is saturated with alumina, is therefore given by Equation [2.17], Section 2.1.

When the NaF- $AlF_3$ - $Al_2O_3$  electrolyte is saturated with both alumina and aluminium fluoride then the gradient in chemical potential of  $Al_2O_3$ ,  $AlF_3$  and NaF,  $\nabla\mu_{Al_2O_3, T}$ ,  $\nabla\mu_{AlF_3, T}$  and  $\nabla\mu_{NaF, T}$ , are all equal to zero. Application of the phase rule to this system (two solid phases and one liquid phase) gives:

$$\Phi = C - P + 1 = 3 - 3 + 1 = 1 \quad [2.45]$$

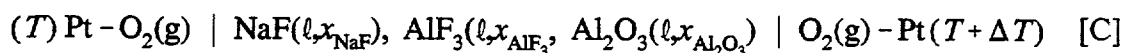
There are no phase composition degrees of freedom. For these conditions the expression for the Pelter effect becomes simply:

$$\frac{\pi}{T} = -S_{Al}^* - \frac{1}{3}(1 - t_{el})(S_{Al} - S_{Al^{3+}}^*) - t_{el}S_{el}^* \quad [2.46]$$

In a liquid solution of cryolite,  $Na_3AlF_6$ , and alumina,  $Al_2O_3$ , in equilibrium with solid alumina, the phase rule gives one degree of freedom,  $\Phi$ , (the temperature) and the Peltier heat can again be expressed by Equation [2.46].

### 2.3.2 Thermocell: $(T)\text{Pt}-\text{O}_2(\text{g}) \mid \text{NaF}, \text{AlF}_3, \text{Al}_2\text{O}_3 \mid \text{O}_2(\text{g})-\text{Pt}(T+\Delta T)$

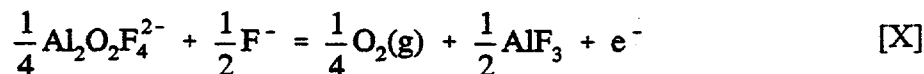
When the liquid aluminium electrodes of thermocell [B] are replaced by oxygen electrodes, we obtain thermocell [C]:



In an alumina saturated electrolyte, the dominating Al-O-F complex anion is probably  $\text{Na}_2\text{Al}_2\text{O}_2\text{F}_4$ . The first experimental evidence for the complex was given by Førland and Ratkje (1973) and Ratkje (1974). The single electrode reaction for cell [C] may formally be written as:



or with the particular complex in question:



In the absence of aluminium there is no electronic conduction in the melt. This means that the sum of ionic transference numbers is one. In the same way as in Section 2.1, the relation between transference coefficients and transference numbers, can be obtained from a local mass balance at the electrodes, which gives (Appendix B, Table A1):

$$t_{\text{NaF}} = t_{\text{Na}^+} \quad [2.47a]$$

$$t_{\text{AlF}_3} = -\frac{1}{3}(1 - t_{\text{Al}^{3+}} - t_{\text{O}^{2-}}) = -\frac{1}{3}t_{\text{Na}^+} \quad [2.47b]$$

$$t_{\text{Al}_2\text{O}_3} = \frac{1}{6}(1 - t_{\text{O}^{2-}}) \quad [2.47c]$$

The expression for the Peltier effect, for thermocell [C], is again obtained from an entropy balance for reversible changes at the electrode - electrolyte interface. From Appendix B Table A2, the Peltier heat at the oxygen electrode can be expressed as:

$$\begin{aligned} \frac{\pi}{T} = & -S_{\text{Pt}}^* + \frac{1}{4}S_{\text{O}_2} - \frac{1}{2}S_{\text{O}^{2-}}^* + t_{\text{Na}^+}(S_{\text{Na}^+}^* - S_{\text{NaF}} - \frac{1}{3}S_{\text{Al}^{3+}}^* + \frac{1}{3}S_{\text{AlF}_3}) \\ & + \frac{1}{6}(1 - t_{\text{O}^{2-}})(3S_{\text{O}^{2-}}^* + 2S_{\text{Al}^{3+}}^* - S_{\text{Al}_2\text{O}_3}) \end{aligned} \quad [2.48]$$

When the melt is saturated with alumina, the heat of transfer of alumina will not contribute to the Peltier effect, and the last term in Equation [2.48] is zero. Equations [2.48], [2.43] and [2.44], combined with the definition of the thermoelectric power, Eq.[2.19], gives the thermoelectric power for thermocell [C], at initial state conditions:

$$F\varepsilon_0 = -\frac{\pi}{T} = -\frac{1}{4}S_{\text{O}_2} + S_{\text{Pt}}^* + \frac{1}{2}S_{\text{O}^{2-}}^* - t_{\text{Na}^+} \frac{Q^*}{T} \quad [2.49]$$

Equation [2.49] is valid only for cryolite melts saturated with alumina, while Equation [2.48]

is valid for any concentration of alumina.

If the electrolyte is saturated with both alumina and aluminium fluoride the expression for the Peltier effect takes the simple form:

$$\frac{\pi}{T} = -S_{\text{Pr}}^* + \frac{1}{4}S_{\text{O}_2} - \frac{1}{2}S_{\text{O}_2}^* \quad [2.50]$$

The same expression is obtained for the Peltier effect for alumina saturated melts with molar ratio NaF/AlF<sub>3</sub> equal to three.

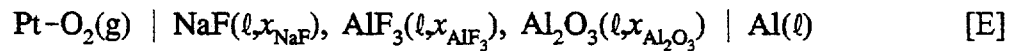
The temperature dependency of the thermoelectric power of the oxygen electrode can be written in a similar way as for the aluminium electrode in Section 2.2. Equation [2.49] can be written:

$$F\varepsilon_0 = \frac{1}{2}[S_{\text{O}_2}^*(T_1) - \frac{1}{2}S_{\text{O}_2}(T_1)] + \frac{1}{4} \left( \frac{\tau_{\text{O}_2} - \frac{1}{2}C_{p,\text{O}_2}}{T_1} \right) \Delta T \quad [2.51]$$

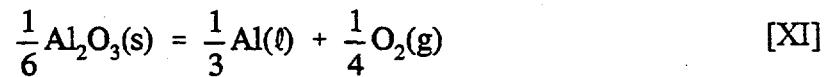
$$- t_{\text{Na}} \frac{Q^*}{T_1} \left( 1 - \frac{\Delta T}{2T_1} \right)$$

## 2.4 CONSISTENCY CONTROL

The isothermal, non-symmetrical formation cell, with one liquid aluminium electrode and one oxygen electrode can be written:



where  $x_{\text{Al}_2\text{O}_3}$  is the mole fraction of alumina. The reduction process in the isothermal cell [E], when  $x_{\text{Al}_2\text{O}_3}$  is the mole fraction of alumina at saturation may be written:



When the transport number for electrons,  $t_{\text{el}}$ , is zero and the contribution from  $(S_{\text{Pt}}^* - S_{\text{Al}}^*)$  is neglected, Equations [2.42] and [2.48] gives the temperature derivative of the electric potential of cell [E], Førlund et al. (1988):

$$\begin{aligned} \left( \frac{\Delta \varphi^{\text{obs}}}{\Delta T} \right)_{\text{cell [B]}} - \left( \frac{\Delta \varphi^{\text{obs}}}{\Delta T} \right)_{\text{cell [C]}} &= - \left( \frac{\pi}{T} \right)_{\text{cell [B]}} + \left( \frac{\pi}{T} \right)_{\text{cell [C]}} \\ &= \frac{1}{3}S_{\text{Al}} + \frac{1}{4}S_{\text{O}_2} - \frac{1}{6}S_{\text{Al}_2\text{O}_3} = \Delta S_{\text{cell [E]}} \end{aligned} \quad [2.52]$$

where  $\Delta S$  refers to one faraday transferred. The change in entropy,  $\Delta S$ , of reaction [XI] is

positive and can be obtained from data of JANAF (1971). At 1173 K,  $\Delta S$  for reaction [XI], is equal to  $55.54 \pm 0.02 \text{ J mol}^{-1} \text{ K}^{-1}$ , using the alpha modification of alumina.

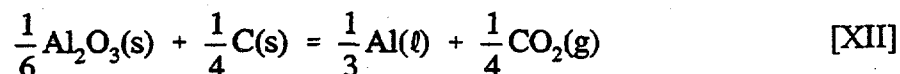
The relation in Equation [2.52] makes a consistency check on separate measurements possibly since all terms in this equation can be obtained independently of each other, Ito et al. (1984).

## 2.5 RELEVANCE TO THE HALL - HÉROULT CELL

Consumable carbon anodes are used instead of inert oxygen electrodes in the aluminium electrolysis process. The Hall - Héroult cell may be written:



When the electrolyte is saturated with alumina, the primary reaction equation for the isothermal cell [A] is:



The Peltier effect at the carbon anode can be found by replacing the temperature derivative of the electric potential of cell [E] with the temperature derivative of the electric

potential of cell [A] in Equation [2.52]. If the thermoelectric power at the aluminium cathode is known, the only unknown is the Peltier effect at the carbon anode:

$$\left(\frac{\Delta \varphi^{\text{obs}}}{\Delta T}\right)_{\text{cell [B]}} - \left(\frac{\Delta \varphi^{\text{obs}}}{\Delta T}\right)_{\text{carbon electrode}} = -\left(\frac{\pi}{T}\right)_{\text{cell [B]}} + \left(\frac{\pi}{T}\right)_{\text{carbon electrode}} = \Delta S_{\text{cell [A]}} \quad [2.53]$$

The temperature derivative of cell [A] when the electrolyte is saturated with alumina,  $d\varphi/dT = \Delta S$ , can be found from data of JANAF (1971). At 1273 K,  $\Delta S$  for reaction [XII] is equal to  $55.77 \pm 0.06 \text{ J mol}^{-1} \text{ K}^{-1}$ . This value differs from the temperature derivative of cell [E] by  $0.23 \text{ J mol}^{-1} \text{ K}^{-1}$ . A shift from consumable anodes to inert oxygen anodes will then only change the Peltier effect or the heat consumption at the anode with  $0.23 \text{ J mol}^{-1} \text{ K}^{-1}$ .

The cathode in the aluminum electrolysis cell is liquid aluminum. The reversible heat production at the aluminium cathode, in an isothermal cell with an electric current density  $i$  is then, where subscript c means cathode:

$$\left(\frac{dq}{dt}\right)_c = \pi_c \frac{i_c}{F} = -T \varepsilon_0 i_c \quad [2.54]$$

The reversible heat production at the anode is accordingly, where subscript a means anode:

$$\left(\frac{dq}{dt}\right)_a = -\pi_a \frac{i_a}{F} = T \varepsilon_0 i_a \quad [2.55]$$

A positive value means that heat is produced by the electrode reaction and a negative value means that heat is consumed.

## 2.6 OTHER SYSTEMS, TRENDS

Thermocells have been investigated experimentally, since the pioneering work of Bouty (1879, 1880, 1881) and by Richards (1897), among others. There are only two available reports on measurements of thermoelectric powers,  $\Delta\phi/\Delta T$ , or Seebeck coefficients,  $\varepsilon_0$ , in systems with cryolite in the literature, the work by Mozhaev and Polyakov (1980) and Ratkje and Sharivker (1995). Examples, from the literature, of Seebeck coefficients in different systems are given in this section.

Usually the Seebeck coefficient is given the sign of the positive electrode

$$\varepsilon = \frac{E^+ - E^-}{T_2^+ - T_1^-} \quad [2.56]$$

but not all authors give the definition they have used in their reports, so sometimes there can be doubt about the sign of the Seebeck coefficient.

There are several reports available on Seebeck coefficients in aqueous solutions of single salts at 298 K. Some examples are given in Table 2.3.

The first thermoelectric power measurement reported on multicomponent systems is the initial thermoelectric power of the  $\text{AgNO}_3\text{-NaNO}_3$  mixture as a function of the composition by Schneebaum and Sundheim (1962). Most of the reported Seebeck coefficients in fused salts are for binary systems with sulfates, nitrates or chlorides. Examples are given in Table 2.4.

There are few reports on Seebeck coefficients of metal-molten salt systems in which mobile electrons as well as ionic species contributes to the transport process. Two examples are given in Table 2.5.

Table 2.3 Seebeck coefficients for aqueous solutions. All data are obtained at 298 K except the last one which is at 328 K.

	Electrodes	Electrolytes	$\epsilon_0 / \mu\text{V K}^{-1}$
Breck et al. (1965)	quinhydrone	0.01 M HCl	$-625 \pm 3$
	"	0.01 M HClO <sub>4</sub>	$-649 \pm 4$
	"	0.01 M HNO <sub>3</sub>	$-632 \pm 5$
	"	0.01 M H <sub>2</sub> SO <sub>4</sub>	$-669 \pm 2$
Breck and Agar (1957)	3.11% Cd amalgam	0.05 M CdSO <sub>4</sub>	810
		0.05 M Cd(ClO <sub>4</sub> ) <sub>2</sub>	768
		0.05 M Cd(NO <sub>3</sub> ) <sub>2</sub>	752
		0.05 M CdCl <sub>2</sub>	710
Haase and Hoch (1965)	Ag/AgCl	0.001 M KCl	831.5
	"	0.001 M LaCl <sub>3</sub>	680.5
	Ag	0.001 M AgNO <sub>3</sub>	-801.5
	"	0.001 M AgClO <sub>4</sub>	-811.3
Levin and Bonilla (1951)	Ag/AgCl	0.001 M KCl	733
	"	0.001 M CsCl	783
Kamata et al. (1986)	Ag	0.001 M AgNO <sub>3</sub>	-780
Ratkje et al. (1990)	Ag/AgCl	0.005 M KCl	740
Quickenden and Veron (1986)	Pt	K <sub>4</sub> Fe(CN) <sub>6</sub> · 3H <sub>2</sub> O + K <sub>3</sub> Fe(CN) <sub>6</sub> (0.07 mol dm <sup>-3</sup> )	$1600 \pm 25$

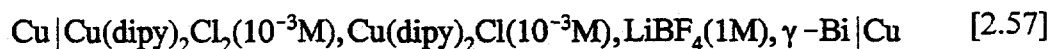
Table 2.4 Seebeck coefficients in fused and solid salt and binary mixtures.

	Electrodes	Electrolytes	$\epsilon_0 / \mu\text{V K}^{-1}$	Temp / K
Schneebaum and Sundheim (1962)	Ag	$\text{AgNO}_3(\ell)$	$-319 \pm 7$	583
	"	$\text{AgNO}_3(0.1 \text{ mol } \%) + \text{NaNO}_3$	$-755 \pm 7$	583
Grimstvedt (1992)	Ag	$\text{Ag}_2\text{SO}_4(\text{s})$	$-438 \pm 8$	773
	"	$\text{Ag}_2\text{SO}_4(\ell)$	$-316 \pm 3$	953
	"	$\text{Ag}_2\text{SO}_4(5.0 \text{ mol } \%) + \text{Li}_2\text{SO}_4$	$-652 \pm 1$	590
Detig and Archer (1963)	$\text{Cl}_2$	$\text{NaCl}(\ell)$	-500	1203
Richter (1977)	Ag	$\text{AgNO}_3(0.1 \text{ mol } \%) + \text{LiNO}_3$	-492	533
	"	$\text{AgNO}_3(0.5 \text{ mol } \%) + \text{NaNO}_3$	-320	563
	"	$\text{AgNO}_3(0.1 \text{ mol } \%) + \text{KNO}_3$	-303	633
	"	$\text{AgNO}_3(0.1 \text{ mol } \%) + \text{RbNO}_3$	-311	633
	"	$\text{AgNO}_3(0.1 \text{ mol } \%) + \text{CsNO}_3$	-308	633
Jacobsen and Broers (1977)	Pt   $\text{O}_2 + \text{CO}_2$	Ekvimolar $(\text{Li}, \text{Na})_2\text{CO}_3$	$-1180 \pm 20$	1248
Ito et al. (1985)	$\text{Cl}_2$	$\text{NaCl}(39 \text{ mol } \%) + \text{ZnCl}_2$	$-960 \pm 150$	643
	Na $\beta$ -alumina	$\text{NaCl}(39 \text{ mol } \%) + \text{ZnCl}_2$	$-42 \pm 1$	643
Ratkje and Sharivker (1995)	Na $\beta$ -alumina	$\text{NaF} + \text{Na}_3\text{AlF}_6$	310	773

Table 2.5 Seebeck coefficients in metal - molten salt system

	Electrodes	Electrolytes	$\varepsilon_0 / \mu\text{V K}^{-1}$	Temp / K
Ichikawa and Shimoji (1967)	W/Graphite	Bi(30 mol %)+BiBr <sub>3</sub> ( $\ell$ )	-132	573
Kuzminskii et al. (1994)	Mo	La(0-9 mol %)+LaCl <sub>3</sub> ( $\ell$ )	- 280	1173
	"	Cd(0-5 mol%)+CdI <sub>2</sub> ( $\ell$ )	1650	650

Table 2.3 shows that even in simple water solutions high Seebeck coefficients can be obtained. It seems as if systems that form complexes or have a complex nature give the highest Seebeck coefficients. In non-aqueous organometallic solutions, as in the thermocell:



extreme high Seebeck coefficients,  $-4170 \mu\text{V K}^{-1}$ , have been reported by Kuzminskii et al. (1994).

Since the transported entropies contributing to the Seebeck coefficient are unknown it is no possible to calculate or predict the magnitude of the Seebeck coefficient. Measurements have to be done in each case.

---

**REFERENCES, CHAPTER 2**

J. N. Agar, *Thermogalvanic Cells*, in *Advances in Electrochemistry and Electrochemical Engineering*, vol. 3, Ed. by P. Delahay, ( Interscience Publ., New York, 1963 )

G. M. Barrow, *Physical Chemistry*, (McGraw-Hill Book Co-Singapore, 5th Ed. 1988)

Yu. V. Borisoglebskii, M. M. Vetyukov and Saber Abu-Zeid, *Tsvetn.Met.*, **51**, p. 43, 1978

G. Borelius and F. Gunneson, *Ann.Physik*, **65**, p. 520, 1921

M. Bouty, *J. Physique*, **8**, p. 341, 1879

M. Bouty, *J. Physique*, **9**, p. 306, 1880

M. Bouty, *J. Physique*, **10**, p. 241, 1881

W. G. Breck, G. Cadenhead and M. Hammerli, *Trans. Faraday Soc.*, **61**, p. 37, 1965

W. G. Breck and J. N. Agar, *Trans. Faraday Soc.*, **53**, p. 179, 1957

R. H. Detig and D. H. Archer, *J. Chem. Phys.*, **38**, p. 661, 1963

E. D. Eastman, *J. Am. Chem. Soc.*, **48**, p. 1482, 1926

E. D. Eastman, *J. Am. Chem. Soc.*, **50**, p. 283, p. 293, 1928

K. S. Førland, T. Førland and S. K. Ratkje, *Irreversible Thermodynamics - Theory and Applications*, (John Wiley & Sons, 1988)

- T. Førland and S. K. Ratkje, *Acta Chem. Scand.*, **27**, p. 1883, 1973
- B. Gilbert, E. Robert, E. Tixhon, J. E. Olsen and T. Østvold, *Light Metals*, p. 181, 1995
- A. Grimstvedt, *Thermocell Studies of Sulphate Mixtures and Melts Relevant for Aluminium Electrolysis*, Dr.Ing. Thesis, The Norwegian Institute of Technology, University of Trondheim, (1992)
- A. Grimstvedt, S. K. Ratkje and T. Førland, *J. Electrochem. Soc.*, **141**, p. 1236, 1994
- K. Grjotheim, C. Krohn, M. Malinovský, K. Matiašovský and J. Thonstad, *Aluminium Electrolysis, Fundamentals of the Hall-Héroult Process*, (Aluminium-Verlag, Düsseldorf, 2nd ed., 1982)
- K. Grjotheim and B. J. Welch, *Aluminium Smelter Technology*, (Aluminium-Verlag, Düsseldorf, 2nd ed., 1988)
- S. R. de Groot, *Thermodynamics of Irreversible Processes*, (North-Holland Publishing Company, Amsterdam, 1966)
- R. Haase, *Thermodynamics of Irreversible Processes*, (Addison Wesley, Dover edition, 1990)
- R. Haase und K. Hoch, *Z. Physik. Chem. Neue Folge*, **46** p. 63, 1965
- G. M. Haarberg, Technical report, Project E3.7 and private communication, Department of Applied Electrochemistry, The Norwegian Institute of Technology, University of Norway, 1994
- G. M. Haarberg, K. S. Osen, J. Thonstad, R. J. Heus and J. J. Egan, *Light Metals*, p. 283, 1990

- K. Ichikawa and M. Shimoji, *Ber. Bun. Ges.*, **71**, p. 1149, 1967
- Y. Ito, R. Takeda, S. Yoshizawa and Y. Ogata, *J. Appl. Electrochem.*, **15**, p. 209, 1985
- Y. Ito, H. Kaiya, S. Yoshizawa, S. K. Ratkje and T. Førland, *J. Electrochem. Soc.*, **131**, p. 2504, 1984
- T. Jacobsen and G. H. J. Broers, *J. Electrochem. Soc.*, **124**, p. 207, 1977
- JANAF Thermochemical Tables, (Clearinghouse, Virginia, 1971, and later supplements)
- M. Kamata, Y. Ito and J. Oishi, *Electrochim. Acta*, **31**, p. 521, 1986
- Y.V. Kuzminskii, V. A. Zasukha and G. Y. Kuzminskaya, *J. Power Sources*, **52**, p. 231, 1994
- H. Levin and C. F. Bonilla, *J. Electrochem. Soc.*, **98**, p. 388, 1951
- J. P. Moore and R. S. Graves, *J. Appl. Phys.*, **44**, p. 1174, 1972
- V. M. Mozhaev and P. V. Polyakov, *Izv. Vyssk. Uchebn. Zav. Tsvet. Met.*, **23** (5), p. 37, 1980
- L. Onsager, *Phys.Rev.*, **37**, p. 405, 1931
- L. Onsager, *Phys.Rev.*, **38**, p. 2265, 1931
- Perry's Chemical Engineer's Handbook*, (McGraw Hill, sixth ed., 1984)
- T. L. Quickenden and C. F. Veron, *Solar Energy*, **36**, p. 63, 1986

H. Rajabu, S. K. Ratkje and T. Førland, Proceedings of the Eighth International Symposium on Molten Salts, St.Louis, 1992

S. K. Ratkje and V. Sharivker, The International Harald A. Øye Symposium, Trondheim, Norway, February 2-3, 1995

S. K. Ratkje, H. Rajabu and T. Førland, *Electrochim. Acta*, **38**, p. 415, 1993

S. K. Ratkje, T. Ikeshoji and K. Syverud, *J. Electrochem. Soc.*, **137**, p. 2088, 1990

S. K. Ratkje, *Complex Formations in Alkali-Aluminium Fluoride Melts*, Dissertation, University of Trondheim, Norway, (1974)

Th. W. Richards, *Z. Physik. Chemi.*, **24**, p. 39, 1897

J. Richter, *Electrochim. Acta*, **22**, p. 1035, 1977

R. Schneebaum and B. R. Sundheim, *Discussions Faraday Soc.*, **32**, p. 197, 1962

C. Wagner, *Ann. Physik*, (5), **3**, p. 629, 1929

C. Wagner, *Ann. Physik*, (5), **6**, p. 370, 1930

R. Ødegård, Å. Sterten and J. Thonstad, *Metall. Trans. B.*, **19B**, p. 449, 1988

### 3. EXPERIMENTAL

The methodology of the thermocell potential measurements of fluoride melts is complicated and needs attention to several details. A full account of material choices, experimental design and procedures is therefore reported. The outer equipment and inner arrangements are given in Section 3.1. Details on the thermocells with aluminium electrodes and oxygen electrodes are discussed in Section 3.2. Criteria that have been considered when designing electrodes for measurements of thermoelectric powers in cryolite melts are pointed out and discussed in Section 3.3. The design of the experimental cell for measurement of the thermoelectric power at stationary state conditions is given in Section 3.4. Section 3.5 gives the qualities of the materials and chemicals. The experimental procedure is outlined in Section 3.6.

#### 3.1 EXPERIMENTAL EQUIPMENT

All thermopotential experiments were performed in a vertical tube furnace with Kanthal heating elements. The construction of the furnace has been described elsewhere, Motzfeldt (1959). All experiments were performed under a controlled atmosphere of argon ( $\geq 99.999\%$ , Hydro Gas). The exiting gas was bubbled through a saturated mixture of  $\text{CaCl}_2$ ,  $\text{CaCO}_3$  and  $\text{Na}_2\text{CO}_3$  to absorb fluoride gases. The amount of gas passing the furnace during the experiments was controlled by a Flow Meter, model 1355, Brookes Instrument. The temperature of the furnace was controlled by an automatic power control unit, Eurotherm model 94. The temperature gradient of the empty furnace is given in Appendix C. Type S thermocouples, platinum-10% rhodium versus platinum, was used to measure the temperature at the electrodes. The thermocouples were made according to the direction given by the National Bureau of Standards (1981, 1991). Ice and distilled water in a dewar flask was used as cold junction. Thermocouple reference tables based on the IPTS-68 given by R.L. Powell et al. (1974) were used. The thermal voltage of the thermocouple was measured by

a multimeter, Hewlett Packard HP 3457A.

The electrode contact, molybdenum -  $\text{TiB}_2/\text{BN}$  (BN Products LTD, England) or platinum, was connected to the same multimeter as the two thermocouples. The multimeter was connected to a GPIB-card that was controlled by a program written in Turbo Pascal 6.0 on a PC, Olivetti M24, Dr.ing Rune Dahl (1992). This gave the possibility to monitor the changes in temperature at the two electrodes and the potential between them with time. The outer experimental arrangement is pictured in Figure 3.1 and a flow diagram for the apparatus is given in Appendix D.

The bottom of the experimental cell, Fig.3.2, was placed about 150 mm above the bottom of the furnace. This gave the possibility to have both positive and negative temperature gradients, Appendix C. A local heating element made from Kanthal wires embedded in high alumina cement, J.H.Bjørklund, Norway, was used to produce different temperature gradients over the electrolyte. The resistance of the heating element was approximately 40 ohms. The thermocouples, for temperature regulation of the furnace and the local heating element, were placed as close as possible to the Kanthal windings to reduce large temperature variations. Radiation shields, made of high alumina cement, were placed above and below the graphite crucible for support and reduction of noise caused by heat radiation.

The local heating element may generate electromagnetic radiation noise that will interfere the measurement of the cell potential. To avoid this a Faraday shield, made of nickel, was surrounding the local heating element and connected to earth ground. Electromagnetic radiation is then absorbed by the shield. A plate of sintered alumina (Alsint), Haldenwanger, Technische Keramik, Germany, was placed on top of the Faraday shield to avoid the graphite crucible to be grounded.

The experimental arrangement inside the furnace, with the experimental cell for measuring thermoelectric powers with aluminium electrodes, is shown in Figure 3.2. A more detailed description of the experimental cells is given in Section 3.2.

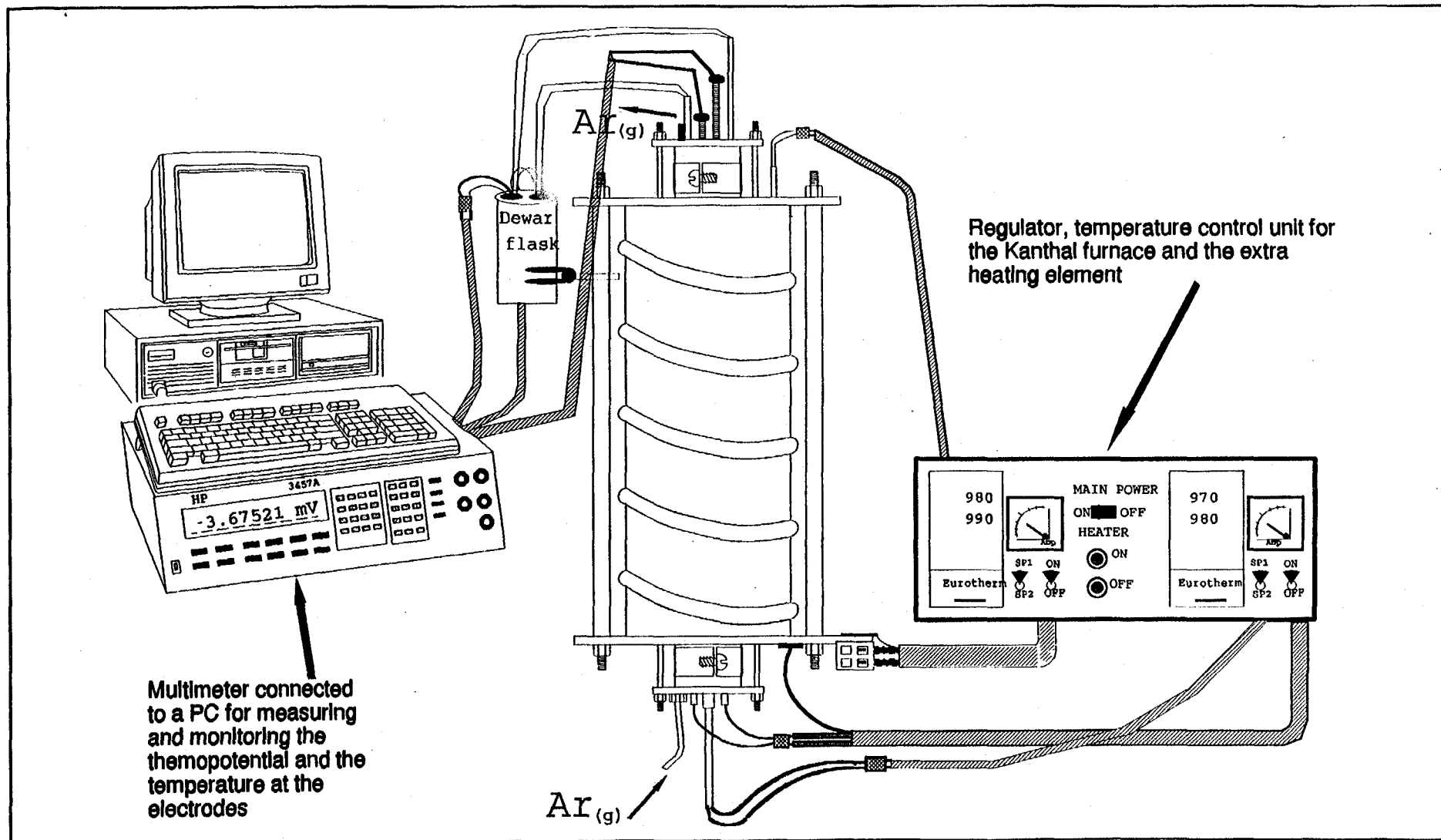
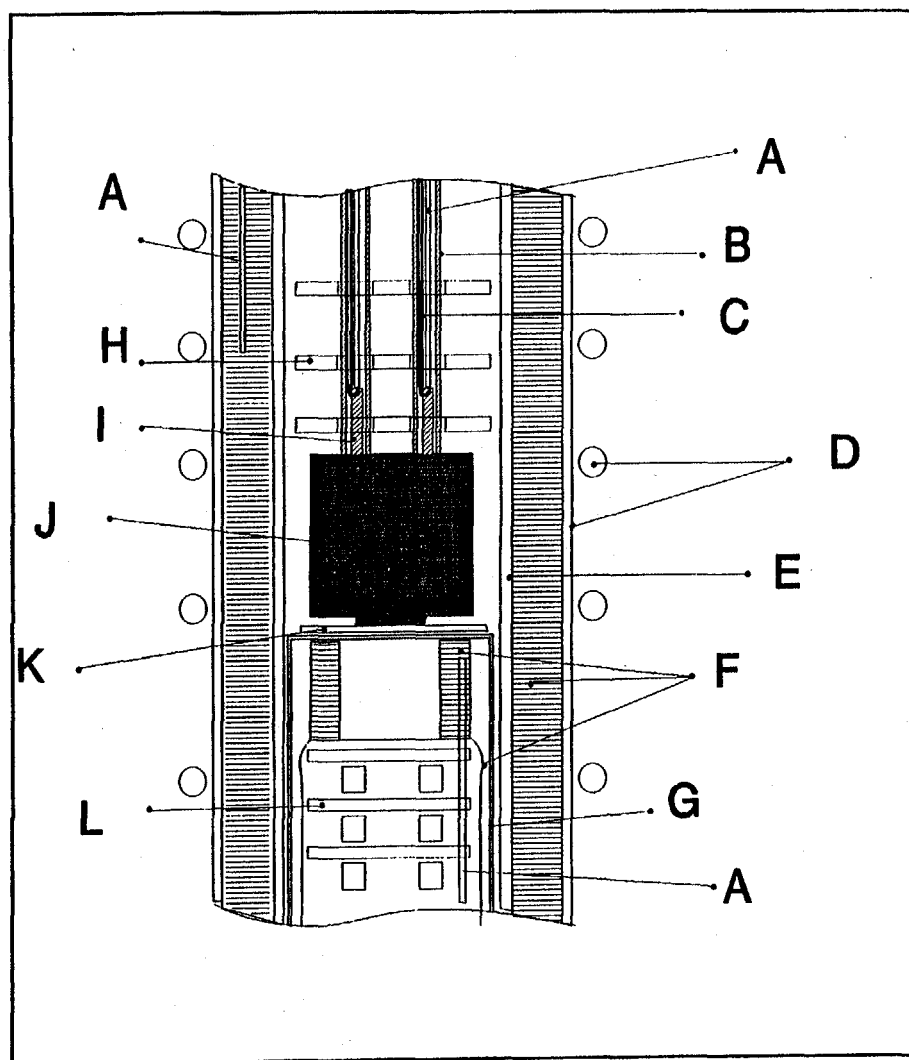


Figure 3.1 Outer experimental arrangement, see text for details.



- A: Type-S thermocouple, Platinum-10% rhodium versus platinum
- B: Alumina ceramic protection tube
- C: Molybdenum wire  $\varnothing 0.5$ , protected by an alumina ceramic tube and connected to the  $\text{TiB}_2/\text{BN}$ -rod
- D: Steel mantle with water cooling tubes
- E: Oxide ceramic tube (Pythagoras-76 wt%  $\text{Al}_2\text{O}_3$ )
- F: Kanthal wires, heating elements
- G: Faraday shield in nickel connected to earth ground
- H: Upper radiation shields
- I:  $\text{TiB}_2/\text{BN}$ -rod, electric connection to the aluminium electrode
- J: Graphite crucible
- K: Insulation between the graphite crucible and grounding
- L: Lower radiation shields and support

Figure 3.2 Sketch of the cross section of the tube furnace with inner arrangement

## **3.2 ALUMINIUM AND OXYGEN ELECTRODES IN CRYOLITE MELTS**

General criteria to be considered when designing the electrodes for measurements of thermoelectric powers in cryolite melts are given in Section 3.2.1. Different electrical contact materials to the liquid aluminium electrode are reviewed in Section 3.2.2. In Section 3.2.3 the possibility of limitation in extension of the aluminium electrode is outlined. The oxygen electrode is discussed in Section 3.2.4.

### **3.2.1 General Criteria**

There are three general criteria that have to be fulfilled for reliable measurements of thermoelectric powers.

1. The electrodes used must give reproducible potentials.
2. There must not be any time dependency on the electric potential.
3. The temperature at the electrodes must be measured as close as possible to the electrode surface. This implies that the extension of the electrode must be known.

### 3.2.2 Stability of Aluminium Electrodes

Burgman et al. (1986) have given a short review of the development of the aluminium reference electrode. They give two designs of the reference electrode, one with the aluminium at the bottom of the crucible (WMH-ref. electrode) and one with the aluminium at the top of the electrolyte (DBI-ref. electrode). The advantage of suspending the aluminium above the electrolyte is that it creates a static, horizontal interface. The disadvantage is that the density of the electrolyte must be increased by the addition of some heavy salts. Molybdenum was used as electric contact material in both designs. Burgman et al. (1986) claim that molybdenum wires are slightly more stable than tungsten and considerably more stable than tantalum. The WMH-ref. electrode reported, showed a stability within a 5 mV window of the theoretical 0 for over 8 hours. The reproducibility of the DBI reference electrode was better than 10 mV for the eight hour period of testing.

The results of Burgman et al. (1986) do not agree with those obtained by Sterten et al. (1976). They report a potential difference of  $0 \pm 2$  mV, which lasted for several hours at constant temperature, between two identical Al-electrodes, with Ta wire as electrical contact. Which is better than Burgman et al. (1986) obtained using molybdenum wires.

It is well known that molybdenum, tungsten and tantalum form alloys in contact with liquid aluminium, Hansen and Anderko (1958), ASM-international (1990). Duruz et al. (1981) state that the limited solubility of tungsten in liquid aluminium, 10 wt% at 1000 °C, makes the tungsten electrode well suited for studying electrodeposition and redissolution of aluminium in cryolite melts.

Rajabu (1993) performed experiments with tungsten as electric contact to the liquid aluminium electrode, to verify if the electrodes were stable and to find the time of stability. In cryolite melts without alumina, she obtained a potential difference of 5-8 mV for 40 minutes, when a tungsten wire with 1mm diameter was used. Several cm of the tungsten wire

were then corroded. A potential difference of  $9 \pm 3$  mV was obtained for four hours when tungsten rods with diameter of 2mm were used. If the liquid aluminium was presaturated with tungsten, before the tungsten rod was in contact with the aluminium, a potential difference of  $-1 \pm 1$  mV was obtained for four hours. Large corrosion of the rod was then avoided. The result of Rajabu (1993) for tungsten as electric contact to the aluminium, is comparable with the result reported by Sterten et al. (1976) for tantalum. From this it can be concluded that tungsten and tantalum are about equal choices.

Due to the solubility of tungsten in contact with liquid aluminium, a titanium diboride rod sintered to inconel was used as electrode contact by Saget (1973) and Saget et al. (1975). He protected the inconel with a boron nitride tube to prevent the inconel from reacting with liquid aluminium and molten cryolite. According to Dewing (1989), the Ti and B contents of aluminium in equilibrium with  $TiB_2$  at  $1000^\circ C$  are less than 1 and 0.1 wt% respectively. Titanium diboride will be susceptible to attack by aluminium and cryolite at the grain boundaries where any impurities are concentrated, Woodfield (1993). To avoid contamination of the aluminium electrode, Woodfield recommended an intermetallic composite material consisting of approximately equal proportions by weight of  $TiB_2$  and BN. The composite is produced from high purity powders which are hot pressed at a temperature above  $1800^\circ C$ .

Experiments run in the experimental cell sketched in Figure 3.3 typically produced a potential of 2.5 mV with standard deviation of 0.3 mV. This potential was stable for at least 13 hours. The experiments were done under the most extreme conditions, a basic melt with molar ratio,  $n_{NaF}/n_{AlF_3}$ , equal to 4 with no alumina present. When using these aluminium electrodes in acidic melts saturated with alumina, one would expect them to be even more stable. The use of this material, for this purpose, has not been reported in the literature.

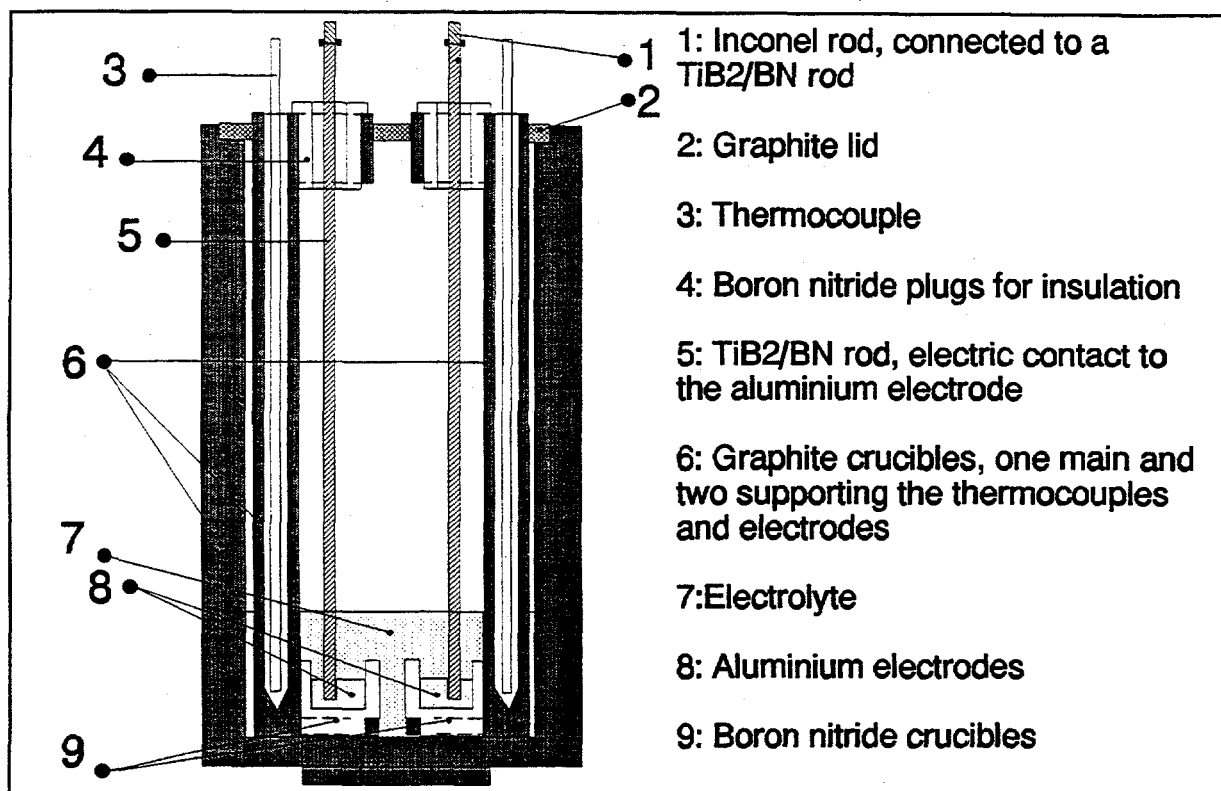


Figure 3.3 Sketch of the experimental cell for testing the stability of the aluminium electrodes

The photograph, in Figure 3.4, shows a cross section of a used boron nitride crucible with a titanium diboride-boron nitride rod in contact with aluminium. Scanning electron microscopy (SEM) was used to analyse the TiB<sub>2</sub>/BN interface that had been in contact with molten aluminium during the experiment. No trace of aluminium nitride at the interface, was detected, but clusters of pure aluminium were observed in the outer parts of the TiB<sub>2</sub>/BN rod. The photograph, in Fig.3.5, of the TiB<sub>2</sub>/BN - aluminium interface is taken with 30 times enlargement. From this picture it is not possible to see any corrosion of the TiB<sub>2</sub>/BN rod.

From the literature study and my laboratory investigations, I draw the conclusion that the intermetallic composite material,  $TiB_2/BN$ , is the best choice with respect to stability. With this choice, the uncontrolled reactions between the electrode contact material and liquid aluminium will also be avoided. Such reactions could cause potential differences between the two electrodes in a temperature gradient.

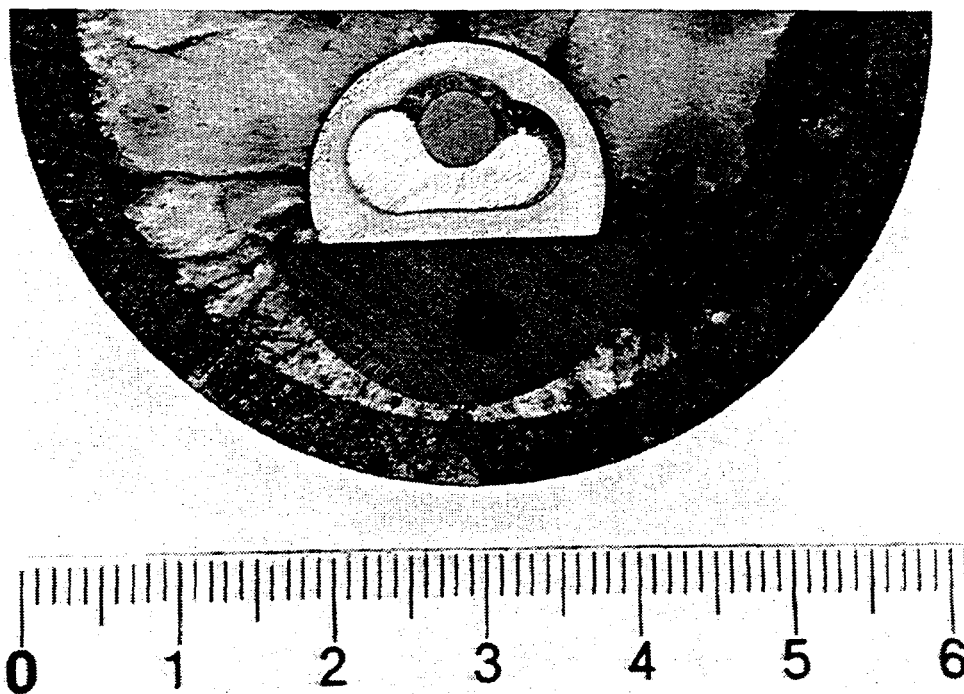


Figure 3.4 Photograph of a cross section of a used boron nitride crucible containing frozen cryolite melt, aluminium metal and a piece of the  $TiB_2/BN$ -rod

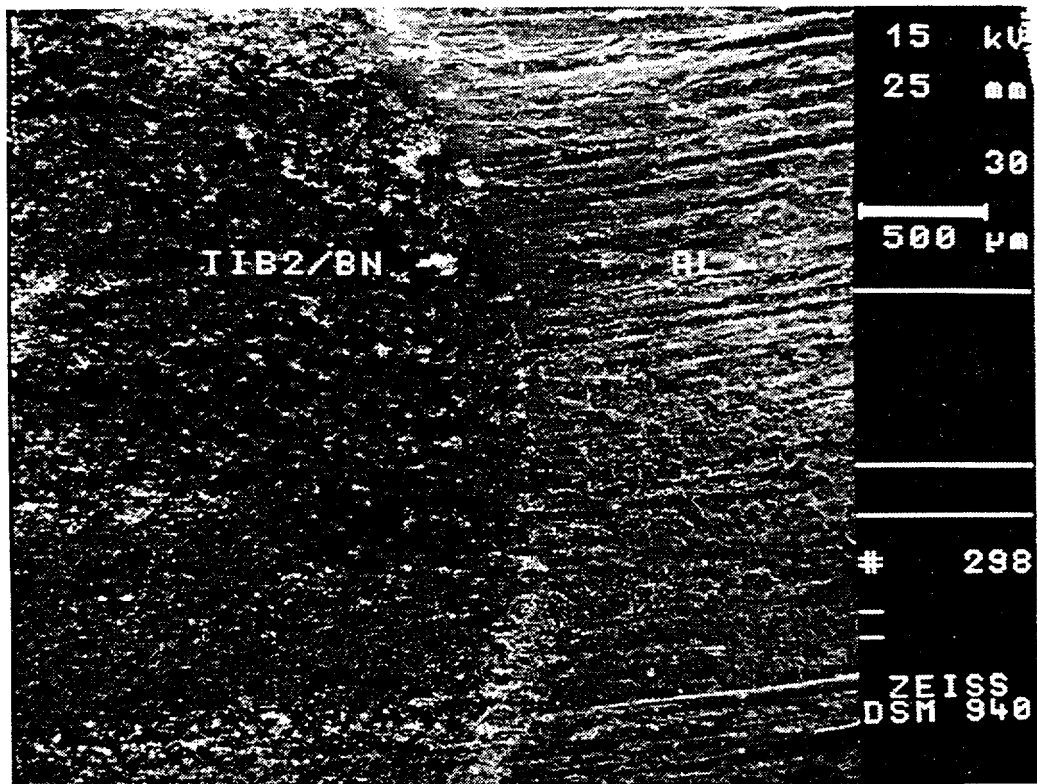


Figure 3.5 Scanning electron microscopy (SEM) -picture of the  $\text{TiB}_2/\text{BN}$ -aluminium interface. The enlargement is 30 times.

### 3.2.3 Limited Extension of the Aluminium Electrode

Molten aluminium wets tungsten, molybdenum and tantalum strongly, aluminium migrates along the lead wire and forms a vertical aluminium cryolite interface. In the present investigation this cannot be allowed. If not, it will be difficult to know where to measure the temperature.

One way of avoiding this is to trap the aluminium in porous aluminium nitride. In order to keep the aluminium in the pores it is important that the aluminium wets the aluminium nitride well. Tungsten, insulated from the cryolite melt by alumina tubes, was used as electric contact to the AlN/Al material. With this construction it was not observed that aluminium migrated along the tungsten wire. With two equal electrodes, at equal temperature, an electrical potential of  $-1.29 \pm 0.02$  mV was obtained for more than 10 hours. The AlN/Al composite material was obtained from SINTEF, Norway.

This electrode could probably also be used in the aluminium industry as a reference electrode. It is easy to handle and it does not need a container as the liquid aluminium electrode does. Further development of an aluminium reference electrode based on this material is continued in our group.

It is well established that  $TiB_2$  is readily wetted by molten aluminium metal, Raj and Skyllas-Kazacos (1992), Billehaug and Øye (1980). Watson and Toguri (1991) claim that hot-pressed  $TiB_2$  is completely wetted by aluminium and cryolite melt. In my experience, aluminium also wets the  $TiB_2$ /BN composite material well, but the aluminium does not creep over it like with tantalum, tungsten and molybdenum. It is also possible to drill a channel through the  $TiB_2$ /BN composite rod, down to the aluminium surface, for a thermocouple. This will make the measurement of the electrode temperature more accurate. This construction will also make it possible to measure thermoelectric powers in cryolite melts that are not saturated with alumina.

I conclude that the  $\text{TiB}_2/\text{BN}$  composite material was the best choice in this context, since it fulfills the three demands stated in Section 3.2.1. Stable cell potential for several hours and the extension of the electrode is limited so it is possible to measure the temperature close to the electrode surface. The composite material aluminium nitride/aluminium may also be a good choice, but the material is not commercially available.

### 3.2.4 The Oxygen Electrode

An electrode that is reversible for oxygen gas and oxygen ions is useful both for thermodynamic measurements involving oxide formation and for determining the oxide ion activity in reactions of metallurgical interest. Flood et al. (1952) showed that a platinum wire surrounded by oxygen and immersed in a fused salt gave reproducible potentials. Hill et al. (1958) experienced that the platinum electrode could be poisoned by foreign cations, such as dissolved iron, present in the melt. This could be avoided by removing the foreign ions from the electrolyte before the electrodes were inserted.

The construction of the oxygen electrode is very simple. The platinum wire on the negative pole of the thermocouple can be used as an electrode. Often it can be an advantage to have a larger electrode areal, than the platinum wire of the thermocouple can give. Figure 3.7 shows the oxygen electrode used in the present work. The thermocouple is placed at the platinum plate that works as an electrode. This makes it possible to measure the temperature very close to the electrode surface.

The solubility of oxygen gas is low in cryolite melts, about a thousandth of that of  $\text{CO}_2$ , Numata and Bockris (1984). It is therefore only necessary to pass a very small amount of oxygen gas through the electrolyte. The oxygen gas is passed through the four-bore alumina tube that supports the thermocouple and the electrode. Sterten et al. (1976) have

examined the stability of the oxygen electrode in  $\text{Na}_3\text{AlF}_6\text{-Al}_2\text{O}_3$  melts. They found the cell potential remained constant within  $\pm 0.5$  mV for several hours at a given temperature and pressure. The cell potential was independent of the depth of immersion of the electrodes.

With this construction, all three criteria stated in Section 3.2.1 are fulfilled for the oxygen electrode.

### 3.3 EXPERIMENTAL CELLS, INITIAL STATE

The initial state is defined at time equal to zero. This means that there can be a temperature gradient, but no concentration gradients between the two electrodes. In these experiments it is therefore important to have a cell with good convection. In Section 3.2.1, the design of the experimental cell with aluminium electrodes is given. The experimental thermocell with oxygen electrodes is described in Section 3.2.2.

#### 3.3.1 The thermocell $(T)Al(\ell) | NaF, AlF_3, Al_2O_3 | Al(\ell)(T+\Delta T)$

The experimental cell, for measurements of cell potentials of thermocell [B], consists of one large graphite crucible, Svensk Spezialgrafitt AB, grade 780GL. The crucible served as a container for the melt and the two liquid aluminium electrodes. A graphite holder worked as support for the upper aluminium electrode, see Fig.3.6. The identical electrodes were placed 7 cm apart in a vertical direction, in order to establish a temperature difference, which could be regulated. Contact between graphite and aluminium, was avoided by placing the aluminium in alumina crucibles, Haldenwanger Technische Keramik, Germany. Rods of  $TiB_2/BN$  - composite material, were used as electrical contact to the liquid aluminium electrodes. Alumina tubes were used to insulate the electrode contact from the graphite lid and the electrolyte. The  $TiB_2/BN$ -rods were obtained from BN Products LTD, England. Maximum length of the rods was 160mm for an outer diameter of 6mm and an inner diameter of 4mm. A molybdenum wire,  $\varnothing 5mm$ , was therefore used to make contact between the  $TiB_2/BN$ -rod and the multimeter. Measurements of thermoelectric powers require that the temperature is measured at the electrode surface. In practice the thermocouples were therefore placed inside the electrode contact material, the  $TiB_2/BN$ -rods. A sketch of the experimental cell is shown in Figure 3.6.

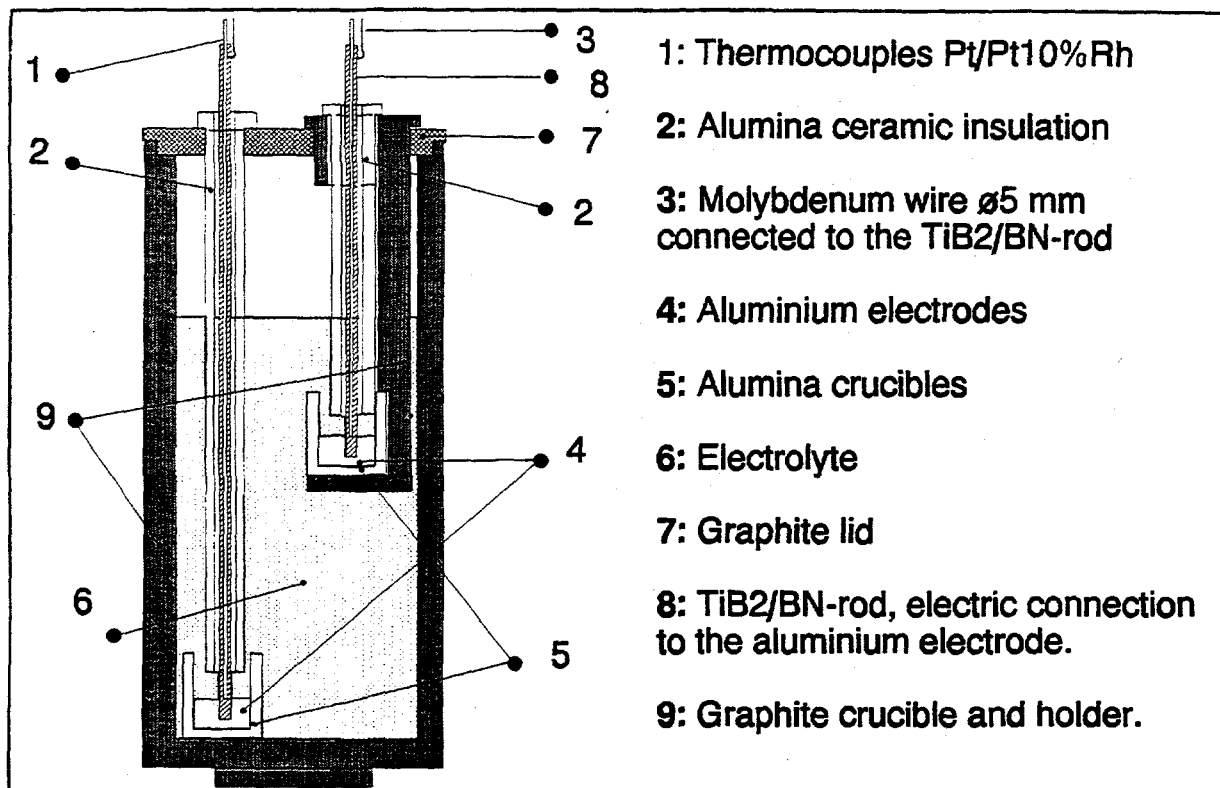


Figure 3.6 Sketch of the experimental cell, used in the experiments at initial state condition, with a pair of aluminium electrodes.

### 3.3.2 The thermocell $(T)\text{Pt}-\text{O}_2(\text{g}) \mid \text{NaF}, \text{AlF}_3, \text{Al}_2\text{O}_3 \mid \text{O}_2-\text{Pt}(T+\Delta T)$

The measurements, of the thermoelectric power in thermocell [C], were performed in an alumina ceramic crucible. The height of the crucible was 200 mm and the inner diameter was 38 mm. Two 4-bore alumina rods worked as support and insulation for the thermocouples and the platinum electrodes. In order to increase the surface of the electrode a platinum plate was placed at the end of the platinum wire, which was connected to the multimeter, Fig.3.1. The thermocouple was placed at the platinum electrode. Oxygen gas was supported through

the 4-bore alumina tube. The gas supply was controlled by two Flow Meters, model 1355, Brookes Instrument. In these experiments the inner arrangement above K in Figure 3.2 is replaced by the experimental cell sketched in Figure 3.7. Details concerning similar oxygen electrodes have been reported by Sterten et al. (1976).

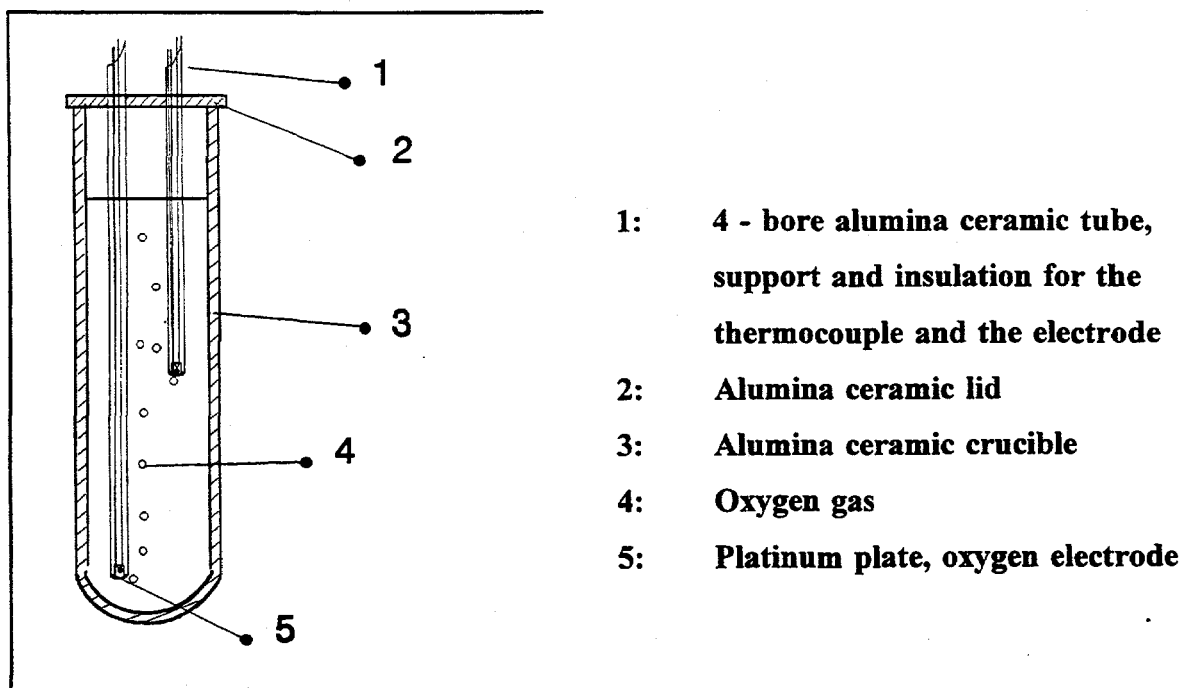


Figure 3.7 Sketch of the experimental cell, used in the experiments at initial state condition, with a pair of oxygen electrodes.

### 3.4 EXPERIMENTAL CELL, STATIONARY STATE

It is not possible to measure the thermoelectric power at stationary state conditions with oxygen electrodes. Mixing of the electrolyte, due to the gas supply, will destroy any concentration gradients. With a pair of aluminium electrodes, it should be possible to measure the thermoelectric power at stationary state conditions, if the time necessary to obtain the stationary state is not longer than 2-3 hours. Then it will be possible to manage five measurements within the limit of the stability time of the electrodes.

The stationary state is defined at time equal to infinity. This means that the system does not change with time. At stationary state there can be both a temperature gradient and a concentration gradient between the two electrodes. In the experiments at stationary state it is therefore important to avoid convection in the melt. To obtain this a plug of boron nitride, BN Products LTD, was placed above the aluminium electrode. The plug had four holes each with 3mm diameter, to obtain contact with the molten aluminium. To avoid contact between graphite and aluminium, the aluminium was placed in boron nitride crucibles.

The boron nitride was cleaned by ultrasonic vibration in acetone for 20 minutes, before removing the water and binder  $B_2O_3$  by evaporation in vacuum at 900 °C, Xue et al. (1992), Hubáček et al. (1991). Tungsten rods with diameter 2 mm and length 50 mm ( 99.95+%, Heraeus) were used as electrode contact, and these were insulated from the graphite lid with boron nitride plugs.

The design of the cell is shown in Figure 3.8.

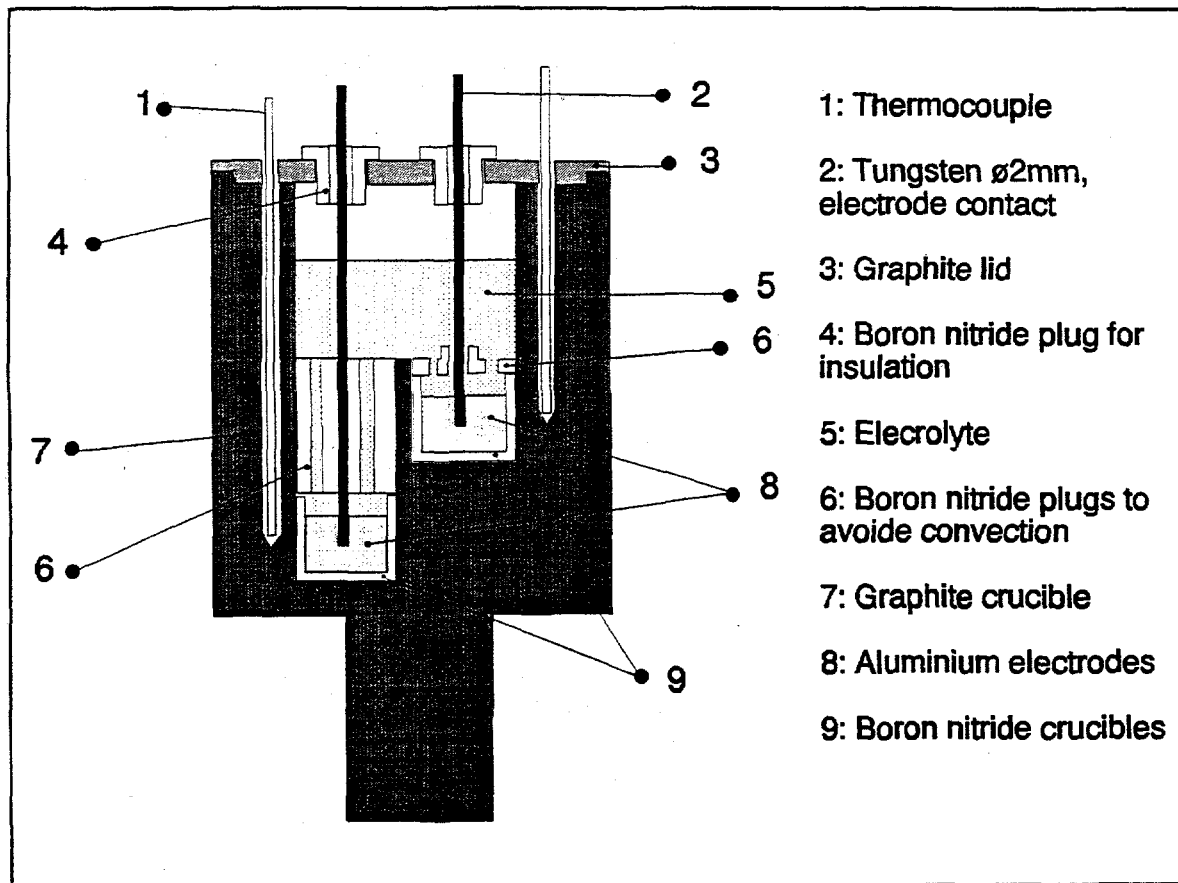


Figure 3.8 Sketch of the experimental cell used to measure the thermoelectric power : stationary state conditions.

### 3.5 MATERIALS AND CHEMICALS USED

The graphite crucible and holder were made from fine grain, extruded, high purity graphite grade 780 GL (The Carbon Graphite Group Inc. USA) by Svensk Spesial Grafit AS. The rods of titanium diboride-boron nitride composite material were made by BN Products LTD. England. High purity aluminium, > 99.99 %, was used for the aluminium electrodes. Both the aluminium and the TiB<sub>2</sub>/BN rods were cleaned by ultrasonic vibration, in acetone for 30 minutes, before each experiment. The graphite crucible and holder were cleaned by ultrasonic vibration in ethanol. After cleaning, all parts were dried at 70°C for 24 hours. All alumina ceramic tubes and crucibles (Alsint) were ordered from Haldenwanger, Germany. Both the oxygen gas, ≥99.99%, and the argon, ≥99.998%, were ordered from Hydro Gas, Rjukan-Norway. Platinum and platinum-10% rhodium were ordered from K.A. Rassmusen, Norway.

Melts with different molar ratio of NaF/AlF<sub>3</sub> were prepared by adding aluminium fluoride, AlF<sub>3</sub>, purified by sublimation, to grounded handpicked natural Greenland cryolite (Kryolitselskabet Øresund A/S). The natural Greenland cryolite is very pure, according to Duruz and Landolt (1985). The cryolite was treated according to the ISO standard 1619 (1976). Alumina, Al<sub>2</sub>O<sub>3</sub>, was used after being fired at 1600°C for four hours. The alumina solubility in the ternary system Na<sub>3</sub>AlF<sub>6</sub>-AlF<sub>3</sub>-Al<sub>2</sub>O<sub>3</sub> was taken from Skybakmoen et al. (1990) and Solheim et al. (1995). The phase diagram was also given by Sterten et al. (1982). A more detailed overview, of quality and producers of the different materials and chemicals used in the experiments, is given in Appendix E.

### 3.6 EXPERIMENTAL PROCEDURE

Measurements of the thermoelectric power at initial state conditions, with two aluminium electrodes, were performed in the experimental cell described in Section 3.3.1. Aluminium cylinders of 4-5 g were placed in the alumina crucibles. The  $\text{TiB}_2/\text{BN}$ -rods were connected to molybdenum wires and the alumina insulation was then put in place. Then the premixed  $\text{Na}_3\text{AlF}_6\text{-AlF}_3\text{-Al}_2\text{O}_3$  powder was filled into the crucible through two holes in the lid. The two holes were closed by graphite plugs. The experimental cell was then placed in the furnace. Upper radiation shields and protection tubes were placed on top of the cell. Then, the thermocouples were placed in the  $\text{TiB}_2/\text{BN}$ -rods. Finally the lid on top of the furnace was put in place and argon gas was connected. Humidity was removed by heating the furnace gradual from room temperature to  $400^\circ\text{C}$  over night. When the electrolyte was melted, the  $\text{TiB}_2/\text{BN}$ -rods were moved down 5mm to make sure that the rods were in contact with the aluminium. The local heating element was used to create different temperature gradients between the two electrodes.

The thermoelectric power measurements, with two oxygen electrodes, were performed in the experimental cell sketched in Figure 3.7, Section 3.3.2. The premixed powder was filled into the alumina ceramic crucible and the alumina lid was placed on top of the crucible. A graphite crucible was used as supporter for the experimental cell. After placing the cell in the furnace and the lid put on top of the furnace, the two 4-bore alumina rods which supported the thermocouples and electrodes, were put in place. In these experiments no upper radiation shields were used. Argon gas was then connected. Humidity was removed by heating the furnace gradual from room temperature to  $400^\circ\text{C}$  over night. When the electrolyte was melted, oxygen gas was supplied through the two 4-bore alumina tubes and the electrodes were moved down in to the electrolyte to the height preferred. The height between the electrodes was also changed during some experiments. The local heating element was used to create different temperature gradients between the two electrodes.

---

**REFERENCES, CHAPTER 3**

ASM-International, The National Standard Reference Data System, *Binary Alloy Phase Diagrams*, 2nd Ed. Vol. 1, (1990)

ASTM Special Technical Publication 470B, *Manual on the use of Thermocouples in Temperature measurement*, American Society of testing Materials, (Philadelphia, 1981)

Annual book of ASTM standards, *General methods and instrumentation*, (Philadelphia, vol. 14.03, 1991)

K. Billehaug and H. A. Øye, *Aluminium*, **56**, p. 642, 1980

J. W. Burgman, J. A. Leistra and P. J. Sides, *J. Electrochem. Soc.*, **133**, p. 496, 1986

R. Dahl, The Norwegian Institute of Technology, University of Trondheim, Norway, private communication, 1992

E. W. Dewing, *Metall. Trans. A*, **20A**, p. 2185, 1989

J. J. Duruz, G. Stehle and D. Landolt, *Electrochim. Acta*, **26**, p. 771, 1981

J. J. Duruz and D. Landolt, *J. Appl. Electrochem.*, **15**, p. 393, 1985

H. Flood, T. Førland and K. Motzfeldt, *Acta Chem. Scand.*, **6**, p. 257, 1952

M. Hansen and K. Anderko, *Constitution of Binary Alloys*, (McGraw-Hill Book Company, Inc. New York, 2nd ed., 1958)

D. G. Hill, B. Porter and A. S. Gillespie Jr., *J. Electrochem. Soc.*, **105**, p. 408, 1958

M. Hubáček, V. Brožek and B. Řehák, *J. Solid Stat Chem.*, **95**, p. 253, 1991

ISO 1619 - *Cryolite, natural and artificial-Preparation and storage of test samples*, 1st Ed. 1976-09-15

K. Motzfeldt, *Means of attending and controlling temperature in Physicochemical Measurements at high Temperature*, eds.: J. O'M. Bockris, J. L. White and J. D. (Mackenzie, London: Butterworths, 1959)

H. Numata and J. O'M. Bockris, *Met. Trans.B*, **15B**, p. 39, 1984

R. L. Powell, W. J. Hall, C. H. Hyink, Jr., L. L. Sparks, G. W. Burns, M. G. Scroger and H. H. Plumb, *Thermocouple reference tables based on the IPTS-69*, NBS monograph; 125, 1974

S. C. Raj and M. Skylas-Kazacos, *Electrochimica Acta*, **37**, p. 1395, 1992

H. M. Rajabu, Technical report no.153, Department of Physical Chemistry, The Norwegian Institute of Technology, The University of Trondheim, Norway, 1993

J. P. Saget, *Electrochimie dans la cryolithe fondue. Interaction de l'aluminium metallique avec les bains cryolithiques. Application au rendement Faraday*, Dr. Sci. Thesis, L'universite Paris VI, (1973)

J. P. Saget, P. Homsy, V. Plichon and J. Badoz - Lambling, *Electrochim. Acta*, **20**, p. 819, 1975

E. Skybakmoen, A. Solheim and Å. Sterten, *Light Metals*, p. 317, 1990

A. Solheim, S. Rolseth, E. Skybakmoen, L. Støen, Å. Sterten and T. Støre, *Light Metals*, p. 451, 1995

Å. Sterten, S. Haugen and K. Hamberg, *Electrochim. Acta*, **21**, p. 589, 1976

Å. Sterten, K. Hamberg and I. Mæland, *Acta Chem.Scand.*, **A36**, p. 329, 1982

K. D. Watson and J. M. Toguri, *Met. Trans. B*, **22B**, p. 617, 1991

M. Woodfield, Director, BN Products LTD, Blackwood Gwent, England, private correspondence, 1993

X. M. Xue, J. T. Wang and F. M. Zhao, *J. Materials Science Letters*, **11**, p. 199, 1992



## 4. RESULTS

In this chapter the experimental results, from measurements of thermoelectric powers at different molar ratios of NaF-AlF<sub>3</sub>, will be given. The measured thermoelectric power in cryolite melts with  $n_{\text{NaF}}/n_{\text{AlF}_3}$  equal to 1.8, 1.2 and 1.0 saturated with alumina are given in Sections 4.1, 4.2 and 4.3, respectively. The transported entropy of O<sup>2-</sup>, Al<sup>3+</sup> and Na<sup>+</sup> is calculated in Section 4.4. The relevance of the Seebeck coefficients to the Hall-Héroult cell is outlined in Section 4.5. The time necessary to obtain the stationary state is found in Section 4.6. Sources of experimental errors are discussed in Section 4.7.

The Seebeck coefficient is determined by plotting the cell potential,  $E$ , versus  $\Delta T$ . I have adopted the sign convention of Agar (1963). That is, the cell potential  $E$  of the non-isothermal cell is positive when the terminal connected to the hotter electrode is positive with respect to that connected to the colder electrode. This means that  $T$  is connected to minus and  $T+\Delta T$  is connected to plus.

### 4.1 THERMOELECTRIC POWER IN CRYOLITE MELT WITH $n_{\text{NaF}}/n_{\text{AlF}_3}=1.8$

Corresponding values of  $E$  and  $\Delta T$  for thermocell [B] are given in Figure 4.1, together with the calculated (principle of last squares) regression curve. Molar ratio  $n_{\text{NaF}}/n_{\text{AlF}_3}$  of the alumina saturated melt was 1.8. The slope of the curve gives the Seebeck coefficient, at temperature  $T$ , equal to  $969.5 \pm 0.5$  °C, Eq.[2.19]. The experiment of Figure 4.1 was reproduced once. The temperatures differed slightly in the two experiments. Table 4.1 gives the slopes of the curves, the Seebeck coefficients, and the Peltier effects. The errors given in the table are the 95 percent confidence intervals. Average temperature, Seebeck coefficient and Peltier effect, with 95 percent confidence interval, based on all the experimental data from

the two experiments, are given in the last line in Table 4.1, Appendix F.

A statistical test with indicator variables was used to find whether the level of the regression lines was equal. This test gives rise to a Fisher distributed test observer  $F_0$ . The problem was formulated as a test of  $H_0$ -hypothesis, where  $H_0$  means that the two regression lines are equal. The statistical test method is described in detail in Appendix F and by Montgomery and Peck (1982). It was found, that  $H_0$  should be accepted at a test level of 99.3% or higher ( $F_0=7.49=F_{0.0067, 1, 220}$ ).

Table 4.1 Experimental results from measurements of thermoelectric powers in thermocell [B]. The molar ratio NaF/AlF<sub>3</sub> of the alumina saturated melt was 1.8. The temperature,  $T$ , the Seebeck coefficient,  $\varepsilon_0$ , and the Peltier effect,  $\pi/T$ , are given with 95% confidence intervals.  $n$  is the number of observations in each experiment. In the bottom line the mean values are given with 95% confidence interval.

No.	$n$	$T / ^\circ\text{C}$	$\varepsilon_0 / \text{mV K}^{-1}$	$\pi/T / \text{J mol}^{-1} \text{K}^{-1}$
1	104	$969.5 \pm 0.5$	$-1.28 \pm 0.03$	$124 \pm 3$
2	120	$955.6 \pm 0.3$	$-1.18 \pm 0.06$	$114 \pm 6$
1, 2	224	$962 \pm 1$	$-1.23 \pm 0.04$	$119 \pm 4$

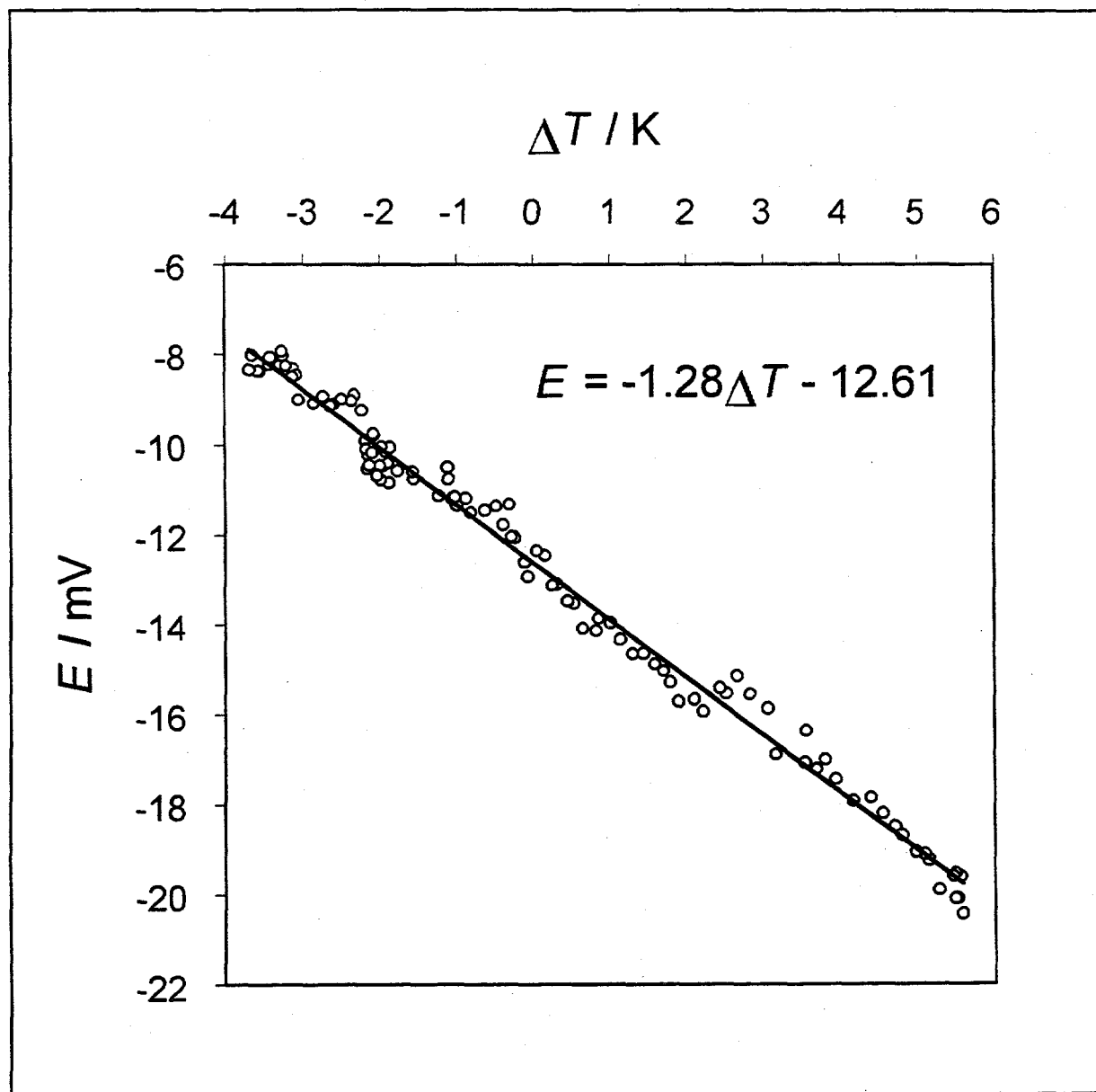


Figure 4.1 Plot of  $E$  versus  $\Delta T$  for thermocell [B].  $E$  is the cell potential. The temperature,  $T$ , on the left-hand side electrode was kept constant at  $969.5 \pm 0.5$  °C. The straight line is the calculated (principle of least squares) regression curve.

A plot of the cell potential,  $E$ , versus  $\Delta T$  for thermocell [C] is given in Figure 4.2, together with the calculated (principle of last squares) regression curve. Molar ratio,  $n_{\text{NaF}}/n_{\text{AlF}_3}$  of the melt was 1.8, and the melt was saturated with  $\alpha$ -alumina. The experiment was reproduced twice for slightly different temperatures. Average temperature, Seebeck coefficient and Peltier effect, with 95 percent confidence interval, based on all the experimental data from the three experiments, are given in the last line in Table 4.2.

The statistical test with indicator variables showed that the three experimental regression lines A, B and C were equal at a test level of 97.1% and higher. That is  $H_0$  should not be rejected,  $F_0 = 3.55 = F_{0.029, 2, 635}$ .

The experimental design of thermocell [C], Figure 3.7, made large temperature differences between the electrodes possible, 50-60°C. With large temperature differences, the possibility for second order heat effects increase, see Section 2.2. However, the test on individual regression coefficients with indicator variable showed that second order term should not be included in the regression model for fitting the experimental data, Appendix F, Section F.3. The problem was formulated as a test of  $H_0$ -hypothesis, where  $H_0$  means that second order heat effects are significant. The statistical test showed that  $H_0$  should be rejected at a test level of 22% and higher,  $F_0 = 0.077 = F_{0.78, 1, 636}$ .

Table 4.2 Experimental results from measurements of the thermoelectric power in thermocell [C]. The molar ratio NaF/AlF<sub>3</sub> of the alumina saturated melt was 1.8. The temperature,  $T$ , the Seebeck coefficient,  $\varepsilon_0$ , and the Peltier effect,  $\pi/T$ , are given with 95% confidence intervals.  $n$  is the number of observations in each experiment.

No.	$n$	$T / ^\circ\text{C}$	$\varepsilon_0 / \text{mV K}^{-1}$	$\pi/T / \text{J mol}^{-1} \text{K}^{-1}$
A	98	$948 \pm 2$	$-1.72 \pm 0.03$	$166 \pm 3$
B	188	$961 \pm 1$	$-1.78 \pm 0.04$	$172 \pm 4$
C	355	$984 \pm 1$	$-1.83 \pm 0.04$	$177 \pm 4$
A, B, C	641	$971 \pm 1$	$-1.80 \pm 0.03$	$174 \pm 3$

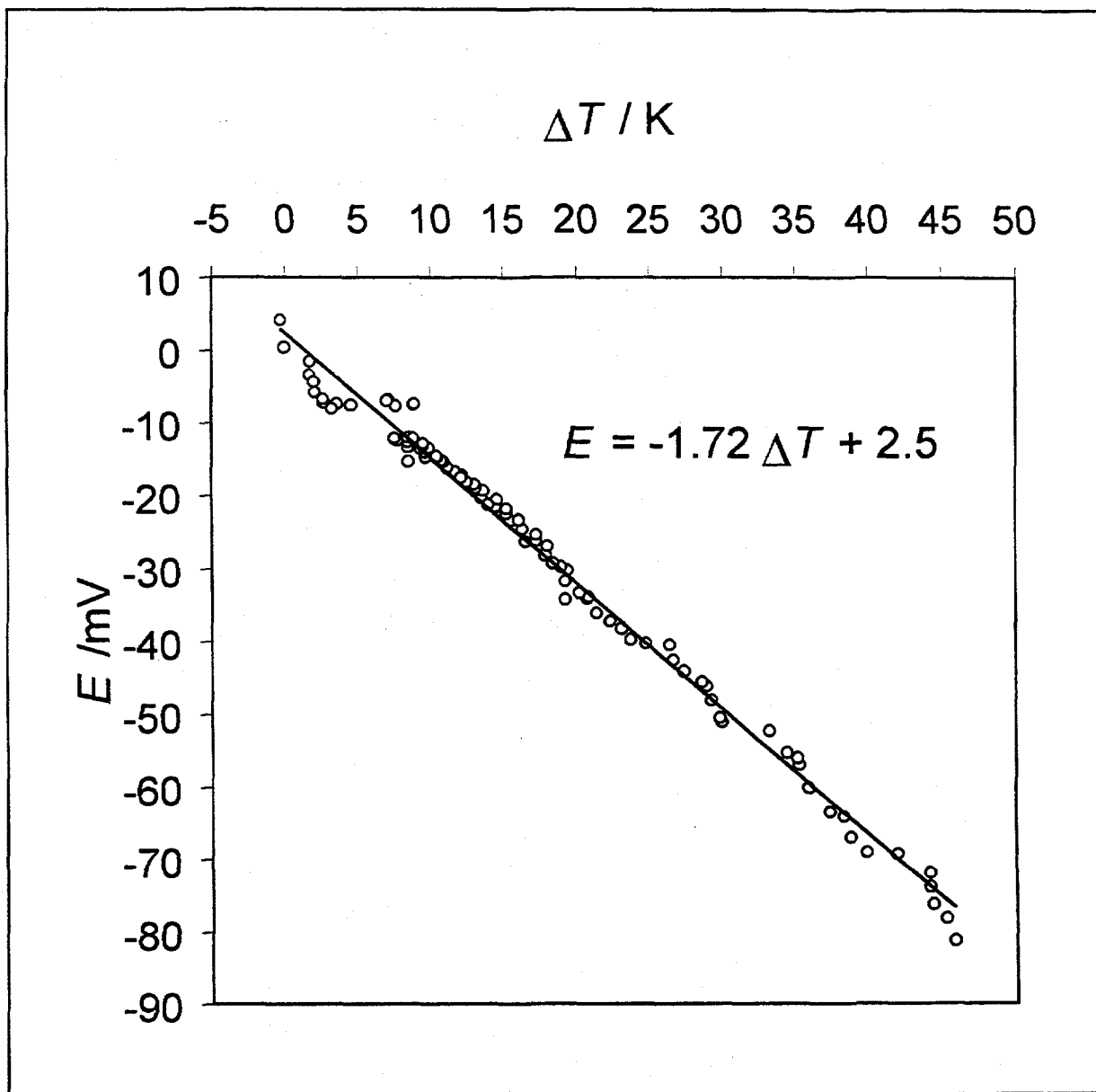


Figure 4.2 Plot of  $E$  versus  $\Delta T$  for thermocell [C] where  $E$  is the cell potential. The temperature,  $T$ , is kept constant at  $948 \pm 2^\circ\text{C}$ . The straight line is the calculated (principle of least squares) regression curve.

#### 4.1.1 Consistency Control, $n_{\text{NaF}}/n_{\text{AlF}_3} = 1.8$

In addition to reproduction of the Seebeck coefficients, the measurements can be controlled for consistency by the entropy change,  $\Delta S$ , of the isothermal cell [E], Section 2.4. The entropy change of Reaction [XI] is equal to  $54.97 \pm 0.02 \text{ J mol}^{-1} \text{ K}^{-1}$ , at 1235 K and  $54.95 \pm 0.02 \text{ J mol}^{-1} \text{ K}^{-1}$  at 1244 K, data from JANAF (1971). The Peltier effect in Tables 4.1 and 4.2 combined with Equation [2.52] gives:

$$\Delta S = 174 - 119 = 55 \pm 5 \text{ J mol}^{-1} \text{ K}^{-1} \quad [4.1]$$

The entropy change of Reaction [XI], calculated from data of JANAF (1971), and the value of  $\Delta S$ , calculated from the measurements of the thermoelectric power, is equal at a 95% confidence interval.

4.2 THERMOELECTRIC POWER IN CRYOLITE MELT WITH  $n_{\text{NaF}}/n_{\text{AlF}_3} = 1.2$ 

The results for corresponding values of the cell potential,  $E$ , and  $\Delta T$  for thermocell [C] are given in Figure 4.3. Molar ratio,  $n_{\text{NaF}}/n_{\text{AlF}_3}$ , of the alumina saturated melt was 1.2. The straight line, in Figure 4.3, is the calculated (principle of least squares) regression curve. One reproduction of the experiment shown in Figure 4.3 was done. The slope of the curves, the Seebeck coefficient and the Peltier effects, are given in Table 4.3. The errors given in the table are the 95 percent confidence intervals. Average temperature, Seebeck coefficient and Peltier effect based on all the experimental data from the two experiments, are given in the last line in Table 4.3.

The Peltier effect of the aluminium electrode in thermocell [B] was calculated to  $102 \pm 3 \text{ J mol}^{-1} \text{ K}^{-1}$ , using Equation [2.52] and the average Peltier effect of the oxygen electrode given in Table 4.3. The entropy of reaction for Equation [XI], at  $813.6 \text{ }^\circ\text{C}$ , is equal to  $55.19 \pm 0.02 \text{ J mol}^{-1} \text{ K}^{-1}$ , data of JANAF (1971). The Peltier effect divided by faradays constant,  $F$ , gives the Seebeck coefficient of the aluminium electrode equal to  $-1.06 \pm 0.03 \text{ mV K}^{-1}$ .

Table 4.3 Experimental results from measurements of thermoelectric powers in thermocell [C]. The molar ratio,  $n_{\text{NaF}}/n_{\text{AlF}_3}$ , is equal to 1.2 and the melts are saturated with alumina. The temperature,  $T$ , the Seebeck coefficient,  $\varepsilon_0$ , and the Peltier effect,  $\pi/T$ , are given with 95% confidence interval.  $n$  is the number of observations in each experiment.

No.	$n$	$T / ^\circ\text{C}$	$\varepsilon_0 / \text{mV K}^{-1}$	$\pi/T / \text{J mol}^{-1} \text{ K}^{-1}$
A	259	$813.5 \pm 0.2$	$-1.64 \pm 0.03$	$158 \pm 3$
B	80	$813.8 \pm 0.2$	$-1.61 \pm 0.07$	$155 \pm 7$
A, B	339	$813.6 \pm 0.2$	$-1.63 \pm 0.03$	$157 \pm 3$

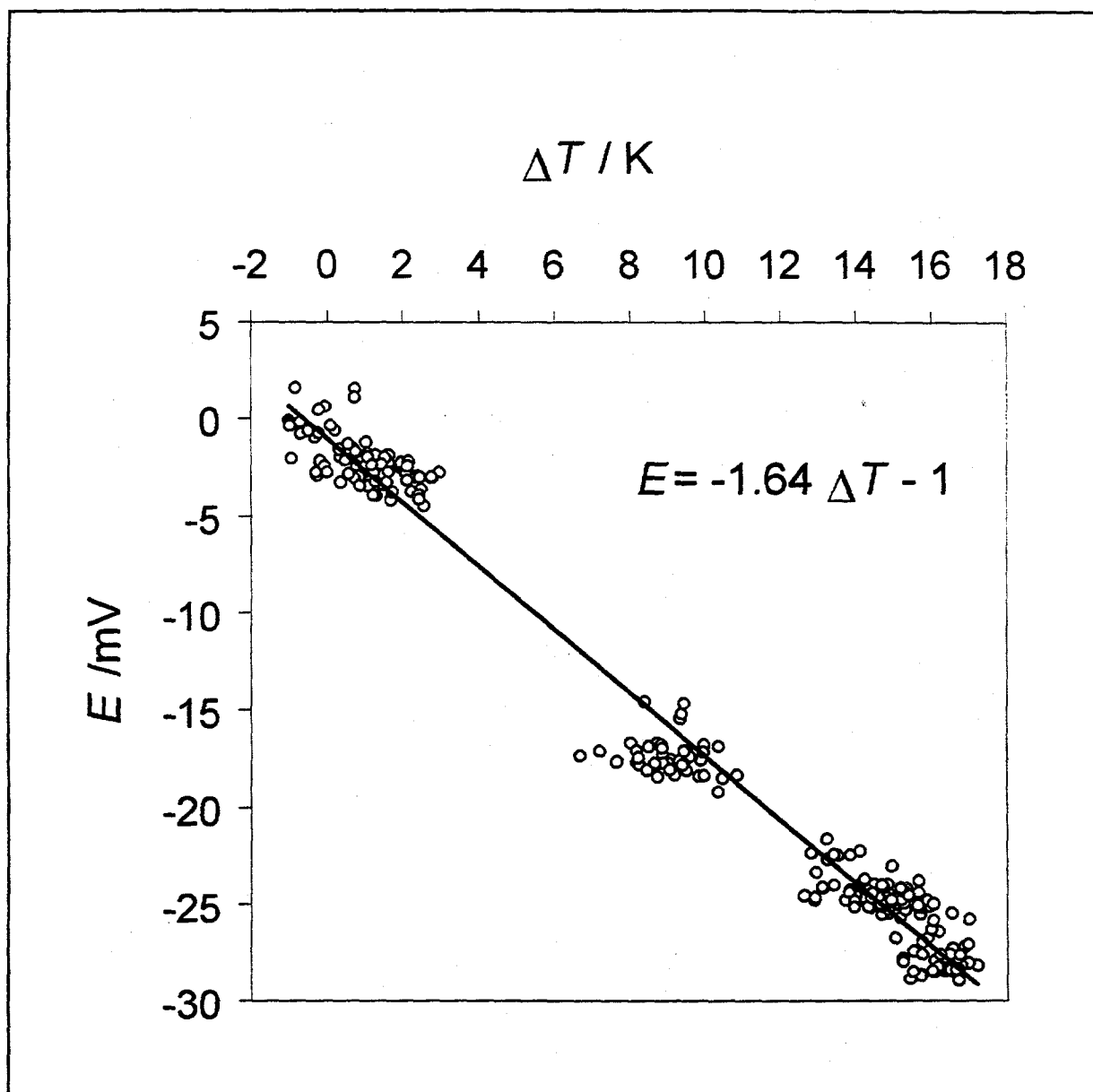


Figure 4.3 Plot of  $E$  versus  $\Delta T$  for thermocell [C].  $E$  is the cell potential. The temperature,  $T$ , was kept constant at  $813.6 \pm 0.2^\circ\text{C}$ . The straight line is the calculated (principle of least squares) regression curve.

### 4.3 THERMOELECTRIC POWER IN CRYOLITE MELT WITH $n_{\text{NaF}}/n_{\text{AlF}_3} = 1.0$

Corresponding values of  $E$  versus  $\Delta T$  for thermocell [C] are given in Figure 4.4. Molar ratio,  $n_{\text{NaF}}/n_{\text{AlF}_3}$ , of the alumina saturated melt was 1.0. The slope of the curve is the Seebeck coefficient at temperature  $T$  equal to  $754.8 \pm 0.9$  °C, Eq.[2.19]. The straight line, in Figure 4.4, is the calculated (principle of last squares) regression curve. The experiment was repeated three times, at slightly different temperatures. Table 4.4 presents the results from the four experiments given with 95% confidence intervals. Average temperature, Seebeck coefficient and Peltier effect based on all the experimental data from the four experiments, are given in the last line in the table.

The Seebeck coefficient and the Peltier effect of the aluminium electrode in thermocell [B] were calculated to  $-0.01 \pm 0.008$  mV K<sup>-1</sup> and  $1.0 \pm 0.8$  J mol<sup>-1</sup> K<sup>-1</sup>, respectively from Table 4.4 and Equation [2.52]. The temperature derivative,  $d\varphi/dT = \Delta S$ , for the isothermal cell [E] was found to be equal to  $55.28 \pm 0.02$  J mol<sup>-1</sup> K<sup>-1</sup> at 758 °C (1031 K), data from JANAF (1971).

Table 4.4 Experimental results from measurements of thermoelectric powers in thermocell [C]. The molar ratio was equal to 1.0 and the melts are saturated with alumina. The temperature,  $T$ , the Seebeck coefficient,  $\epsilon_0$ , and Peltier effect,  $\pi/T$ , are given with 95% confidence interval.  $n$  is the number of observations in each experiment.

No.	$n$	$T / ^\circ\text{C}$	$\epsilon_0 / \text{mV K}^{-1}$	$\pi / T / \text{J mol}^{-1} \text{K}^{-1}$
A	181	$754.8 \pm 0.9$	$-0.61 \pm 0.01$	$59 \pm 1$
B	195	$762 \pm 2$	$-0.55 \pm 0.01$	$53 \pm 1$
C	53	$735.2 \pm 0.4$	$-0.58 \pm 0.01$	$56 \pm 1$
D	112	$769 \pm 1$	$-0.62 \pm 0.01$	$60 \pm 1$
A, B, C, D	541	$758 \pm 1$	$-0.583 \pm 0.008$	$56.3 \pm 0.8$

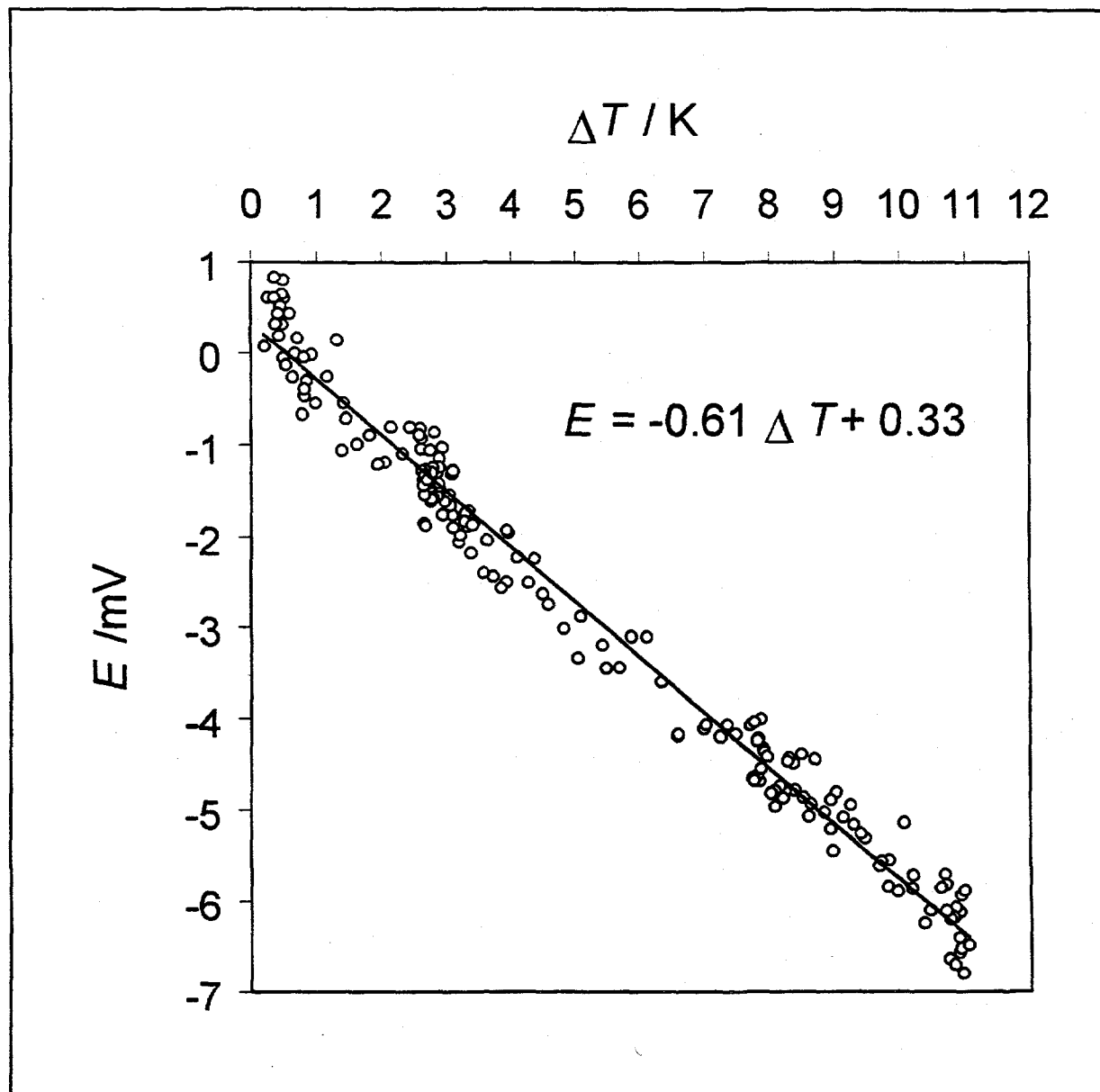


Figure 4.4 Plot of  $E$  versus  $\Delta T$  for thermocell [C] with molar ratio  $\text{NaF}/\text{AlF}_3$  equal to 1.0.  $E$  is the cell potential. The temperature,  $T$ , was kept constant at  $754.8 \pm 0.9$  °C. The straight line is the calculated (principle of least squares) regression curve.

#### 4.4 TRANSPORTED ENTROPIES IN CRYOLITE MELTS

In cryolite melt with molar ratio of NaF/AlF<sub>3</sub> lower than two, the transport number of Na<sup>+</sup>,  $t_{\text{Na}^+}$ , is approximately equal to one, Sterten et al. (1982), Ratkje et al. (1993). With this simplification, the transported entropy of sodium,  $S_{\text{Na}^+}^*$ , can be estimated from Equations [2.42] or [2.48]. Equation [2.48] gives the following relation between the transported entropy of sodium, the Peltier effect and the partial molar entropies:

$$S_{\text{Na}^+}^* = \frac{\pi}{T} + S_{\text{Pt}}^* - \frac{1}{4}S_{\text{O}_2} + S_{\text{NaF}} - \frac{1}{3}S_{\text{AlF}_3} + \frac{1}{6}S_{\text{Al}_2\text{O}_3} \quad [4.2]$$

The transported entropy through the electrode,  $S_{\text{Pt}}^*$ , is negligible, Borelius and Gunneson (1921), More and Graves (1972). Since the cryolite melt is saturated with alumina, the activity of Al<sub>2</sub>O<sub>3</sub> is equal to unity. By introducing the Peltier effect for the oxygen electrode in Tables 4.2 and 4.3 and the data given in Table 4.5 into Equation [4.2], the transported entropy of sodium can be estimated. For molar ratios of NaF/AlF<sub>3</sub> equal to 1.8 and 1.2,  $S_{\text{Na}^+}^*$  was found to be  $238 \pm 4 \text{ J mol}^{-1} \text{ K}^{-1}$  and  $244 \pm 4 \text{ J mol}^{-1} \text{ K}^{-1}$ , respectively.

Table 4.5 The molar entropy and the activity of  $\text{Al}_2\text{O}_3$ ,  $\text{NaF}$ ,  $\text{AlF}_3$  and  $\text{O}_2$  at molar ratio  $\text{NaF}/\text{AlF}_3$  equal to 1.8 and 1.2, data of JANAF (1971) and Sterten et al. (1982).

$n_{\text{NaF}}/n_{\text{AlF}_3}=1.8 \quad T = 971^\circ\text{C}$		$n_{\text{NaF}}/n_{\text{AlF}_3}=1.2 \quad T = 814^\circ\text{C}$	
Molar entropy /J mol <sup>-1</sup> K <sup>-1</sup>	activity	Molar entropy /J mol <sup>-1</sup> K <sup>-1</sup>	activity
$S_{\text{Al}_2\text{O}_3}=207.82$	$a_{\text{Al}_2\text{O}_3}=1$	$S_{\text{Al}_2\text{O}_3}=190.63$	$a_{\text{Al}_2\text{O}_3}=1$
$S_{\text{AlF}_3}=201.7$	$a_{\text{AlF}_3}=0.0063$	$S_{\text{AlF}_3}=187.9$	$a_{\text{AlF}_3}=0.23$
$S_{\text{NaF}}=154.26$	$a_{\text{NaF}}=0.094$	$S_{\text{NaF}}=144.61$	$a_{\text{NaF}}=0.0087$
$S_{\text{O}_2}=251.27$	$a_{\text{O}_2}=1$	$S_{\text{O}_2}=246.49$	$a_{\text{O}_2}=1$

When the cryolite melt is saturated with both alumina and aluminium fluoride, the gradients in chemical potential of  $\text{Al}_2\text{O}_3$ ,  $\text{AlF}_3$  and  $\text{NaF}$ ,  $\nabla\mu_{\text{Al}_2\text{O}_3, T}$ ,  $\nabla\mu_{\text{AlF}_3, T}$  and  $\nabla\mu_{\text{NaF}, T}$  are all equal to zero. Application of the phase rule to an equilibrium system with two solid phases and one liquid phase gives one degree of freedom, Eq.[2.45]. There are no composition degrees of freedom. Consequently, Equations [2.46] and [2.50] can be applied. At this concentration the electronic conduction of the melt will be approximately equal to zero, Haarberg et al. (1990), Haaberg (1994). The transported entropy of  $\text{Al}^{3+}$  and  $\text{O}^{2-}$  was calculated to  $77 \pm 2 \text{ J mol}^{-1} \text{ K}^{-1}$  and  $10 \pm 2 \text{ J mol}^{-1} \text{ K}^{-1}$  respectively from the experimental results at molar ratio  $\text{NaF}/\text{AlF}_3$  equal to 1.0 and  $758^\circ\text{C}$ , Table 4.4, and Equations [2.46] and [2.52]. The molar entropies used in the calculation of aluminium,  $S_{\text{Al}}$ , and oxygen,  $S_{\text{O}_2}$ , was  $74.338 \text{ J mol}^{-1} \text{ K}^{-1}$  and  $244.61 \text{ J mol}^{-1} \text{ K}^{-1}$  at  $758^\circ\text{C}$ , data from JANAF (1971).

In Section 2.5 it was shown that the Peltier heat at the carbon electrode is equal to the Peltier heat at the oxygen electrode in the limit of the experimental error. When the cryolite melt is saturated with both alumina and aluminium fluoride, the Peltier effect at the carbon electrode is:

$$\left(\frac{\pi}{T}\right)_{\text{carbon electrode}} = -S_{\text{C}}^* - \frac{1}{4}S_{\text{C}} - \frac{1}{2}S_{\text{O}^{2-}}^* + \frac{1}{4}S_{\text{CO}_2} \quad [4.3]$$

The average Peltier effect in Table 4.4 and data for the molar entropy of carbon and carbon dioxide from JANAF (1971), give the transported entropy of oxygen ions at the carbon electrode equal to  $10 \pm 2 \text{ J mol}^{-1} \text{ K}^{-1}$ . Which is the same as the transported entropy of oxygen ions at the oxygen electrode.

#### 4.5 RELEVANCE TO THE HALL-HÉROULT CELL

In the Hall - Héroult cell consumable carbon electrodes are used as anodes, instead of oxygen electrodes. In Section 2.5 it was shown that when the oxygen electrode in the isothermal cell [E] is exchanged with a carbon electrode, cell [A], the  $\Delta S$  for the cell will change with only  $0.23 \text{ J mol}^{-1} \text{ K}^{-1}$ . This implies that the Peltier heat or the heat consumption at the carbon anode is equal to the Peltier heat of the oxygen electrode (within limits of experimental errors).

The reversible heat production at the aluminium cathode and the carbon anode in the Hall - Héroult cell can be calculated from Equations [2.54] and [2.55], respectively. In Table 4.6, the reversible heat production at the cathode and the anode is given for a current density of  $0.7 \text{ A cm}^{-2}$ . The table shows that there will be a large heat production at the cathode and a large heat consumption at the anode, for the molar ratio  $\text{NaF}/\text{AlF}_3$  equal to 1.8 and 1.2.

Table 4.6 The reversible heat production at the cathode and the anode in the Hall-Héroult cell. The current density is chosen equal to  $0.7 \text{ A cm}^{-2}$  and Faraday's constant,  $F$ , is equal to  $96500 \text{ C mol}^{-1}$ .

Electrode	$n_{\text{NaF}}/n_{\text{AlF}_3}$	$T / \text{K}$	$\pi/T / \text{J mol}^{-1} \text{ K}^{-1}$	$dq/dt / \text{J s}^{-1} \text{ cm}^{-2}$
Al-cathode	1.8	$1235 \pm 1$	$119 \pm 4$	$1.07 \pm 0.04$
O <sub>2</sub> -anode		$1244 \pm 1$	$174 \pm 3$	$-1.57 \pm 0.03$
Al-cathode	1.2	$1086.6 \pm 0.2$	$102 \pm 3$	$0.80 \pm 0.03$
O <sub>2</sub> -anode			$157 \pm 3$	$-1.24 \pm 0.03$
Al-cathode	1.0	$1031 \pm 1$	$1.0 \pm 0.8$	$0.007 \pm 0.006$
O <sub>2</sub> -anode			$56.3 \pm 0.8$	$-0.421 \pm 0.006$

#### 4.6 THERMOELECTRIC POWER AT STATIONARY STATE CONDITIONS

The time dependency of the thermoelectric power for systems with one degree of freedom for diffusion can be found from Equation [4.4], Tyrrell (1961).

$$\frac{\varepsilon_t - \varepsilon_0}{\varepsilon_\infty - \varepsilon_0} = 1 - \frac{8}{\pi^2} \exp\left(-\frac{t}{\Theta}\right) \quad [4.4]$$

The quantity  $\Theta$  is the "characteristic time" and governs the rate at which the steady state equilibrium is established. The definition of  $\Theta$  is given by Equation [4.5], where  $h$  is the height between the electrodes,  $D_{12}$  the interdiffusion coefficient, Richter and Prüser (1977), and  $\pi$  is equal to 3.1416.

$$\Theta = \frac{h^2}{\pi^2 D_{12}} \quad [4.5]$$

If it is assumed that the diffusion coefficient in NaF-AlF<sub>3</sub> melts is  $1.64 \times 10^{-4} \text{ cm}^2 \text{ s}^{-1}$ , the time necessary to obtain the stationary state can be calculated from Equations [4.4] and [4.5]. Table 4.7 shows the time necessary to obtain 70.2 to 99.9% of the stationary state, for a cell with a height of 2 cm between the two electrodes.

Table 4.7 Percent of stationary state with time,  $\Theta = 41.19$  min,  $h = 2$  cm,  
 $D_{12} = 1.64 \times 10^{-4}$  cm<sup>2</sup> s<sup>-1</sup>

$t = x\Theta$ /min	$(\varepsilon_t - \varepsilon_0)/(\varepsilon_t - \varepsilon_0)$	% of stationary state
41.19 = $\Theta$	0.702	70.2
82.37 = $2\Theta$	0.890	89.0
123.56 = $3\Theta$	0.960	96.0
164.75 = $4\Theta$	0.985	98.5
205.94 = $5\Theta$	0.995	99.5
247.12 = $6\Theta$	0.998	99.8
288.31 = $7\Theta$	0.999	99.9

One experiment was run to find the time necessary to obtain the stationary state and verify the calculations above. The experiment was done in the experimental cell sketched in Figure 3.8 in Section 3.5. The thermocouples were placed in the graphite next to the electrodes. This will produce a systematic error in the temperature measurement, but in this experiment it is only necessary to know that the temperature is constant.

In Figure 4.5, the cell potential,  $E$ , and the temperature difference,  $\Delta T$ , between the electrodes are given as function of time. The cell potential starts to stabilize around 17 minutes. After, roughly, 30 minutes the graph shows that the stationary state is reached. The mean temperature difference between the electrodes between 17 and 45 minutes was measured to  $3.38 \pm 0.01^\circ\text{C}$ . In the same period the mean temperature at the electrode connected to minus was equal to  $991.24 \pm 0.03^\circ\text{C}$ . The result obtained from the experiment in Figure 4.5 is not consistent with the calculations in Table 4.7. The diffusion coefficient has to be higher than  $1.64 \times 10^{-4}$  cm<sup>2</sup> s<sup>-1</sup>.

If 99.9% of stationary state is reached after 30 minutes in Figure 4.5, then the interdiffusion coefficient can be estimated to  $1.5 \times 10^{-3} \text{ cm}^2 \text{ s}^{-1}$  from Equations [4.4] and [4.5]. If the stationary state is assumed to occur 10 minutes later, the estimated interdiffusion coefficient will be reduced to  $1.1 \times 10^{-3} \text{ cm}^2 \text{ s}^{-1}$ . This is in the same order of magnitude as found by Dewing (1984) in  $\text{LiF-AlF}_3$  melts.

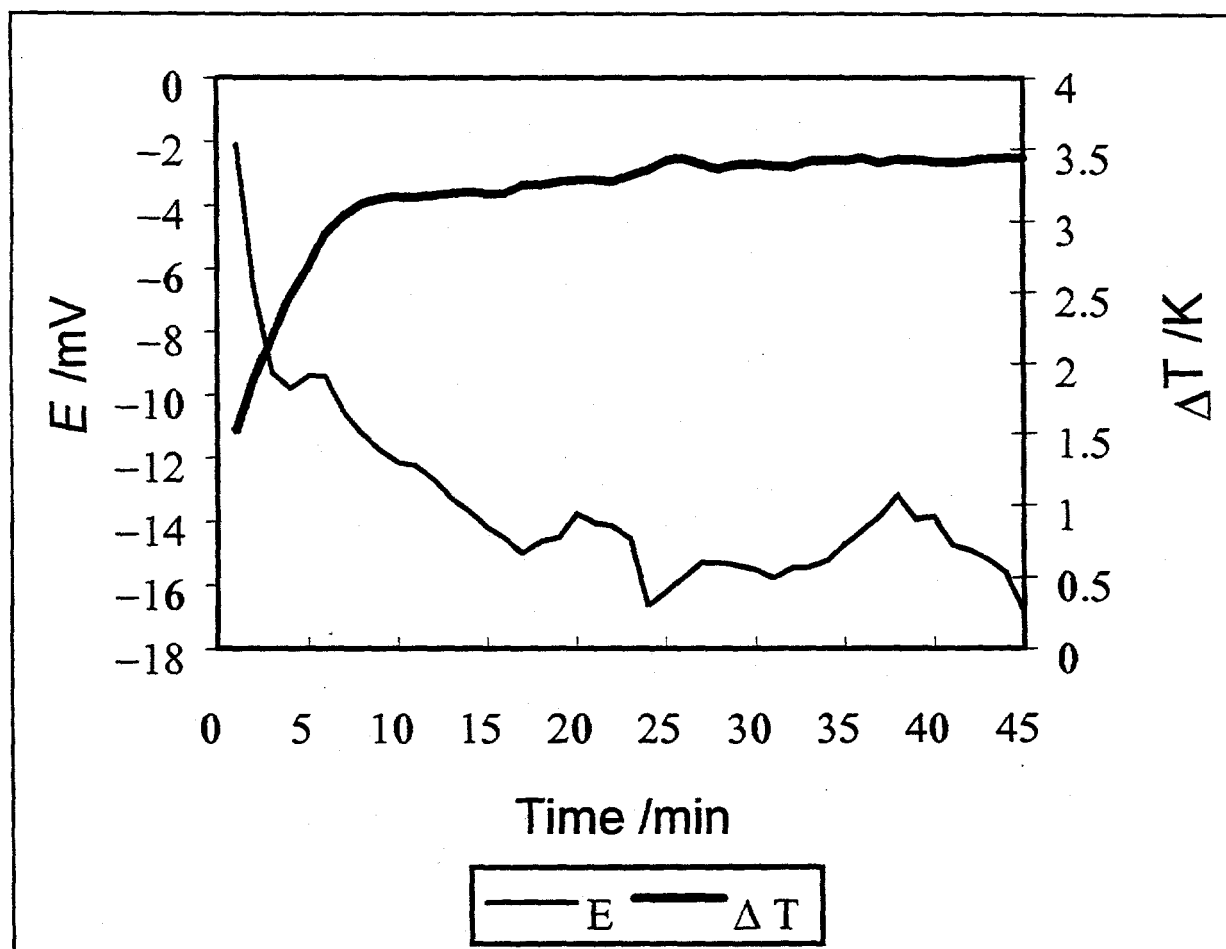


Figure 4.5 The molar ratio  $\text{NaF/AlF}_3$  of the electrolyte was equal to 4.0. The average temperature difference between the electrodes between  $t = 17$  and 45 minutes was  $3.38 \pm 0.01^\circ\text{C}$ . In the same period the mean temperature at the electrode connected to minus was equal to  $991.24 \pm 0.03^\circ\text{C}$ .

#### 4.7 SOURCES OF EXPERIMENTAL ERRORS

For all experiments the 95% confidence intervals are less than 5% of the Seebeck coefficient. This implies that there are no large sources of random errors in the experiments. The consistency check, in Section 4.1.1, implies that there cannot be any major sources of systematic errors in the experiments. Possible sources of error are discussed below.

New thermocouples had to be made for each experiment. For economical reasons, they were therefore not calibrated. Since a linear relation between measured potential and temperature difference was found, an error in the thermocouple would not matter. It will only cause the intercept to be different from zero when a zero temperature difference is present. The slope will not be influenced. Usually the error in a thermocouple, made after the instructions given by the ASTM standard (1981, 1991), is not larger than  $\pm 1$  °C.

There may be a conduction of heat up the thermocouple wires. The potential generated by a thermocouple is a function of the temperature difference between the connection between the platinum and platinum-10% rhodium wires and the zero point. Heat is transferred to the thermocouple through the melt by convection or through the molten aluminium and TiB<sub>2</sub>/BN rod. Heat is then lost through conduction along the length of the thermocouple. When the system is in thermal equilibrium, the rates of conduction of heat along the thermocouple length and into the thermocouple junction are equal. This may cause a difference between the temperature of the thermocouple junction and the surroundings, the electrode. The thermocouple does not give the absolute temperature, but as long as changes in temperature are reflected in the thermocouple readings it should not affect the slope of the curves.

Inequalities between the electrodes and between contact materials will contribute to the deviation of the potential from zero at zero temperature difference. Aluminium electrodes, typically give a potential difference between 0 and 10 mV, at zero temperature difference, Burgman et al. (1986), Yoshida and Dewing (1972), Duruz and Landolt (1985). In Section

4.1, Figure 4.1, a potential of 12.61 mV was obtained instead of the theoretical 0 mV. This deviation from the theoretical value is not unreasonable and can be explained by inequalities between electrodes, electrode contact materials and errors in temperature readings (due to uncalibrated thermocouples).

In the experiments with oxygen electrodes the deviation from the theoretical potential at zero temperature difference was  $\leq 2.5$  mV. The deviation from the theoretical potential at zero temperature difference is generally less with oxygen electrodes than with aluminium electrodes. This is due to the simpler construction of the oxygen electrode. It is not necessary to have an electrode contact material for the oxygen electrode that is different from the electrode material. Platinum dissolves easily in aluminium and must be insulated from the liquid aluminium electrode. When oxygen electrodes are used it is not necessary to insulate the thermocouple junction. The temperature can therefore be measured closer to the platinum electrode surface than to the surface of the liquid aluminium electrode.

The solubility of aluminium in alumina saturated cryolite with molar ratio of NaF/AlF<sub>3</sub> equal to 2.0 is 0.0630 w% at 1000 °C. Dissolution of aluminium metal into the electrolyte increases when the melt gets more basic, when the temperature increases and when the proportion of additives (Al<sub>2</sub>O<sub>3</sub>, CaF<sub>2</sub>, MgF<sub>2</sub>) decreases, Ødegård (1986). The diffusion coefficient of dissolved aluminium,  $D_{Al}$ , is high,  $2.3 \times 10^{-5}$  cm<sup>2</sup> s<sup>-1</sup> (Lantelme et al. 1980),  $1.5 \times 10^{-4}$  cm<sup>2</sup> s<sup>-1</sup> (Ødegård 1986),  $3.2 \times 10^{-4}$  cm<sup>2</sup> s<sup>-1</sup> (Tellenbach and Landolt 1988). Dissolved aluminium is predominantly present as the monovalent species AlF<sub>2</sub><sup>-</sup>, Ødegård et al. (1988). In the experimental cell with aluminium electrodes, Figure 3.6, the liquid aluminium was placed in alumina crucibles, to avoid contact between aluminium and carbon. Since aluminium is dissolving in the cryolite melt there may be some reaction between dissolved aluminium and carbon. This reaction will give formation of aluminium carbide (Al<sub>4</sub>C<sub>3</sub>), which is soluble in the electrolyte. If this reaction is significant, concentration gradients may occur in the melt. The consequence would be that the consistency control in Section 4.1.1 failed. Section 4.1.1 showed however that the measurements in Tables 4.1 and 4.2 was consistent. I therefore conclude that the solubility of aluminium metal into the electrolyte does not deflect the

measurements done in this work.

All 95% confidence limits in Chapter 4 given for the Seebeck coefficients, are random errors from the standard deviation of the regression analysis. The main contribution to the standard deviation is random noise from the potential and temperature measurements. In the confidence limit for the average value of the Seebeck coefficient in each series, the variation in concentration and temperature,  $T$ , will also be included. The precision of the average temperature is less than the confidence limits given for each experiment indicated. This is because a systematic error is introduced by the uncalibrated thermocouples. The magnitude of this systematic error is less than 1 °C.

---

**REFERENCES, CHAPTER 4**

ASTM Special Publication 470, American Society of testing Materials, (Philadelphia, 1981)

Annual book of ASTM standards, General methods and instrumentation, (Philadelphia, vol 14.03, 1991)

J. N. Agar, *Thermogalvanic Cells*, in *Advances in Electrochemistry and Electrochemical Engineering*, vol. 3, Ed. by P. Delahay, (Interscience Publ., New York, 1963 )

G. Borelius and F. Gunneson, *Ann. Physik*, **65**, p. 520, 1921

J. W. Burgman, J. A. Leistra and P. J. Sides, *J. Electrochem. Soc.*, **133**, p. 496, 1986

E. W. Dewing, *J. Electrochem. Soc.*, **131**, p. 1073, 1984

J. J. Duruz and D. Landolt, *J. Appl. Electrochem*, **15**, p. 393, 1985

G. M. Haarberg, K. S. Osen, J. Thonstad, R. J. Heus and J. J. Egan, *Light Metals*, p. 283, 1990

G. M. Haarberg, Technical report, Project E3.7, Department of Applied Electrochemistry, The Norwegian Institute of Technology, The University of Trondheim, Norway, 1994

JANAF Thermochemical Tables, (Clearinghouse, Virginia, 1971, and later supplements)

F. Lantelme, D. Damianacos and M. Chemla, *J. Electrochem. Soc.*, **127**, p. 498, 1980

D.C. Montgomery and E.A. Peck, *Introduction to Linear Regression Analysis*, (Wiley, New York, 1982)

J.P. Moore and R.S.Graves, *J.Appl.Phys.*, **44**, p. 1174, 1972

S.K. Ratkje, H.Rajabu and T.Førland, *Electrochim. Acta*, **38**, p. 415, 1993

J. Richter and U. Prüser, *Ber. Bunsenges. physik. Chem.*, **81**, p. 508, 1977

Å. Sterten, K. Hamberg and I. Mæland, *Acta Chem. Scand.*, **A36**, p. 329, 1982

J. M. Tellenbach and D. Landolt, *Electrochim. Acta*, **33**, p. 221, 1988

H.J.V. Tyrrel, *Diffusion and Heat Flow in Liquids*,

- Kap 8. *Experimental aspects of thermal diffusion*, (Butterworths, 1961)

K. Yoshida and E. W. Dewing, *Met. Trans.*, **3**, p. 683, 1972

R. Ødegård, *On the Solubility and Electrochemical Behavior of Aluminium and Aluminium Carbide in Cryolite Melts*, Dr. Techn. thesis, The Norwegian Institute of Technology, University of Trondheim, (1986)

R. Ødegård, Å. Sterten and J. Thonstad, *Metall. Trans. B.*, **19B**, p. 449, 1988



## 5. LOCAL HEAT EFFECTS IN HALL-HÉROULT CELLS

All contributions from heat sinks and sources are important for the total heat balance of the aluminium reduction cell. All heat sinks and sources are, in some way, linked to the electric current density. The main contributions like joule heat, overvoltages, bubble resistance and the reversible heat production at the electrodes will be examined in this chapter.

### 5.1 JOULE HEAT

The main voltage loss in the aluminium reduction cell is due to ohmic resistance in the electrolyte. In addition there are minor losses in the anode and the cathode, Grjotheim and Kvande (1986). These heat sources will be quantified in this section.

#### 5.1.1 Electrolyte

The temperature and concentration dependence of the conductivity of molten cryolite, of binary mixtures of cryolite with  $\text{Al}_2\text{O}_3$ ,  $\text{AlF}_3$ ,  $\text{CaF}_2$ ,  $\text{KF}$ ,  $\text{Li}_3\text{AlF}_6$  and  $\text{MgF}_2$ , and for ternary mixtures of  $\text{Na}_3\text{AlF}_6$ - $\text{Al}_2\text{O}_3$ - $\text{CaF}_2$  ( $\text{MgF}_2$ ) and  $\text{Na}_3\text{AlF}_6$ - $\text{AlF}_3$ - $\text{KF}$  ( $\text{Li}_3\text{AlF}_6$ ), were investigated by Hiveš et al. (1994). From experimental data and calculations they proposed a model of the conductivity of a multicomponent system, described by the equation:

$$\begin{aligned} \ln \kappa = & 1.977 - 0.0200[\text{Al}_2\text{O}_3] - 0.0131[\text{AlF}_3] - 0.0060[\text{CaF}_2] \\ & - 0.0106[\text{MgF}_2] - 0.0019[\text{KF}] + 0.0121[\text{LiF}] - \frac{1204.3}{T} \end{aligned} \quad [5.1]$$

where  $T$  represents the temperature in K, and the brackets denote the concentration of the additives in wt%. The maximum relative error of equation is reported to be less than 2.5%.

In a molten mixture of cryolite, with 2.5 wt%  $\text{Al}_2\text{O}_3$  and 20.5 wt%  $\text{AlF}_3$ , ( $n_{\text{NaF}}/n_{\text{AlF}_3} = 1.8$ ) the electrical conductivity will be equal to 1.988  $\text{S cm}^{-1}$  at 1240 K, according to Equation [5.1]. If the amount of alumina is increased to saturation, 9.6 wt%, Skybakmoen et al. (1990) and Solheim et al. (1995), then the electrical conductivity of the mixture is reduced to 1.725  $\text{S cm}^{-1}$ .

The heat production in the electrolyte is proportional to the square of the current density, and may be written as:

$$\left( \frac{dq}{dt} \right)_{\text{electrolyte}} = i^2 \frac{\ell}{\kappa} \quad [5.2]$$

where  $\kappa$  is the electric conductivity of the electrolyte and  $\ell$  is the distance between the electrodes. The inter polar distance is, usually, in Hall-Héroult cells with prebacked anodes between 4 - 5 cm. Table 5.1 gives the heat production in the electrolyte, due to passage of current for several current densities.

Table 5.1 Heat production due to ohmic resistance, in cryolite melts with molar ratio NaF/AlF<sub>3</sub> equal to 1.8, at different current densities. Column two gives the heat production in melt saturated with alumina. Column three is for melt with 2.5 wt% alumina. The inter polar distance,  $\ell$ , is chosen equal to 4.5 cm.

Current density / Acm <sup>-2</sup>	Heat production / Js <sup>-1</sup> cm <sup>-2</sup> ( $\kappa = 1.725 \text{ S cm}^{-1}$ )	Heat production / Js <sup>-1</sup> cm <sup>-2</sup> ( $\kappa = 1.988 \text{ S cm}^{-1}$ )
0.0	0.000	0.000
0.1	0.026	0.023
0.2	0.104	0.091
0.3	0.235	0.204
0.4	0.417	0.362
0.5	0.652	0.566
0.6	0.939	0.815
0.7	1.278	1.109
0.8	1.670	1.449
0.9	2.113	1.833
1.0	2.609	2.263

### 5.1.2 Anode

Prebaked anodes, which are made from coke and coal tar pitches, are heated to 1050-1250 °C to balance coke and binder properties. This controlled heating process of a composite carbon product, to coke the binder phase and substantiate structural changes, is called baking. The specific electrical resistance of the anode,  $R$ , depends on the electrical resistivity of the coke and the final baking temperature. Typical values for the specific electrical resistance are 66 and 74  $\mu\Omega\text{m}$ , Smith et al. (1991). The heat production in the anode due to passage of current may be expressed as:

$$\left(\frac{dq}{dt}\right)_{\text{anode}} = i^2 R h \quad [5.3]$$

where  $h$  is the height of the anode. Equation [5.3] shows that the heat production in the anode is proportional to the square of the current density. If the height of the anode is 0.55m, and the mean specific electrical resistance of the anode are equal to 70  $\mu\Omega\text{m}$ , then the heat production in the anode is equal to 0.39  $\text{J s}^{-1} \text{cm}^{-2}$  if the current density is equal to 1.0  $\text{A cm}^{-2}$ . Compared to the joule heat in the electrolyte, the heat production in the anode is a minor heat source in the aluminium reduction cell.

### 5.1.3 Cathode

The cathode in the Hall-Héroult cell typically consists of semi-graphitic blocks with a layer of liquid aluminium on top. The molten aluminium is the acting electrochemical cathode. In a semi-graphitic block the aggregate is graphitized, but the block (binder coke) has only been heated to normal baking temperatures, up to 1200 °C. Semi-graphitic blocks have low electrical resistance, 16 - 20  $\mu\Omega\text{m}$ , Sørli and Øye (1994). The specific electrical resistance of liquid aluminium, at 950 K, is equal to  $11.0 \times 10^{-8} \Omega\text{m}$ , Samsonov (1968). The heat production in the cathode is the sum of the heat production in the molten aluminium and in the carbon, due to resistance to current passage, and might be expressed as:

$$\left(\frac{dq}{dt}\right)_{\text{cathode}} = i^2 (R_C h_C + R_{Al} h_{Al}) \quad [5.4]$$

where  $h_C$  and  $h_{Al}$  are the height of the carbon and the molten aluminium, respectively. If the height of the aluminium is 0.20 m, and the cathode carbon is 0.45 m high and has a mean specific electrical resistance of 18  $\mu\Omega\text{ m}$ , then the heat production in the cathode is equal to 0.08  $\text{J s}^{-1} \text{ cm}^{-2}$ , at a current density of 1.0  $\text{A cm}^{-2}$ . Under the condition selected, the heat production in the cathode is even less than in the anode, and must be considered as a minor heat source in the aluminium reduction cell.

## 5.2 OVERVOLTAGE

If current passes through an electrolyte cell, then the potential of each electrode attains a value different from the equilibrium value that the electrode should have in the same system without current passage. This phenomenon is usually termed electrode polarization. When a single electrode reaction occurs at a given current density at the electrode, then the degree of polarization can be defined in terms of the overvoltage. The overvoltage,  $\eta$ , is equal to the electrode potential,  $E$ , under the given conditions, minus the value of the equilibrium electrode potential corresponding to the considered electrode reaction,  $E_e$ , Koryta and Dvořák (1987). In this section, the importance of heat evolution due to the anodic and the cathodic overvoltages will be considered

### 5.2.1 Anode

The anodic overvoltage is an activation overvoltage, due to a slow chemical reaction or a slow charge transfer, and to some extent, anodic concentration overvoltage, Solli (1994). The activation part of the anodic overvoltage is purely dissipative, and the heat evolution is equal to:

$$\left(\frac{dq}{dt}\right)_{\text{anode}} = i \eta \quad [5.5]$$

where  $\eta$  is the overvoltage of the anode. Equation [5.5] shows that the heat production due to the overvoltage increases with increasing current density. Table 5.2 gives the heat production due to anodic activation overvoltage for several current densities. The cell potential at zero current density is referred to the main cell reaction, Eq.[XI], and is calculated from

data of JANAF (1971). The newest data reported on anode potentials in the literature are the data reported by Solli (1994). Her anode potentials give however very high overvoltages compared with earlier reports. Thonstad (1970) determined the anodic overvoltage to be 0.5 V at a current density of  $1 \text{ A cm}^{-2}$ . The anodic overvoltage was determined to be 0.71 V at a current density of  $1 \text{ A cm}^{-2}$  by Dewing and van der Kouwe (1975) and Jarek and Thonstad (1987) found the anodic overvoltage to be 0.51 V at a current density of  $1 \text{ A cm}^{-2}$ . All results are obtained from laboratory experiments and are strongly dependent on the experimental conditions.

Table 5.2 Heat production due to anodic overvoltage, in  $\text{Na}_3\text{AlF}_6$  melt saturated with  $\text{Al}_2\text{O}_3$  and with 10 wt%  $\text{AlF}_3$  and 5 wt %  $\text{CaF}_2$ , at 1243 K. The anodic potential at different current densities is given in column two, Haarberg et al. (1994), Haaberg (1995). The overvoltage is equal to the anodic potential minus the reversible cell potential given at zero current density. The reversible potential of equation [XI] is calculated to 1.187 at 1243 K.

Current density / $\text{Acm}^{-2}$	Potential of anode / V	Heat production / $\text{Js}^{-1}\text{cm}^{-2}$
0.0	1.187	0.00
0.1	1.91	0.07
0.2	1.94	0.15
0.3	1.97	0.23
0.4	1.98	0.32
0.5	1.99	0.40
0.6	1.99	0.48
0.7	2.10	0.64
0.8	2.20	0.81
0.9	2.50	1.18
1.0	2.60	1.41

### 5.2.2 Cathode

The major part of the cathodic overvoltage is diffusion controlled, caused by a shift in concentration towards higher molar ratio  $\text{NaF}/\text{AlF}_3$  near the cathode, Thonstad and Rolseth (1978). A concentration gradient gives a reversible contribution to the cell potential and does not contribute to the dissipation function,  $T\theta$ , of the cell, Førland et al. (1988). The diffusion controlled part of the cathodic overvoltage, should therefore be related to the reversible emf of the cell. Since the cathodic overvoltage is predominantly diffusion controlled, it will depend on the experimental conditions. The rather large discrepancies in the literature data can probably be ascribed to this fact. Thonstad and Rolseth (1978) found that the cathodic overvoltage on aluminium in  $\text{NaF}-\text{AlF}_3-\text{Al}_2\text{O}_3$  melts decreases strongly when the molar ratio  $\text{NaF}/\text{AlF}_3$  is varied from 1 to 8. For molar ratios  $\text{NaF}/\text{AlF}_3$  equal to 1 and 8 and a current density of  $1 \text{ A cm}^{-2}$  they found the overvoltage to be 0.23 and 0.035 V, respectively.

### 5.3 BUBBLE LAYER RESISTANCE

Besides the voltage drop caused by the resistance of the bath, there will be a voltage drop caused by gas bubbles present in the electrolyte. This bubble overvoltage typically has a size of about 0.15 - 0.20 V, Grjotheim and Kvande (1986).

A model cell was constructed by Solheim and Thonstad (1989) in order to measure accumulated gas volume and ohmic resistance as function of the gas inlet rate, interpolar distance and angle of inclination. The cell consisted of an aqueous mixture of glycerol and 1-propanol representing the bath and a porous plate through which air was passed representing the anode. They found that the gas volume as well as the resistance were strongly dependent on the size of the gas bubbles. With a current density of  $0.8 \text{ A cm}^{-2}$  and an inter polar

distance of 4.5 cm they report a gas volume between 0.28 and 0.16 cm<sup>3</sup> cm<sup>-2</sup> and an increase in ohmic resistance between 0.45 and 0.24 V. These results are comparable with the data of Haupin (1971).

In a laboratory aluminium reduction cell, with inter polar distance of 4 cm and 0.8 A cm<sup>-2</sup>, Aaberg (1995) reports a bubblelayer potential between 15 and 60 mV and a gas volume between 0.5 and 0.7 cm<sup>3</sup> cm<sup>-2</sup>. The bubblelayer area resistance is between 25 and 80 mΩ cm.

From the reports available in the literature, it can be concluded that the voltage drop due to the bubble overvoltage, is in the same order of magnitude as the cathodic and anodic voltage losses.

#### 5.4 REVERSIBLE HEAT PRODUCTION AT THE ELECTRODES

The reversible heat production of an electrochemical cell is the entropy of reaction,  $\Delta S$ , times the temperature,  $T$ , of the electrolyte. The heat production per unit area and time is then:

$$\left(\frac{dq}{dt}\right)_{\text{rev}} = T\Delta S j \quad [5.6]$$

where  $j$  is the electric current density divided by Faraday's constant. This heat effect can be decomposed into electrolyte and electrode contributions. Reversible contributions from the electrolyte are negligible for all practical purposes (the Thomson effect). The electrode contributions are obtained from reversible heat balances at each electrode, Eqs. [2.42] and

[2.48]. The reversible heat production at the anode and the cathode in the aluminium reduction cell can be calculated from the measurements in Section 4.1 Tables 4.1 and 4.2 and Equations [2.54] and [2.55]. Table 5.3 gives the heat production at the anode and the cathode for several current densities. The temperature at the cathode and the anode is 1235 K and 1244 K, respectively.

Table 5.3 Reversible heat production at the anode and the cathode, in alumina saturated melt with molar ratio of NaF/AlF<sub>3</sub> equal to 1.8 at several current densities. Faraday's constant,  $F$ , is equal to 96500 C mol<sup>-1</sup>.

Current density / Acm <sup>-2</sup>	Heat production at the cathode / Js <sup>-1</sup> cm <sup>-2</sup>	Heat production at the anode / Js <sup>-1</sup> cm <sup>-2</sup>
0.0	0.00	0.00
0.1	0.152 ± 0.005	-0.224 ± 0.004
0.2	0.30 ± 0.01	-0.449 ± 0.008
0.3	0.46 ± 0.02	-0.67 ± 0.01
0.4	0.61 ± 0.02	-0.90 ± 0.02
0.5	0.76 ± 0.03	-1.12 ± 0.02
0.6	0.91 ± 0.03	-1.35 ± 0.02
0.7	1.07 ± 0.04	-1.57 ± 0.03
0.8	1.22 ± 0.04	-1.79 ± 0.03
0.9	1.37 ± 0.04	-2.02 ± 0.03
1.0	1.52 ± 0.05	-2.24 ± 0.04

---

**REFERENCES, CHAPTER 5**

- E. W. Dewing and E. Th. van der Kouwe, *J. Electrochem. Soc.*, **22**, p. 358, 1975
- K. S. Førland, T. Førland and S. K. Ratkje, *Irreversible Thermodynamics-Theory and Applications*, (John Wiley & Sons, 1988)
- K. Grjotheim and H. Kvande, *Understanding the Hall-Héroult Process for Production of Aluminium*, (Aluminium-Verlag, Düsseldorf, 1986)
- W. E. Haupin, *J. Metals*, **23** (10), p. 46, 1971
- J. Hiveš, J. Thonstad, Å. Sterten and P. Fellner, *Light Metals*, p. 187, 1994
- G. M. Haarberg, L. N. Solli and Å. Sterten, *Light Metals*, p. 227, 1994
- G. M. Haarberg, Department of Applied Electrochemistry, The Norwegian Institute of Technology, The University of Trondheim, Norway, Private communication, 1995
- JANAF Thermochemical Tables, (Clearinghouse, Virginia, 1971, and later supplements)
- S. Jarek and J. Thonstad, *J. Appl. Electrochem.*, **17**, p. 1203, 1987
- J. Koryta and J. Dvořák, *Principles of Electrochemistry*, (John Wiley & Sons, 1987)

- G. V. Samsonov, *Handbook of the Physicochemical Properties of the Elements*, Translated from Russian (IFI/Plenum, New York-Washington, 1968)
- E. Skybakmoen, A. Solheim and Å. Sterten., *Light Metals*. p. 317, 1990
- M. A. Smith, R. C. Perruchoud, W.K. Fischer and B. J. Welch, *Light Metals*, p. 651, 1991
- A. Solheim, S. Rolseth, E. Skybakmoen, L. Støen, Å. Sterten and T. Støre., *Light Metals*, p. 451, 1995
- A. Solheim and J. Thonstad, *Light Metals*, p. 397, 1989
- L. N. Solli, *Carbon Anodes in Aluminium Electrolysis Cells. Factors Affecting Anode Potential and Carbon consumption*, Dr. Ing. thesis, The Norwegian Institute of Technology, University of Trondheim, (1994)
- M. Sørli and H. A. Øye, *Cathodes in Aluminium Electrolysis*, (Aluminium-Verlag GmbH, Düsseldorf, 2nd ed., 1994)
- J. Thonstad, *Electrochem. Acta*, **15**, p. 1569, 1970
- J. Thonstad and S. Rolseth, *Electrochem. Acta*, **23**, p. 233, 1978
- R. J. Aaberg, *Bubblelayer Resistance in Cells with Horizontal Electrodes*, Siviling.thesis (Msc-level), The Norwegian Institute of Technology, University of Trondheim, 1995

## 6. DISCUSSION AND CONCLUSIONS

In this chapter the experimental results will be discussed and conclusions will be drawn. The Seebeck coefficients and the Peltier heats, obtained from measurements and calculations, will be discussed in Section 6.1. Other methods, than measurement of the thermoelectric power, for determination of the Peltier heat are reviewed in Section 6.2. The importance of electronic conduction in cryolite melts in contact with aluminium is examined in Section 6.3. In Section 6.4 the transported entropies in cryolite melts are reviewed. The reversible heat effects, due to the electrode reactions, are compared with other local heat effects in the Hall-Héroult cell in Section 6.5. Technical consequences, due to suggested local heating of the cathode and the local cooling of the anode, will be outlined in Section 6.6. The limitations and the advantages of the theory of irreversible thermodynamics are outlined in Section 6.7. Recommendations for further investigations of the Peltier heat in the cryolite system are given in Section 6.8.

### 6.1 SEEBECK COEFFICIENTS AND PELTIER HEATS

Because of the difficult circumstances for the measurements of Seebeck coefficients, emphasis was put on obtaining reliable data. The results for the different electrodes were checked by reproduction at least once. At molar ratio  $n_{\text{NaF}}/n_{\text{AlF}_3}$  equal to 1.8 the results were also checked for consistency, by application of Equation [2.52], and consistency was indeed found within the experimental error, see Section 4.1.1.

For the oxygen electrodes, the values,  $-1.80 \pm 0.03 \text{ mV K}^{-1}$  at  $971^\circ\text{C}$ ,  $-1.63 \pm 0.03 \text{ mV K}^{-1}$  at  $813.6^\circ\text{C}$  and  $-0.583 \pm 0.008 \text{ mV K}^{-1}$  at  $758^\circ\text{C}$ , were obtained, for molar ratios of  $\text{NaF}/\text{AlF}_3$  equal to 1.8, 1.2 and 1.0, respectively. Carbon electrodes give the same Seebeck

coefficients as oxygen electrodes, in the limit of the experimental error, see Section 2.5.

For the aluminium electrode, the Seebeck coefficient  $-1.23 \pm 0.04 \text{ mV K}^{-1}$  at  $962^\circ\text{C}$ , was obtained for molar ratio of  $\text{NaF}/\text{AlF}_3$  equal to 1.8. At molar ratios  $\text{NaF}/\text{AlF}_3$  equal to 1.2 and 1.0, the Seebeck coefficients were calculated to  $-1.06 \pm 0.03 \text{ mV K}^{-1}$  at  $813.6^\circ\text{C}$  and  $-0.01 \pm 0.008 \text{ mV K}^{-1}$  at  $758^\circ\text{C}$ , respectively. The Peltier effect at the aluminium cathode at molar ratio  $\text{NaF}/\text{AlF}_3$  equal to 1.0 is approximately equal to zero,  $1.0 \pm 0.8 \text{ J mol}^{-1} \text{ K}^{-1}$ , Section 4.3. Then the heat consumption, due to reaction [XI], is located at the oxygen or carbon electrode.

Seebeck coefficients for fluoride melts have only been reported by Mozhaev and Polyakov (1980) before. They reported a Seebeck coefficient of  $-100 \mu\text{V K}^{-1}$  with a relative error of 13% at  $1000^\circ\text{C}$ , for an electrolyte consisting of cryolite and alumina,  $n_{\text{NaF}}/n_{\text{AlF}_3} = 2.7$ , using aluminium electrodes. Their Seebeck coefficient differs widely from the results of cells [B] and [C] in Sections 4.1-4.3. The reproducibility of the measurement was not given, and only a small temperature difference between the electrodes was used,  $6^\circ\text{C}$ . Mozhaev and Polyakov (1980) also reported that no variation in cell potential with alumina concentration was found. This seems unlikely from Equations [2.42] and [2.48]. The activity of  $\text{NaF}$  and  $\text{AlF}_3$  depends on the amount of alumina present in the melt, Sterten et al. (1982). In cryolite melts with molar ratio  $\text{NaF}/\text{AlF}_3$  higher than 2.0, the transport number of sodium is less than one, Sterten et al. (1982), Rajabu et al. (1992). Therefore, there might be a contribution from the heat of transfer of  $\text{Al}_2\text{O}_3$  to the Seebeck coefficient in melts unsaturated with alumina. The heat of transfer can be both negative or positive, depending on the relative magnitude of the transported entropy of  $\text{Al}^{3+}$  and  $\text{O}^{2-}$  and the entropy of  $\text{Al}_2\text{O}_3$ , Eq.[2.44]. It is therefore impossible to predict whether a contribution from  $Q_{\text{Al}_2\text{O}_3}^*$  will increase or decrease the Seebeck coefficient.

Mozhaev et al. (1972) measured the cathode polarization temperatures at varying alumina concentrations in a laboratory cell. At a current density of  $0.8 \text{ A cm}^{-2}$  and 2.5 wt%  $\text{Al}_2\text{O}_3$  they found a temperature increase of  $2^\circ\text{C}$ . At the same current density, but with 10

wt%  $\text{Al}_2\text{O}_3$  they found a temperature increase of 5 °C. Their measurements imply that a lower Peltier heat should be expected at the cathode in cells with industrial melt compositions, than in baths saturated with alumina.

The Seebeck coefficient  $-10 \pm 8 \mu\text{V K}^{-1}$  ( $-1.0 \pm 0.8 \text{ J mol}^{-1} \text{ K}^{-1}$ ) at 758 °C that we obtained for  $n_{\text{NaF}}/n_{\text{AlF}_3} = 1$  is small, however. At this composition, the melt is saturated with  $\text{AlF}_3$  as well as with alumina. The low value can be explained by lack of participation of the heats of transfers,  $Q_{\text{NaF}}^*$ ,  $Q_{\text{AlF}_3}^*$  and  $Q_{\text{Al}_2\text{O}_3}^*$ , to the Seebeck coefficient, see Equations [2.46] and [2.50]. The variation in the Seebeck coefficient, from molar ratio  $\text{NaF}/\text{AlF}_3$  equal to 1.2 to 1.0, is consistent with the loss of compositional degrees of freedom. For molar ratio 1.2, the composition can vary, and the heat of transfer will contribute to the Peltier heat, Eqs. [2.42] and [2.49]. For a molar ratio of 1.0 and temperatures below 850 °C, the phase diagram imposes one more equilibrium restriction on the system, see Fig. 1.2 and Sterten et al. (1982).

The results from the present study are reproducible, they show a behaviour which can be expected from theory by varying  $\Delta T$  and types of electrodes and their concentration dependence can be explained. Therefore I conclude that the measurements are correct.

At molar ratio  $\text{NaF}/\text{AlF}_3$  equal to 1.0, there are two solid phases in equilibrium with one liquid phase, see Fig. 1.2. The liquid phase has a different composition than the total mixture. The composition of the liquid melt is found at the phase boundary line, Fig. 1.2. If the molar ratio of the mixture is equal to 1.0 and the temperature is 758 °C, then the real melt has a molar ratio of  $\text{NaF}/\text{AlF}_3$  equal to 1.08. By decreasing the temperature by 25 °C the molar ratio  $\text{NaF}/\text{AlF}_3$  is changed to 1.12. The composition of the melt in this area of the phase diagram is dependent on the temperature. The experiments at molar ratio  $\text{NaF}/\text{AlF}_3$  equal to 1.0 were therefore carried out with temperature gradients less than 15 °C, and the electrodes were not moved during the experiment. Four experiments were done at molar ratio  $\text{NaF}/\text{AlF}_3$  equal to 1.0 at slightly different temperatures, Table 4.4. However, it does not look like there are any systematic variations in the Peltier effect with temperature. It may be concluded that the Peltier effect is not strongly dependent on the concentration of the melt, but there may be

a concentration dependency over large concentration ranges.

Using the thermodynamic data given in Table 4.5, the change in the Seebeck coefficient with temperature and composition due to the change in entropies can be estimated. Assuming the transported entropies to be constant and the transport number of  $\text{Na}^+$  to be equal to one, the changes in the partial molar entropies,  $S_{\text{NaF}}$ ,  $S_{\text{AlF}_3}$ ,  $S_{\text{Al}_2\text{O}_3}$  and  $S_{\text{O}_2}$  will cause a reduction in the Seebeck coefficient of  $0.24 \pm 0.04 \text{ mV K}^{-1}$ , when the molar ratio of  $\text{NaF}/\text{AlF}_3$  is changed from 1.8 to 1.2. This value is larger than the difference between the measured values of the Seebeck coefficient at molar ratios of  $\text{NaF}/\text{AlF}_3$  equal to 1.8 and 1.2,  $0.17 \pm 0.04 \text{ mV K}^{-1}$ . The concentration dependency of the transported entropies is not known, and cannot be found from this investigation. A systematic temperature variation is likely, Borelius and Gunneson (1921), and is seen in Tables 4.1 and 4.2. Since the regression lines are statistically equal on test levels of 99.3 and 97.1 %, respectively, the data do not allow us to derive any temperature variation of the Seebeck coefficients.

Some examples from the literature of Seebeck coefficients in aqueous solutions, fused and solid salts and metal - molten salt systems are given in Section 2.6. The only trend, that can be seen in Tables 2.3-2.5, is that the Seebeck coefficient seems to increase when the system becomes more complex. The theory of the present experiments show that the Seebeck coefficients cannot be understood by any simple model. The single contributions to the Seebeck coefficient are needed to achieve an understanding. This means that the heat of transfer and the transported entropies must be known in detail. The present results allow us to get such information in some cases. Before any prediction of the size of the Seebeck coefficient is possible, a better understanding of the heat of transfer and the transported entropies is necessary.

## 6.2 OTHER METHODS OF FINDING THE PELTIER EFFECT

The most common way of finding the Peltier effect is to use the relation between the Peltier effect and the Seebeck coefficient, Eq.[2.19]. This method was used in the present work. Two other more direct methods, using the definition of the Peltier heat, Equation [2.15], have been used in the literature and are briefly described below.

Ito, Hayashi and Hayafuji (1985) measured the single electrode Peltier heat of the anodic chlorine evolution reaction in the electrolysis of molten NaCl-ZnCl, using a  $\beta$ -alumina diaphragm, with an electrolytic calorimeter employing a heat flux transducer. They measured the single Peltier heat to  $0.697 \text{ J C}^{-1}$  at  $377^\circ\text{C}$ . This value is close to the value  $0.614 \text{ J C}^{-1}$  previously obtained by Ito, Takeda, Yoshizawa and Ogata (1985) by a thermoelectric power measurement. Coincidence between the values suggests that both experimental techniques are appropriate. Ito, Hayashi and Hayafuji (1985) expressed the single electrode heat to be supplied as:

$$X = \pi i - |\eta| i - \rho_0 \left( \frac{k}{a} \right)^{0.5} i \tanh \left[ \left( \frac{a}{k} \right)^{0.5} \ell i \right] \quad [6.1]$$

where  $\rho$  and  $\rho_0$  are the resistivity at temperatures  $T$  and  $T_0$  respectively, and  $a$  is the positive temperature coefficient,  $i$  is the current density and  $k$  is the thermal conductivity. The first term on the right-hand side in Equation [6.1] corresponds to the single electrode Peltier heat, and the second corresponds to the heat due to overvoltage. The third term on the right is a function of heat conductivity and resistivity. In Equation [6.1], the second and third terms on the right converge to zero rapidly when the current density approaches zero (parabolically), though the first term does so slowly (linearly). Thus:

$$\lim_{i \rightarrow 0} \left( \frac{X}{i} \right) = \pi \quad [6.2]$$

Ito, Hayashi and Hayafuji (1985) measured the heat evolved or absorbed at the single electrode at several steady state electrolytic current densities, the single electrode Peltier heat was then obtained by extrapolation according to Equation [6.2].

Another calorimetric method was used by Kuz'minskii and Gorodyskii (1988). Instead of extrapolating to zero current density in a single electrode heat versus current density plot, Kuz'minskii and Gorodyskii (1988) determined the Peltier heat graphically by extrapolating to  $\Delta T/I$  equal to zero in a  $\Delta T/I$  versus the electrode overvoltage plot. The basic equation used by Kuz'minskii and Gorodyskii (1988) was:

$$\frac{\Delta T_{st}}{I} k_q = -\pi + \eta \quad [6.3]$$

where  $\Delta T_{st} = T_b - T_v$  and  $T_b$  is the electrode surface (i.e. the interface) temperature and  $T_v$  is the bulk electrolyte temperature. The constant  $k_q$  is the coefficient of heat emission from the electrode surface into the electrolyte under conditions of convective exchange, or the thermal conductivity coefficient for systems with allowance for heat transfer by conduction. From Equation [6.3] it follows that the relation described is linear in  $\Delta T_{st}/I - \eta$  coordinates and that the Peltier coefficient can be determined graphically or from the relation  $\Delta T_{st}/I = f(\eta)$  by the least - squares method.

In solid and molten electrolytes and semiconductors, the Peltier effect has been studied by the temperature wave method by Mogilevskii and Usmanov (1967). To find the Peltier effect, they passed periodic sequences of rectangular current pulses of variable polarity from

accumulator batteries through the test sample. The frequencies were varied within limits of 1-0.02 Hz. During passage of current of variable polarity through the test sample, the liberation and absorption of heat were periodically observed on the electrodes and recorded. A method for determining Peltier heats based on the analysis of electrode /molten electrolyte interface temperature oscillations, when applying symmetric rectangular current pulses to an electrochemical cell, was also proposed by Kuz'minskii and Andriiko (1988). This method is a modification of the temperature wave method of Mogilevskii and Usmanov (1967).

All the experimental techniques described in this Section will give the Peltier heat. For each system in question the researcher has to choose the method that is easiest and most accurate. The method used in the present work is the most common one, probably because it is easy to handle and demands a minimum of equipment.

### 6.3 ELECTRONIC CONDUCTION

Electronic conduction in NaF-AlF<sub>3</sub> melts was first demonstrated by Borisoglebskii et al. (1978). The increase in conductivity in the presence of aluminium was about 3% in Na<sub>3</sub>AlF<sub>6</sub> at 1000°C. However, they did not take the evaporation of sodium into account. When sodium evaporates from the melt, the contribution to the current transport from dissolved metal becomes smaller. This leads to lower electronic conduction. Later more reliable measurements have been done by Haarberg et al. (1990), Haarberg (1994). They found the electronic conductivity to be over 20% in Na<sub>3</sub>AlF<sub>6</sub> saturated with Al<sub>2</sub>O<sub>3</sub> and Al at 1000°C. The electronic conduction in the cell can be looked upon as a short-circuit effect and treated as a parallel coupling. The relationship between the gradient in electric potential,  $\nabla\phi^{\text{obs}}$ , of a cell with both electronic and ionic conduction and the gradient in electric potential,  $\nabla\phi$ , of a cell with ionic conduction only, can be illustrated by the two electrical circuits in Figure 6.1. It is assumed that the composition is uniform and that the electrodes in the cells are equal and at same temperature, so that they will not contribute to the electric potential gradient. Consider also that the electric current density,  $j$ , is constant and equal in the two cases. The electric potential for circuit 1 can then be written as:

$$\Delta\phi^{\text{obs}} = \left( \frac{1/(\kappa_{\text{el}}\kappa_{\text{ion}})}{1/\kappa_{\text{el}} + 1/\kappa_{\text{ion}}} \right) \ell j \quad [6.4]$$

where  $\kappa_{\text{el}}$  is the electronic conductivity and  $\kappa_{\text{ion}}$  is the ionic conductivity of the melt. The relation between conductivity and resistance is  $\kappa = \ell/(AR)$  where  $\ell$  is the distance between the electrodes and  $A$  is the electrode area.

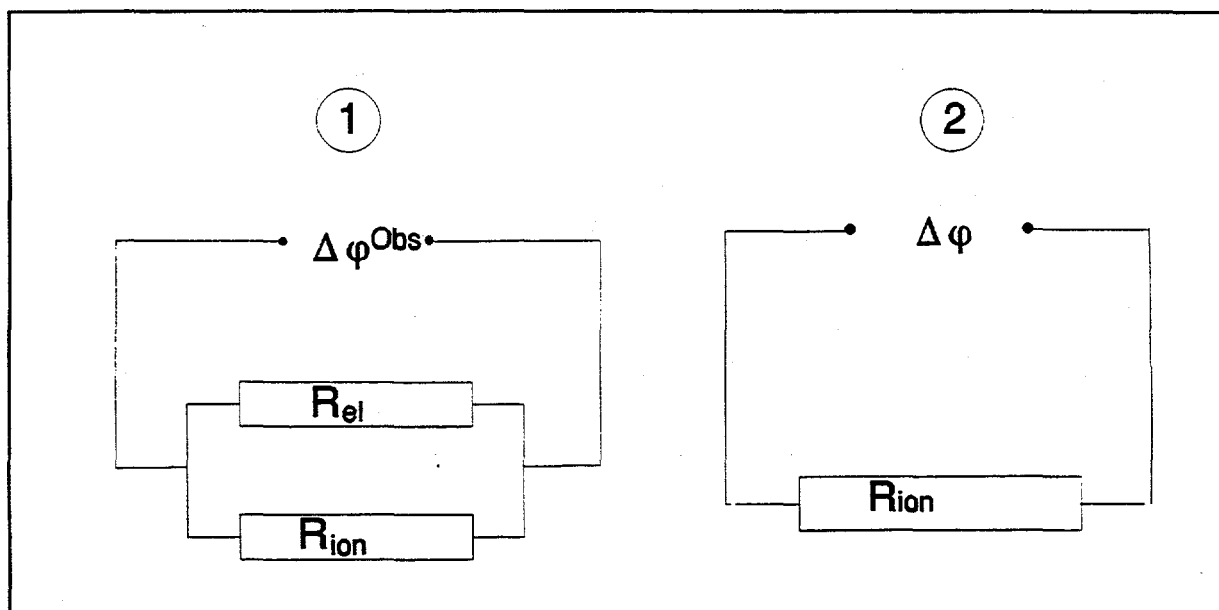


Figure 6.1 1. Illustration of an electrolyte with both electronic and ionic conductivity  
 2. Illustration of an electrolyte with only ionic conductivity

Similarly for circuit 2 in Figure 6.1:

$$\Delta \varphi = \frac{1}{\kappa_{ion}} l j \quad [6.5]$$

If the ionic conductivity,  $\kappa_{ion}$ , is numerically equal in electrolytes 1 and 2, the relation between the two potentials can be obtained by combining Equations [6.4] and [6.5]:

$$\Delta \varphi^{\text{obs}} = \frac{\kappa_{\text{ion}}}{\kappa_{\text{el}} + \kappa_{\text{ion}}} \Delta \varphi \quad [6.6]$$

The fraction of electric current carried by all ions,  $t_{\text{ion}}$ , and by electrons,  $t_{\text{el}}$ , was defined by Haarberg et al. (1990) as:

$$t_{\text{ion}} = \frac{\kappa_{\text{ion}}}{\kappa_{\text{el}} + \kappa_{\text{ion}}} \quad [6.7]$$

and

$$t_{\text{el}} = \frac{\kappa_{\text{el}}}{\kappa_{\text{el}} + \kappa_{\text{ion}}} \quad [6.8]$$

The relationship between the two electric potentials is obtained from Equations [6.6] to [6.8]:

$$\Delta \varphi^{\text{obs}} = t_{\text{ion}} \Delta \varphi \quad [6.9]$$

If there is a gradient in temperature and concentration, between the two electrodes, the terms  $-(\pi/T)\nabla T$  and  $\sum(t_i\nabla\mu_i)$  have to be included in Equations [6.4] and [6.5].

The measurements of thermoelectric powers in Section 4.1 were done at initial state conditions, then there are no gradients in concentration and the gradients in chemical potential are equal to zero. If there is no electronic conduction in thermocell [B], then the initial state thermoelectric power in melt saturated with alumina would be:

$$F \varepsilon_0 = \left( \frac{\nabla \varphi}{\nabla T} \right)_{j=0, t=0} = S_{\text{Al}}^* + \frac{1}{3} (S_{\text{Al}} - S_{\text{Al}^{3+}}^*) - t_{\text{Na}^+}' (S_{\text{Na}^+}^* - \frac{1}{3} S_{\text{Al}^{3+}}^* - S_{\text{NaF}} + \frac{1}{3} S_{\text{AlF}_3}) \quad [6.10]$$

where  $t_{\text{Na}^+}' = 1 - t_{\text{Al}^{3+}} - t_{\text{O}^{2-}}$ . The relation between  $\Delta \varphi^{\text{obs}}$  and  $\Delta \varphi$ , when there is only a temperature gradient between the two equal aluminium electrodes and the melt is saturated with  $\text{Al}_2\text{O}_3$ , can be found from Equations [2.42] and [6.10]:

$$F \varepsilon_0 = \frac{\Delta \varphi^{\text{obs}}}{\Delta T} = (1 - t_{\text{el}}) \frac{\Delta \varphi}{\Delta T} + t_{\text{el}} S_{\text{Al}}^* + t_{\text{el}} S_{\text{el}}^* \quad [6.11]$$

It can be seen from Equation [6.11], that if  $t_{\text{el}} = 0$  then  $\Delta \varphi^{\text{obs}} = \Delta \varphi$ . If  $t_{\text{el}}$  is different from zero, then the first term in Equation [6.11] will reduce the thermoelectric power compared to the condition where  $t_{\text{el}}$  is equal to zero. When  $t_{\text{el}}$  is known, this reduction can be calculated. Since the transported entropies are always positive, the two last terms will increase the thermoelectric power. The transported entropy through the electrode is in order of magnitude less than  $1 \text{ J mol}^{-1} \text{ K}^{-1}$ , and can usually be neglected, Borelius and Gunneson (1921), Moore and Graves (1972).

The magnitude of the transported entropy of electrons through the electrolyte,  $S_{\text{el}}^*$ , is not known. If  $S_{\text{el}}^*$  is similar to  $S_{\text{Na}^+}^*$ , the last term in Equation [6.11] can contribute significantly to  $\Delta \varphi^{\text{obs}}/\Delta T$ . Amezawa (1995) and Amezawa and Ratkje (1996) have measured the transported entropy of protons,  $S_{\text{H}^+}^*$ , in 5 mol%-Sr-doped  $\text{LaPO}_4$  and found values that can be compared with transported entropies of ions in molten salts,  $113 \pm 1 \text{ J mol}^{-1} \text{ K}^{-1}$  at  $600 \text{ }^\circ\text{C}$ . Since the transported entropy of protons has the same magnitude as transported entropies of ions, it is not unreasonable that electrons localized in salt melts have transported entropies that are of the same order of magnitude as transported entropies of ions. The reduction in the observed thermoelectric power caused by the first term, in Equation [6.11], might then be

compensated for by an increase in the thermoelectric power due to the last term in Equation [6.11]. It can be concluded that the change in the thermoelectric power due to electronic conduction is dependent on the importance of the transported entropy of electrons in the electrolyte, and this dependence can only be found by experiments.

The consistency control in Section 4.1.1, gave the change in entropy of the isothermal cell [E] equal to  $55 \pm 5 \text{ J mol}^{-1} \text{ K}^{-1}$  between 1235-1244 K. The entropy change was obtained from data of JANAF (1971) in the limit of the experimental error. The contribution to the thermoelectric power due to electronic conduction must then be smaller than the experimental error at molar ratio of NaF/AlF<sub>3</sub> equal to 1.8. Support for this conclusion can be obtained from Figure 6.3, which shows that the ionic transport number is approximately equal to 1 at molar ratio NaF/AlF<sub>3</sub>  $\leq 2$  and temperatures below 967 °C.

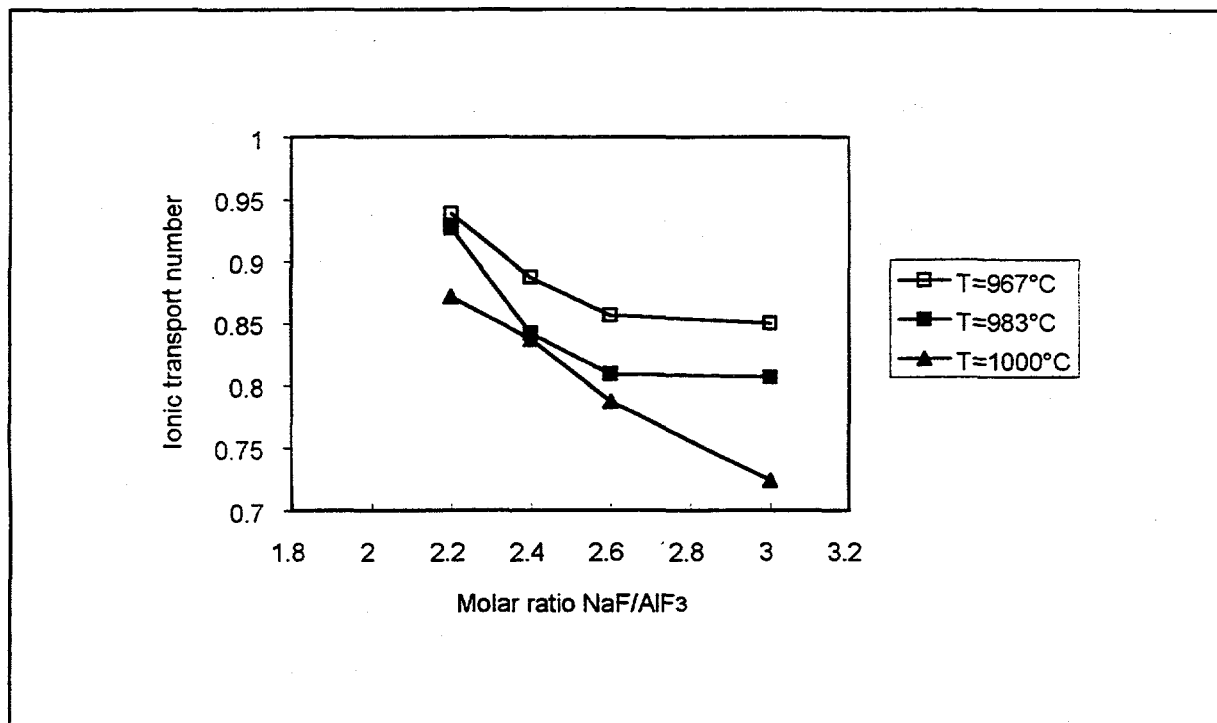


Figure 6.2 Relations between electronic conduction and molar ratio of NaF/AlF<sub>3</sub> at different temperatures, Haaberg (1994).

#### 6.4 TRANSPORTED ENTROPIES IN CRYOLITE MELTS

In Section 4.4, the transported entropy of sodium ions,  $S_{\text{Na}^+}^*$ , was calculated to  $238 \pm 4 \text{ J mol}^{-1} \text{ K}^{-1}$  at  $971^\circ \text{C}$  and  $244 \pm 4 \text{ J mol}^{-1} \text{ K}^{-1}$  at  $814^\circ \text{C}$ , when the molar ratios of  $\text{NaF}/\text{AlF}_3$  were equal to 1.8 and 1.2 respectively. These values are high, but transported entropies of the same order of magnitude have been reported in simpler systems. For instance, in the thermocell  $(T)\text{Ag} | \text{AgCl} | \text{Ag}(T+\Delta T)$  the transported entropy of silver ions,  $S_{\text{Ag}^+}^*$ , was calculated to  $220 \text{ J mol}^{-1} \text{ K}^{-1}$  at  $150^\circ \text{C}$ , Christy (1961).

The results of Ratkje and Sharivker (1995) support the high values obtained for the transported entropy of sodium ions. They found the transported entropy of sodium ions in solid cryolite with 16 - 22 mole %  $\text{AlF}_3$  equal to  $140 \pm 5 \text{ J mol}^{-1} \text{ K}^{-1}$  at  $380^\circ \text{C}$ . The variation in the transported entropy with temperature is given by the Thomson coefficient, Section 2.2. Equation [2.33] shows that the transported entropy increases with temperature. It is not unreasonable that the transported entropy of sodium ions in molten cryolite with  $\text{AlF}_3$  is higher than in the solid state.

We may therefore correct the first estimate of Ratkje (1991) for the transported entropy of  $\text{Na}^+$  ( $89 \pm 5 \text{ J mol}^{-1} \text{ K}^{-1}$  at  $1000^\circ \text{C}$ ), which was based on the Seebeck coefficient of Mozhaev and Polyakov (1980). As pointed out earlier, Section 6.1, these measurements did not seem to be reliable. Also the assumption of Ødegård et al. (1991):

$$S_{(\text{Na}^+ + e^-)}^0 \approx S_{\text{Na}(l)}^0 \quad [6.12]$$

is not correct. The partial molar entropy of an ion is fundamentally different from the transported entropy. The partial molar entropy of an ion is not operationally defined, and should be avoided.

For molar ratio NaF/AlF<sub>3</sub> equal to 1.0, the transported entropy of Al<sup>3+</sup> and O<sup>2-</sup> were calculated to  $77 \pm 2 \text{ J mol}^{-1} \text{ K}^{-1}$  and  $10 \pm 2 \text{ J mol}^{-1} \text{ K}^{-1}$  respectively at 758 °C. In Section 4.4 it was found that the transported entropy of oxygen ions at the carbon electrode was equal to  $10 \pm 2 \text{ J mol}^{-1} \text{ K}^{-1}$ , the same as the transported entropy of oxygen ions at the oxygen electrode. The identical result may be accidental, however. It does not necessarily mean that the transported entropy is independent of the electrode material.

The transported entropies generally vary with concentrations. A large variation in the transported entropy of silver is seen in different silver systems, Table 6.1. For multicomponent systems, only the transported entropy of the ion reversible to the electrode is reported in the literature, and they are estimated from measurements of the thermoelectric power at stationary state conditions. There is still no theoretical explanation for the magnitude of the transported entropies. The transported entropy of an ion has to be determined for all systems and concentrations of interest, like transport numbers.

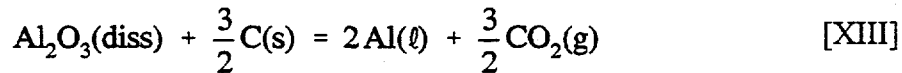
Some authors report a systematic variation with the size of the ions and with the mobility of the ion in question eg. Levin and Bonilla (1951), Ratkje et al. (1990). A short review of models of the transported entropy is given by Grimstvedt (1992). The present data are too few to allow for a systematic analysis.

Table 6.1 The transported entropy of silver ions,  $S_{Ag^+}^*$ , from selected literature. The thermocells are symmetrical.

References	Thermocell	Temp./K	$S_{Ag^+}^* / J mol^{-1} K^{-1}$
Christy (1961)	Ag AgCl	423	220
Grimstvedt (1992)	Ag Ag <sub>2</sub> SO <sub>4</sub>	500	110.1 ± 0.7
	Ag Ag <sub>2</sub> SO <sub>4</sub> (5 mole%)-Li <sub>2</sub> SO <sub>4</sub>	590	135.3 ± 0.1
Haase et al. (1977)	Ag AgNO <sub>3</sub>	533	88.9
	Ag AgNO <sub>3</sub> (x <sub>AgNO<sub>3</sub></sub> =0.7)-LiNO <sub>3</sub>	533	93.1
	Ag AgNO <sub>3</sub> (x <sub>AgNO<sub>3</sub></sub> =0.7)-NaNO <sub>3</sub>	533	89.8
Mogilevskii and Usmanov (1967)	Ag AgF	493	162 ± 4
	Ag α-AgI	473	116 ± 2
	Ag β-AgI	373	166 ± 5
	Ag AgBr	448	182 ± 5
Polishchuk et al. (1978)	Ag α-AgI	473	113 ± 1
	Ag β-AgI	373	184 ± 5

## 6.5 COMPARISON WITH OTHER LOCAL HEAT EFFECTS IN THE HALL-HÉROULT CELL

In the Hall-Héroult cell there are several heat sinks and sources. The main contributions, which were quantified in Chapter 5, will be discussed in this section. In an industrial Hall-Héroult cell, the cell voltage during normal operation is usually between 3.8 and 4.6 V. The reversible potential,  $E^{\text{rev}}$ , for the main cell reaction, Eq.[XIII], demands about 1.18-1.2 V.



In addition, the applied voltage must overcome the anodic and cathodic overvoltages. The anodic overvoltage is an activation overvoltage, due to a slow chemical reaction or a slow charge transfer, and to some extent, anodic concentration overvoltage, Solli (1994), Haaberg (1995). It can be seen from Table 5.2 and Figure 6.3, that the anodic overvoltage is one of the main heat source in the aluminium reduction cell. At current densities,  $i > 0.8 \text{ A cm}^{-2}$  is the slope higher compared to the slope at  $i < 0.8 \text{ A cm}^{-2}$ . According to Solli (1994) the concentration overvoltage may become significant when the current density exceeds  $0.8 \text{ A cm}^{-2}$ . A concentration gradient, however, gives a reversible contribution to the cell potential and does not contribute to the entropy production of the cell, Førland et al. (1988).

The ohmic voltage loss in the electrolyte depends on  $i^2$ , Eq. [5.2]. As can be seen from lines 4a and 4, the Joule heat in the electrolyte is higher in a melt saturated with alumina than in a melt with 2.5 wt% alumina. At current densities higher than  $0.7 \text{ A cm}^{-2}$ , the heat evolution due to ohmic voltage loss in the electrolyte is the largest heat source and its importance increases with increasing current densities.

Figure 6.3 shows that the reversible heat production at the anode is the main heat sink in the cell. More than half of this heat consumption is compensated by the anodic overvoltage. The remaining heat, necessary to maintain the temperature at the anode surface, must be delivered from the heat production in the bath due to bath resistance and bubble overvoltage and from the heat production at the aluminium cathode.

It must be remembered that Figure 6.3 is for cryolite melt saturated with alumina. The picture will probably change for a melt that is unsaturated with alumina. As explained in Section 6.1, it is not possible to predict whether the reversible heat production at the electrodes will increase or decrease in cryolite melts that is not saturated with alumina. The ions being discharged at the anode are some kind of oxygen-containing ions. Both the reversible potential versus an aluminium electrode and the overvoltage are expected to increase with decreasing alumina content in the melt, Grjotheim et al. (1982).

Besides the ohmic drop caused by the resistance of the bath, there will be an ohmic drop caused by gas bubbles present in the electrolyte, resistance in the anode and cathode materials and external electric connections. The sum of these heat sources is large, but the individual ones are small, see Chapter 5.

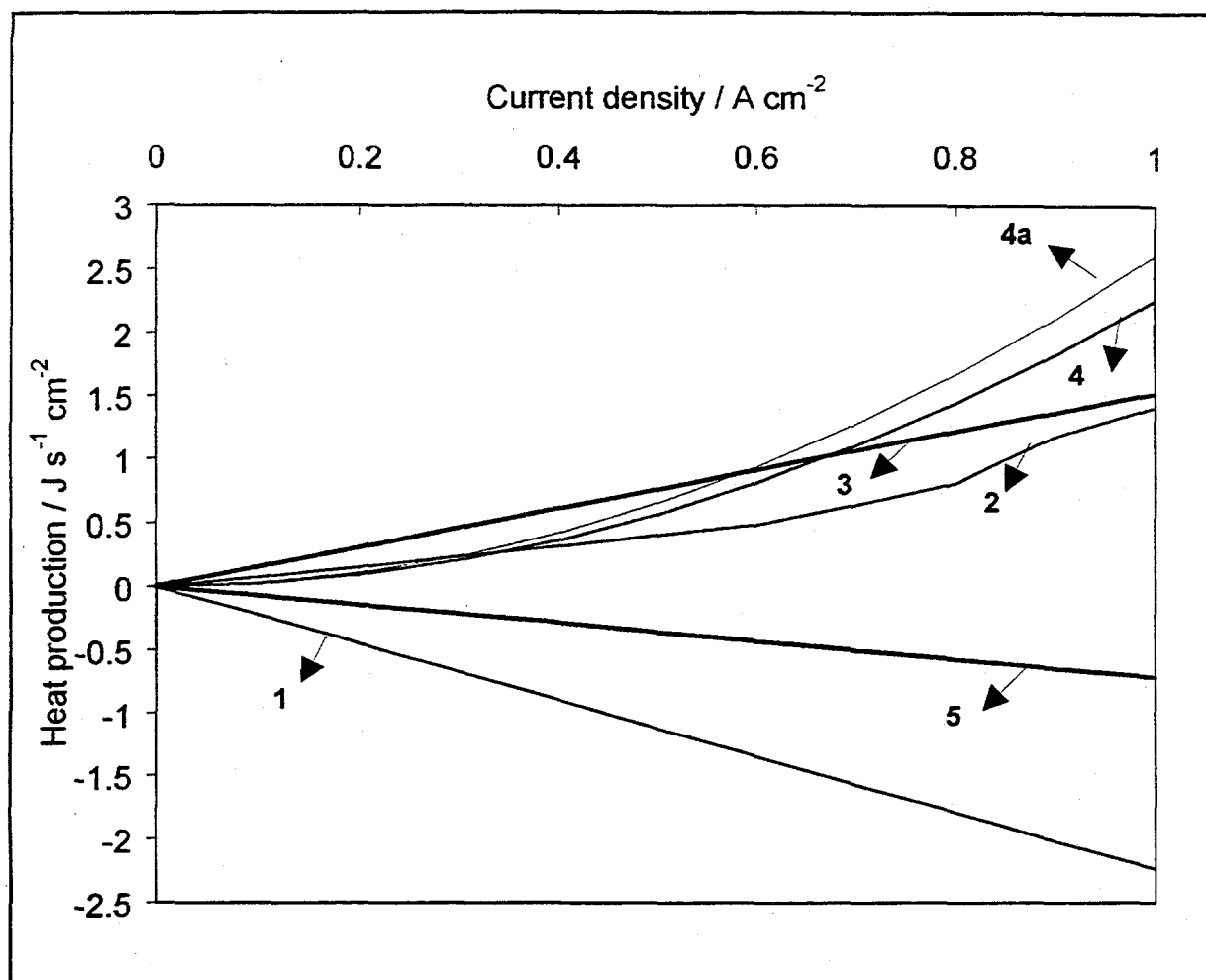


Figure 6.3 Local heat production during aluminium production as function of the current density. Molar ratio  $\text{NaF}/\text{AlF}_3$  is equal to 1.8. The electrode distance is 4.5 cm.

1: Reversible heat production at the anode, alumina saturated melt 2: Anodic overvoltage, Haaberg et al. (1994) 3: Reversible heat production at the cathode, alumina saturated melt 4: Joule heat, electrolyte, 2.5 wt%  $\text{Al}_2\text{O}_3$ , Híveš et al. (1994) 4a: Joule heat, electrolyte, alumina saturated melt, Híveš et al. (1994) 5: Net reversible heat production due to the electrode reactions, lines 1+3.

## 6.6 INDUSTRIAL SCALE MEASUREMENTS AND TECHNICAL CONSEQUENCES

Typical baths used in the aluminium industry have a molar ratio of NaF/AlF<sub>3</sub> in the range 2.2 to 2.6 and temperatures in the range 960 to 1000 °C. Sodium ions, Na<sup>+</sup>, are the major charge carriers, while Al is deposited at the cathode. Therefore, there will be an accumulation of NaF and a depletion of AlF<sub>3</sub> at the cathode, giving rise to a higher NaF / AlF<sub>3</sub> molar ratio, at the cathode, Thonstad and Rolseth (1978). If the bath has a molar ratio NaF / AlF<sub>3</sub> of 2.2, the molar ratio NaF / AlF<sub>3</sub> at the cathode may be as high as 2.7. If there is 2.5 wt% alumina in the bath, the liquidus temperatures will be about 965 °C and 995 °C at molar ratio of NaF/AlF<sub>3</sub> 2.2 and 2.7, respectively, Skybakmoen et al. (1990). Conventionally, the bath temperature is 10 to 15 °C above the liquidus temperature to provide sufficient heat to dissolve alumina additions, Haupin (1992). The bath at the cathode will then have a liquidus temperature higher or very close to the bath temperature. The large heat production due to the Peltier effect at the cathode may explain why there is not any extensive crystallisation of cryolite at the aluminium surface. This also implies that the highest temperature in the Hall-Héroult cell is closer to the cathode surface than to the anode surface. Hansen et al. (1996) have shown that it is possible to have a temperature at the cathode surface higher than both surrounding bulk temperatures. In the heat balance model of the aluminium industry, it is assumed that the highest temperature in the cell is in the bath. If the temperature is significantly higher at the cathode-bath interface this model may have to be changed.

Ødegård et al. (1991) measured the temperature close to the anode surface in industrial-scale cells. From their measurements and thermodynamic calculations they found that the anodic overvoltages is balanced by an electrochemically induced cooling, which results from the large positive  $\Delta S$  of the anode reaction. It is very difficult to measure local heat effect in industrial cells, especially if it is not possible to measure the temperature exactly where the heat effect occurs, in this context on the anode surface. The temperature measurements of Ødegård et al. (1991) were performed inside the carbon anode about two

centimetres above the horizontal anode surface. Two centimetres in this context is nearly half the distance between the anode and the cathode. Heat evolution due to the anodic overvoltage, the bubble and electrolyte resistance together with the mixing of the electrolyte, due to the  $\text{CO}_2$  evolution, will smooth out the temperature differences and interfere their measurements. The results of the present work and the results of Ødegård et al. (1991), imply that there is a heat consumption at the carbon anode in cells having melts that are unsaturated with alumina, which may be in the same order of magnitude as the anodic overpotential, see Chapter 5.

Formation of anode point deformations or protrusions called "spikes" or "tits" are frequently observed in high amperage, prebaked Hall - Héroult cells, Ødegård and Midtlyng (1991). The formation of such protrusions is hardly treated in the literature. Low  $\text{NaF}/\text{AlF}_3$  ratio, bath temperature close to the liquidus temperature, low alumina concentration, low setting of the anode and combinations of these four incidents are conditions that might initiate anode protrusions, Sterten (1995). Ødegård and Midtlyng (1991) did laboratory experiments that indicated that there is a correlation between electrodeposition of carbon from dissolved aluminium carbide and formation of "spikes" on anodes. The heat consumption due to the Peltier heat at the anode may offer another explanation for the initiation of anode point deformations. The heat generated by the anodic overvoltage and heat supplied from the surroundings may occasionally be smaller than the heat consumption of the anode reaction. This can lead to a local temperature below the liquidus temperature. Freezing out of bath may follow, as a result a protrusion may be initiated.

One of the earliest temperature measurements in Hall-Héroult cells reported in the literature is the work of Korobov and Yanko (1968). They reported that the bath temperature beneath the anode centre was 11-13 °C higher than in the molten metal. At the cell periphery close to the crust they found the bath temperature to be about 3 °C higher than the temperature of the metal. Zhuxian et al. (1994) found that under the anode, the bath temperature was 3-6 °C higher than that in metal. If the bath temperature was measured outside the anode shadow the bath temperature was 5-7 °C higher than that of the metal. The bath

temperature under the anode was found to be 5-10 °C higher than outside the anode. This implies that the temperature of the cell is not uniform. The alumina content is varying at different positions in the bath and is highest close to the feeding points. The measurements of Mozhaev et al. (1972) implies that a lower Peltier heat should be expected at the cathode with decreasing alumina content.

The work by Thonstad and Liu (1981) together with the earlier work by Kent (1970) and Kozmin et al. (1976) show that excess alumina, which is added in such a way that no lumps are formed, will settle at the interface between the liquid aluminium and the cryolite-alumina melt, due to the high interfacial tension (~450 mN/m). The alumina layer formed will have a very open structure. Samples taken from commercial cells showed in some cases an enrichment of alumina near the metal surface, eg. ~16 wt% near the metal compared with ~4 wt% Al<sub>2</sub>O<sub>3</sub> in the bulk, Kozmin et al. (1976). This implies that the electrolyte at the cathode can be saturated or is close to saturation with respect to alumina. Then a Peltier effect as large as measured in the present work can occur at the aluminium cathode-electrolyte interface.

The anode-cathode distance is typically 4-5 cm in a cell with prebaked anodes. There are several forces that cause mixing of the electrolyte, eg. thermal convection, gas release from beneath the anode, magnetic movements in the metal pad which also affects the electrolyte and Marangoni flow resulting from interfacial tension differences. Despite this there might be temperature jumps at the electrode surfaces, Bedeaux and Ratkje (1996), Hansen et al. (1996). When estimating the temperature profiles through the cell these temperature jumps should be considered.

The Seebeck coefficients measured in the present work are for melts saturated with alumina and are probably different from the Seebeck coefficients in melts of industrial compositions. Equations [2.42] and [2.48] give the Peltier effect for any melt composition, but there are too many unknowns to allow us to calculate the heat effect at low oxide concentrations. Any final conclusions on the magnitude of the reversible heat effect at the electrodes cannot be drawn before experiments with melts of industrial composition are done.

This start of a more detailed mapping of the heat consumption due to the anodic reaction and the heat production due to the cathodic reaction may give a new way of looking at the heat balance of the Hall-Héroult cell. Up to now, only the total heat consumption due to the general reduction process in the aluminium cell has been used in the heat balance model. Usually it is also assumed that the highest temperature in the cell is in the bath, but the present work indicates that the highest temperature might be at the cathode surface. By including the heat effects at the electrodes, the heat balance model will become more detailed.

## 6.7 THE THEORY OF IRREVERSIBLE THERMODYNAMICS

Irreversible thermodynamics is an extension of classical thermodynamics to give a unified method of treating transport processes. It is particularly useful when several interacting transport processes occur simultaneously.

In contrast to Agar (1963), who describes the electromotive force by local electric potential differences due to charge separation, Førland et al. (1988) use only well defined thermodynamic functions and measurable quantities.

Irreversible thermodynamics is limited to near equilibrium situations with microscopic reversibility, that is local equilibrium, and linear transport processes. It is assumed that although the total system is not in equilibrium there exists, within small control volumes, a state of local equilibrium for which the local entropy  $S$  is the same function of  $U$ ,  $V$  and  $n$  as in real equilibrium. In equilibrium, the total differential of  $S$  is given by the Gibbs relation:

$$dS = \frac{dU}{T} + \frac{p}{T}dV - \frac{1}{T}\sum_i \mu_i \quad [6.13]$$

Hafskjold and Ratkje (1995) have found, using molecular dynamics simulations, that the assumption of local equilibrium is good in systems with severe temperature and concentration gradients. The empirical laws for processes such as heat conduction, electrical conduction and diffusion express fluxes as linear functions of forces. Linear relations are approximations that are valid when there is microscopic reversibility.

The first attempt to describe surfaces by use of the theory of irreversible thermodynamics has been done recently, Ratkje and Bedeaux (1996), Bedeaux and Ratkje (1996). Hansen et al. (1996) have derived the theoretical expression for the dissipated energy for the cathode surface in the aluminium reduction cell. The main difficulty in using non-equilibrium thermodynamics on surfaces, lies in the estimating or measuring of surface properties.

## 6.8 FINAL CONCLUSIONS AND PERSPECTIVES

Further work, to map the reversible heat effect at the electrodes due to the Peltier heat in the aluminium reduction cell, is discussed in Section 6.8.1. Section 6.8.2 summarizes the information on the heat of transfer and the transported entropies that can be obtained from thermoelectric power measurements at stationary state conditions. With a proper design, thermocells can also be used for determination of diffusion coefficients. The estimation of the interdiffusion coefficient in the NaF-AlF<sub>3</sub> system is discussed in Section 6.8.3.

### 6.8.1 Thermoelectric Power at Initial State Conditions

The Peltier heat, at the aluminium and the oxygen electrode, in the system NaF-AlF<sub>3</sub>-Al<sub>2</sub>O<sub>3</sub> has been described by irreversible thermodynamics for any composition of alumina and any molar ratio of NaF/AlF<sub>3</sub>, Eqs.[2.42] and [2.48]. The theory of irreversible thermodynamics is well suited for describing local heat effects such as the Peltier heat.

Thermocells have been constructed for measurements of the thermoelectric power between a pair of aluminium electrodes and a pair of oxygen electrodes in cryolite melt. From the measurements, it was found that in melts saturated with alumina and with molar ratios of NaF/AlF<sub>3</sub> equal to 1.8 and 1.2, there is a Peltier heating of the aluminium cathode. This heating is in the same order of magnitude as the anodic overvoltage, when the current density is 1 A cm<sup>-2</sup>. At molar ratio of NaF/AlF<sub>3</sub> equal to 1.0 the Peltier effect at the aluminium electrode approaches zero.

At the anode there will be a Peltier cooling which is larger than the anodic overvoltage, in melts with NaF/AlF<sub>3</sub> molar ratios 1.8 and 1.2, saturated with alumina. At

molar ratio  $\text{NaF}/\text{AlF}_3$  equal to 1.0, the heat of transfer does not contribute to the Peltier heat and the Peltier cooling of the anode is reduced to about one third of the Peltier effect in melts with  $\text{NaF}/\text{AlF}_3$  molar ratio equal to 1.2.

In this work, reproduction and control of the measurements has been emphasized more than getting measurements for a wide range of compositions. The reason for this strategy was that the obtained results, for the reversible heat production, were unexpectedly high and in large variation with results reported earlier, Mozhaev and Polyakov (1980), Ødegård et al. (1991).

Final conclusions on the magnitude of the reversible heat effect at the electrodes in the Hall-Héroult process cannot be drawn from the present work. Experiments have to be done for melts with industrial composition. The only modification of the experimental cells that is necessary to measure thermoelectric powers in melts without alumina is to exchange the parts that consist of alumina with boron nitride.

Methods for thermoelectric power measurements in the cryolite system have been established and are described in the present work. More work in the field can therefore be concentrated on obtaining the concentration variations of the thermoelectric power, at various alumina contents and  $\text{NaF}/\text{AlF}_3$  molar ratios.

### 6.8.2 Thermoelectric Power at Stationary State Conditions

In Section 4.6, the time necessary to obtain the stationary state was measured to be approximately 30 minutes in NaF-AlF<sub>3</sub> melts with molar ratio  $n_{\text{NaF}}/n_{\text{AlF}_3}$  equal to 4.0. Even if the diffusion coefficient is as low as  $1.64 \times 10^{-4} \text{ cm}^2 \text{ s}^{-1}$ , as in the calculations in Table 4.7, is it possible to manage 5-6 measurements in each experiment. This because it is not necessary to run the experiment to 100% stationary state. It can therefore be concluded that the thermoelectric power at stationary state conditions can be measured in the cell sketched in Figure 3.8. An improvement of the experimental conditions will be to replace the tungsten rods with TiB<sub>2</sub>/BN rods and place the thermocouples inside them as in Figure 3.6. These aluminium electrodes were found to be stable for more than 13 hours, Section 3.2.2. During this time it should be easy to manage to measure the stationary state potential at 8 - 10 different temperature differences.

Seebeck coefficients at stationary state conditions, are found from plots of the cell potential versus  $\Delta T$ . It can be seen from Figure 4.5 that the Seebeck coefficient at molar ratio of NaF/AlF<sub>3</sub> equal to 4.0 is negative. In Chapter 4, the Seebeck coefficient at initial state conditions was found to be negative for all compositions investigated, for both the aluminium and the oxygen electrode. If  $\epsilon_0$  is more negative than  $\epsilon_\infty$ , then the heat of transfer,  $Q^*$ , will become positive, Eq.[2.32]. Which means that NaF will be enriched at the cold side in a temperature gradient, see Eq.[2.30]. If the heat of transfer becomes negative, then NaF will be enriched on the hot side.

From measurements of the thermoelectric power, at stationary state conditions, the transported entropy of the ion reversible to the electrode can be found. The observable heat of transfer can be obtained from the combination of the measurements at initial and stationary state conditions, Eq.[2.32]. Then all terms in the Peltier heat, Equations [2.42] and [2.48], can be found.

Further work should put effort in determining the transported entropy and the heat of transfer in cryolite melts at different concentrations. It is also important to obtain a better understanding of these quantities.

### 6.8.3 Diffusion Coefficients

Very little has been done to determine the interdiffusion coefficients in the NaF-AlF<sub>3</sub> system. Dewing (1984) measured the interdiffusion coefficient in LiF-AlF<sub>3</sub> melts. He found the interdiffusion coefficient to be  $1.6 \times 10^{-3} \text{ cm}^2 \text{ s}^{-1}$ , when the equivalent fraction of AlF<sub>3</sub> was equal to 0.685 ( $n_{\text{LiF}}/n_{\text{AlF}_3} \approx 1.5$ ) at 1273 K. When the equivalent fraction of AlF<sub>3</sub> was decreased to 0.5 ( $n_{\text{LiF}}/n_{\text{AlF}_3} = 3$ ), the interdiffusion coefficient decreased to  $1.6 \times 10^{-4} \text{ cm}^2 \text{ s}^{-1}$ . Burgman and Sides (1988) measured the effective diffusivities for aluminium fluoride species in alumina saturated NaF-AlF<sub>3</sub> melts. Depending on the concentration model used for the aluminium fluoride species, they found an effective diffusion coefficient between  $1.9 \pm 0.6 \times 10^{-5}$  and  $9.2 \pm 7.2 \times 10^{-5} \text{ cm}^2 \text{ s}^{-1}$ , at molar ratio of NaF/AlF<sub>3</sub> equal to 4.0. The diffusion coefficients determined by Burgman and Sides (1988) are probably too low, due to the experimental technique they used. The technique they used, for determining the diffusion coefficients, demands 100% current efficiency and the cathodic overvoltage must be known.

In Section 4.6, the inter-diffusion coefficient in NaF-AlF<sub>3</sub> melts were given a rough estimate to be  $1.5 \times 10^{-3} \text{ cm}^2 \text{ s}^{-1}$ . The unsurety of this value is however high. The calculations are based on only one experiment and as seen from Figure 4.5 it is difficult to know when the stationary state appears due to noise. The inter-diffusion coefficient at molar ratio of NaF/AlF<sub>3</sub> equal to 4.0 is probably between  $1.0 \times 10^{-3}$  and  $1.5 \times 10^{-3} \text{ cm}^2 \text{ s}^{-1}$ . In alumina saturated NaF-AlF<sub>3</sub> melts, the diffusion coefficient is probably lower.

Thermocells where convection is avoided and the distance between the electrodes is known, can be used to determine inter diffusion coefficients. Effort should be put down in determining the diffusion coefficients in cryolite melts as function of the composition.

---

**REFERENCES, CHAPTER 6**

- J. N. Agar, *Thermogalvanic Cells*, in *Advances in Electrochemistry and Electrochemical Engineering*, vol. 3, Ed. by P. Delahay, (Interscience Publ., New York, 1963 )
- K. Amezawa, Graduate School of Human and Environmental Studies, Kyoto University, Sakyo-ku Kyoto 606, Japan, Private communication, 1995
- K. Amezawa and S. K. Ratkje, *in print Denki Kagaku (J. Electrochem. Soc. Japan)*, 1996
- D. Bedeaux and S. K. Ratkje, *J. Electrochem. Soc.*, accepted 1995
- Y. V. Borisoglebskii, M. M. Vetyukov and S. Abu-Zeid, *Tsvetn. Met.* **51**, p.43, 1978
- G. Borelius and F. Gunneson, *Ann. Physik*, **65**, p. 520, 1921
- J. W. Burgman and P. J. Sides, *Light Metals*, p. 673, 1988
- R. W. Christy, *J. Chem. Phys.*, **34**, p. 1148, 1961
- K. S. Førland, T. Førland and S. K. Ratkje, *Irreversible Thermodynamics - Theory and Applications*, (John Wiley & Sons, 1988)
- A. Grimstvedt, *Thermocell Studies of Sulphate Mixtures and Melts Relevant for Aluminium Electrolysis*, Dr. Ing. Thesis, The Norwegian Institute of Technology, University of Trondheim, (1992)

- K. Grjotheim, C. Krohn, M. Malinovský, K. Matiašovský and J. Thonstad, *Aluminium Electrolysis, Fundamentals of the Hall-Héroult Process*, (Aluminium-Verlag, Düsseldorf, 2nd ed., 1982)
- B. Hafskjold and S. Ratkje, *J. Stat. Phys.*, **78**, p. 463, 1995
- E. M. Hansen, S. K. Ratkje, B. Flem and D. Bedeaux, *in print Light Metals*, 1996
- G. M. Haarberg, Department of Applied Electrochemistry, Norwegian Institute of Technology, The University of Trondheim, Norway, Private communication, 1995
- G. M. Haarberg, L. N. Solli and Å. Sterten, *Light Metals*, p. 227, 1994
- G. M. Haarberg, Technical report, Project E3.7, Department of Applied Electrochemistry, Norwegian Institute of Technology, The University of Trondheim, Norway, 1994
- G. M. Haarberg, K. S. Osen, J. Thonstad, R. J. Heus and J. J. Egan, *Light Metals*, p. 283, 1990
- W. Haupin, *Light Metals*, p. 477, 1992
- J. Híveš, J. Thonstad, Å. Sterten and P. Fellner, *Light Metals*, p. 187, 1994
- R. Haase, U. Prüser and J. Richter, *Ber. Bunsenges. Physik. Chem.*, **81**, p. 577, 1977
- Y. Ito, H. Hayashi and N. Hayafuji, *J. Appl. Electrochem.*, **15**, p. 671, 1985
- Y. Ito, R. Takeda, S. Yoshizawa and Y. Ogata, *J. Appl. Electrochem.*, **15**, p. 209, 1985
- J. H. Kent, *J. Metals*, **22 (11)** p. 30, 1970

M. A. Korobov, E. A. Yanko and V. N. Deryagin, *Tsvetn. Met. J. Non-Ferrous Met.*, **41 (1)**, p. 59, 1968

M. A. Korobov, E. A. Yanko, *Tsvetn. Met. Sov. J. Non-Ferrous Met.*, **41 (2)** p. 70, 1968

G. D. Koz'min, P. V. Polyakov, A. V. Sysoev, A. M. Tsyplakov and V. A. Kryukovskii, *Tsvetn. Met. J. Non-Ferrous Met.*, **17 (7)** p. 31, 1976

Y. V. Kuz'minskii and A. V. Gorodyskii, *J. Electroanal. Chem.*, **252**, p. 21, 1988

Y. V. Kuz'minskii and A. A. Andriiko, *J. Electroanal. Chem.*, **252**, p. 39, 1988

H. Levin and C. F. Bonilla, *J. Electrochem. Soc.*, **98**, p. 388, 1951

B. M. Mogilevskii and O. U. Usmanov, *Soviet Electrochem.*, **3**, p. 1002, 1967

J. P. Moore and R. S. Graves, *J. Appl. Phys.*, **44**, p. 1174, 1972

V. M. Mozhaev and P. V. Polyakov, *Tsvet. Met. Sov. J. Non Ferrous Met.*, **23 (5)**, p. 37, 1980

V. M. Mozhaev, P. V. Polyakov and L. M. Afans'eva, *Tsvet. Met. Sov. J. Non Ferrous Met.*, **13 (9)**, p. 28, 1972

A. F. Polishchuk, V. Ya. Loichenko and N. A. Glagoleva, *Soviet Electrochem.* **14**, p. 892, 1978

H. Rajabu, S. K. Ratkje and T. Førlund, Proceedings of the Eighth International Symposium on Molten Salts, St.Louis, 1992

- S. K. Ratkje and D. Bedeaux , submitted 1996
- S. K. Ratkje and V. Sharivker, The International Harald A. Øye Symposium, Trondheim-Norway, February 2-3, 1995
- S. K. Ratkje, *Electrochem. Acta*, **36**, p. 661, 1991
- S. K. Ratkje, T. Ikeshoji and K. Syverud, *J. Electrochem. Soc.*, **137**, p. 2088, 1990
- E. Skybakmoen, A. Solheim and Å. Sterten, *Light metals*, p. 317, 1990
- L. N. Solli, *Carbon Anodes in Aluminium Electrolysis Cells. Factors Affecting Anode Potential and Carbon Consumption*, Dr. Ing. Thesis, The Norwegian Institute of Technology, University of Trondheim, (1994)
- Å. Sterten, K. Hamberg and I. Mæland, *Acta Chem.Scand.*, **A36**, p. 329, 1982
- Å. Sterten, Report, Forskningscenteret, Norsk Hydro, Årdal, 1995 (unpublished work)
- J. Thonstad and Ye-xiang Liu, *Light Metals*, p. 303, 1981
- J. Thonstad and S. Rolseth, *Electrochim. Acta*, **23**, p. 233, 1978
- Q. Zhuxian, L. Jingjiang, C. Xiaoli, K. Grjotheim, H. Kvande and H.A. Øye, *JOM - J. Minerals, Met. Mat. Soc.*, **46 (8)**, p. 28, 1994
- R. Ødegård, S. Julsrud, A. Solheim and K. Thovsen., *Met. Trans. B*, **22B**, p. 831, 1991
- R. Ødegård and S. H. Midtlyng, *J. Electrochem. Soc.*, **138**, p. 2612, 1991



# APPENDICES



## APPENDIX A The Relation Between $l_{ij}$ and $r_{ij}$

In Section 2.1 it was stated that the following relation between  $l_{ij}$  and  $r_{ij}$  had to exist:

$$\sum_{i=1}^{k+1} l_{ii} r_{ii} = 1 \quad \text{and} \quad \sum_{i=1}^{k+1} l_{ji} r_{ii} = 0 \quad (j=2,3,\dots,k+1) \quad [\text{A-1}]$$

Here the derivation will be shown for a two component system,  $j = 2$ . The two components are named 2 and 3. If there is a temperature gradient in the system there will be three forces,  $-\nabla \ln T$ ,  $-\nabla \mu_{2,T}$  and  $-\nabla \mu_{3,T}$ . The corresponding fluxes to the forces are  $J_q$ ,  $J_2$  and  $J_3$ . The fluxes expressed by the forces may then be written:

$$J_q = -l_{11} \nabla \ln T - l_{12} \nabla \mu_{2,T} - l_{13} \nabla \mu_{3,T} \quad [\text{A-2a}]$$

$$J_2 = -l_{21} \nabla \ln T - l_{22} \nabla \mu_{2,T} - l_{23} \nabla \mu_{3,T} \quad [\text{A-2b}]$$

$$J_3 = -l_{31} \nabla \ln T - l_{32} \nabla \mu_{2,T} - l_{33} \nabla \mu_{3,T} \quad [\text{A-2c}]$$

and the forces expressed by the fluxes may be written:

$$-\nabla \ln T = r_{11} J_q + r_{12} J_2 + r_{13} J_3 \quad [\text{A-3a}]$$

$$-\nabla \mu_2 = r_{21} J_q + r_{22} J_2 + r_{23} J_3 \quad [\text{A-3b}]$$

$$-\nabla \mu_3 = r_{31} J_q + r_{32} J_2 + r_{33} J_3 \quad [\text{A-3c}]$$

A combination of Equations [A-2a] to [A-2c] with Equation [A-3a] gives:

$$\begin{aligned} -\nabla \ln T = & r_{11}(-l_{11} \nabla \ln T - l_{12} \nabla \mu_2 - l_{13} \nabla \mu_3) + r_{12}(-l_{21} \nabla \ln T - l_{22} \nabla \mu_2 - l_{23} \nabla \mu_3) \\ & + r_{13}(-l_{31} \nabla \ln T - l_{32} \nabla \mu_2 - l_{33} \nabla \mu_3) \end{aligned} \quad [\text{A-4}]$$

Reorganisation of Equation [A-4] with respect to the forces gives:

$$\begin{aligned} -\nabla \ln T = & -(r_{11} l_{11} + r_{12} l_{21} + r_{13} l_{31}) \nabla \ln T - (r_{11} l_{12} + r_{12} l_{22} + r_{13} l_{32}) \nabla \mu_2 \\ & - (r_{11} l_{13} + r_{12} l_{23} + r_{13} l_{33}) \nabla \mu_3 \end{aligned} \quad [\text{A-5}]$$

The only way the right hand and left hand sides in Equation [A-5] can be equal is if:

$$\begin{aligned}(r_{11}l_{11} + r_{12}l_{21} + r_{13}l_{31}) &= \sum_{i=1}^3 r_{i1}l_{i1} = 1 \\(r_{11}l_{12} + r_{12}l_{22} + r_{13}l_{32}) &= \sum_{i=1}^3 r_{i1}l_{i2} = 0 \\(r_{11}l_{13} + r_{12}l_{23} + r_{13}l_{33}) &= \sum_{i=1}^3 r_{i1}l_{i3} = 0\end{aligned}\tag{A-6}$$

If there are k components in the system Equation [A-6] can be written as Equation [A-1].



## APPENDIX B Mass and Entropy Balance at the Oxygen Electrode

The method of determination of the transference coefficients and the Peltier effect for thermocell [C] is the same as for thermocell [D] in Section 2.1.

The transference coefficients, and the relation between transference coefficients and transference numbers can be found from a local mass balance at the electrodes. Table A1 lists the mass changes upon the passage of one faraday of positive charges.

Table A1 Local mass changes in thermocell [C]

A quasi stationary lattice of fluoride ions is chosen as the frame of reference for the changes at the electrode - electrolyte interface when one faraday of positive charges is transferred from left to right.

	Left-hand side electrode ( $T$ )	Right-hand side electrode ( $T+\Delta T$ )
$\text{Al}^{3+}$ :	$-\frac{1}{3}t_{\text{Al}^{3+}}$	$\frac{1}{3}t_{\text{Al}^{3+}}$
$\text{F}^-$ :	$t_{\text{F}^-} = 0$	$t_{\text{F}^-} = 0$
$\text{Na}^+$ :	$-t_{\text{Na}^+}$	$t_{\text{Na}^+}$
$\text{O}^{2-}$ :	$-\frac{1}{2} + \frac{1}{2}t_{\text{O}^{2-}}$	$\frac{1}{2}(1 - t_{\text{O}^{2-}})$
$\text{NaF}$ :	$-t_{\text{Na}^+}$	$t_{\text{Na}^+}$
$\text{AlF}_3$ :	$\frac{1}{3}t_{\text{Na}^+}$	$-\frac{1}{3}t_{\text{Na}^+}$
$\text{Al}_2\text{O}_3$ :	$-\frac{1}{3}(\frac{1}{2} - \frac{1}{2}t_{\text{O}^{2-}})$	$\frac{1}{3}(\frac{1}{2} - \frac{1}{2}t_{\text{O}^{2-}})$
$\text{O}_2$	$\frac{1}{4}$	$-\frac{1}{4}$

The expression for the Peltier effect can be found from a reversible entropy balance. For thermocell [C], the different contributions to the entropy balance are listed in Table A2.

Table A2 Reversible entropy balance at the left-hand side  
electrode-electrolyte interface.

The entropy received and consumed is given for the transfer of one Faraday of positive electric charge passing from the left to the right electrode.

ENTROPY RECEIVED	
$\pi/T$	the interface receives entropy from the heat reservoir
$S_{Pt}^*$	entropy transported through the electrode to the interface
$t_{Na^+}S_{NaF}$	the disappearance of $t_{Na^+}$ mole NaF liberates entropy
$\frac{1}{3}(\frac{1}{2} - \frac{1}{2} t_{O^{2-}})S_{Al_2O_3}$	the disappearance of $\frac{1}{3}(\frac{1}{2} + \frac{1}{2} t_{O^{2-}})$ mole $Al_2O_3$ liberates entropy
$\frac{1}{2} t_{O^{2-}} S_{O^{2-}}^*$	entropy transported through the electrolyte to the interface
ENTROPY CONSUMED	
$\frac{1}{4}S_{O_2}$	the formation of $\frac{1}{4}$ mole $O_2$ consumes entropy
$\frac{1}{3}t_{Na^+}S_{AlF_3}$	the formation of $\frac{1}{3}t_{Na^+}$ mole $AlF_3$ consumes entropy
$t_{Na^+}S_{Na^+}^*$	entropy transported through the electrolyte away from the interface
$\frac{1}{3}t_{Al^{3+}}S_{Al^{3+}}^*$	entropy transported through the electrolyte away from the interface

---

## **APPENDIX C    Temperature Gradient of the Vertical Tube Furnace.**

The vertical tube furnace used in the experiments performed in the present work, had an oxide ceramic furnace tube with length 60 cm and inner diameter 10 cm (Pythagoras 1800 Z, 76%  $\text{Al}_2\text{O}_3$ , Haldenwanger Technische Keramik, Germany). Kanthal wire was used as resistor material in the heating element of the furnace. The resistance of the heating element was around 30 ohm.

The top and bottom lids of the furnace were water-cooled and made from brass, with rubber gaskets resting on the edges of the oxide ceramic tube. The rubber gaskets were lubricated with high vacuum grease (N.V.Dow Corning s.a. Belgium) to avoid gas leakage.

Temperatures measured at different vertical positions in the furnace tube are shown in Figure A1. The temperature was measured in the empty furnace with a type-S thermocouple, platinum - 10% rhodium versus platinum. A small flow of argon was maintained through the furnace during the measurement. Within experimental error ( $0.1^\circ\text{C}$ ) no horizontal temperature gradient was detected. From the temperature profile of the furnace it was decided to place the bottom of the crucible 150 mm from the bottom end of the oxide ceramic tube. This position will give the possibility to have both positive and negative temperature differences between the two electrodes.

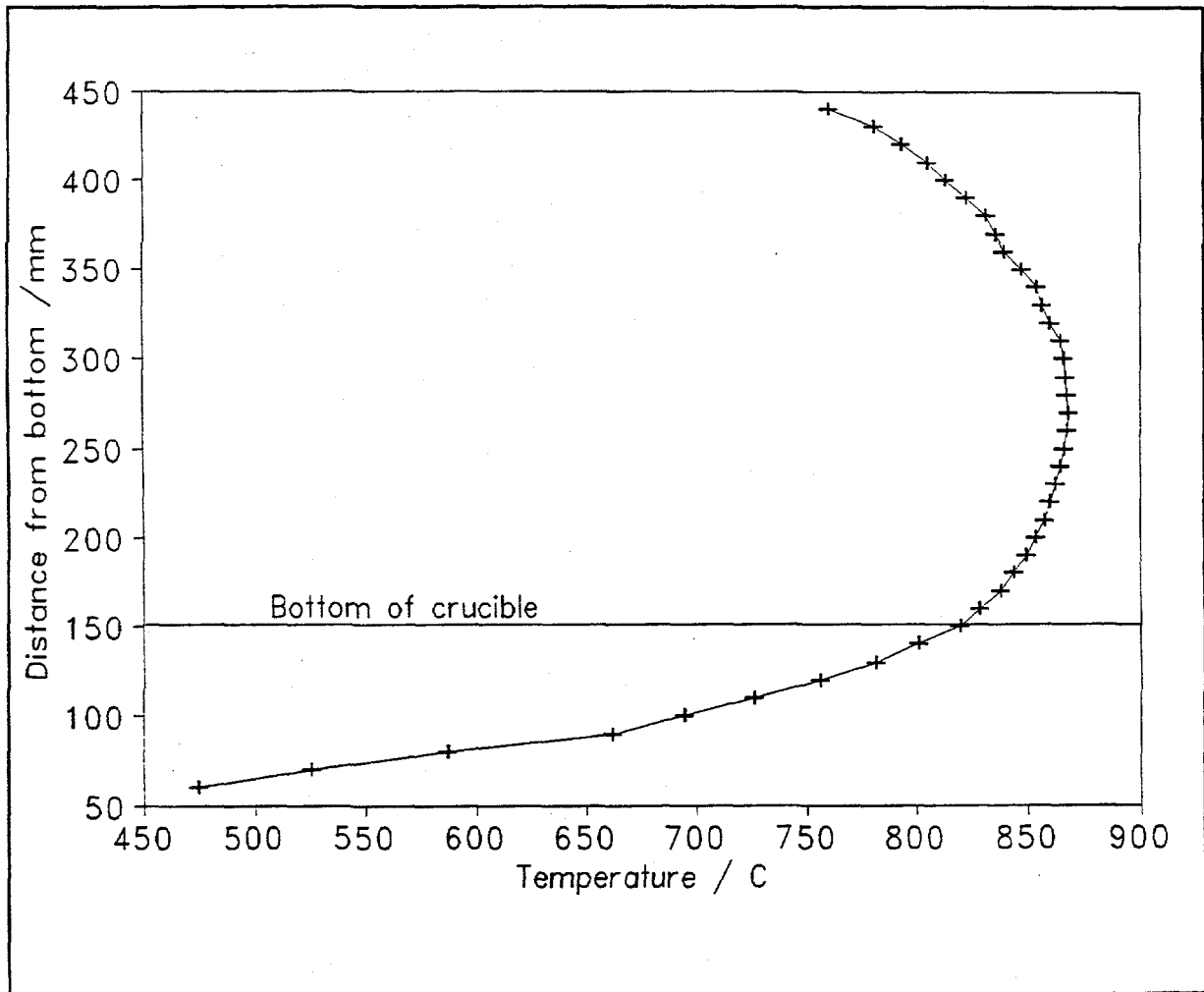


Figure A1 The temperature gradient in the empty tube furnace used in the present work. Position of the experimental cell is indicated.

## APPENDIX D Flow Diagram for the Apparatus

Figure A2 shows the different apparatus used in the experiments with a pair of aluminium electrods. Specifications for the different parts are given underneath.

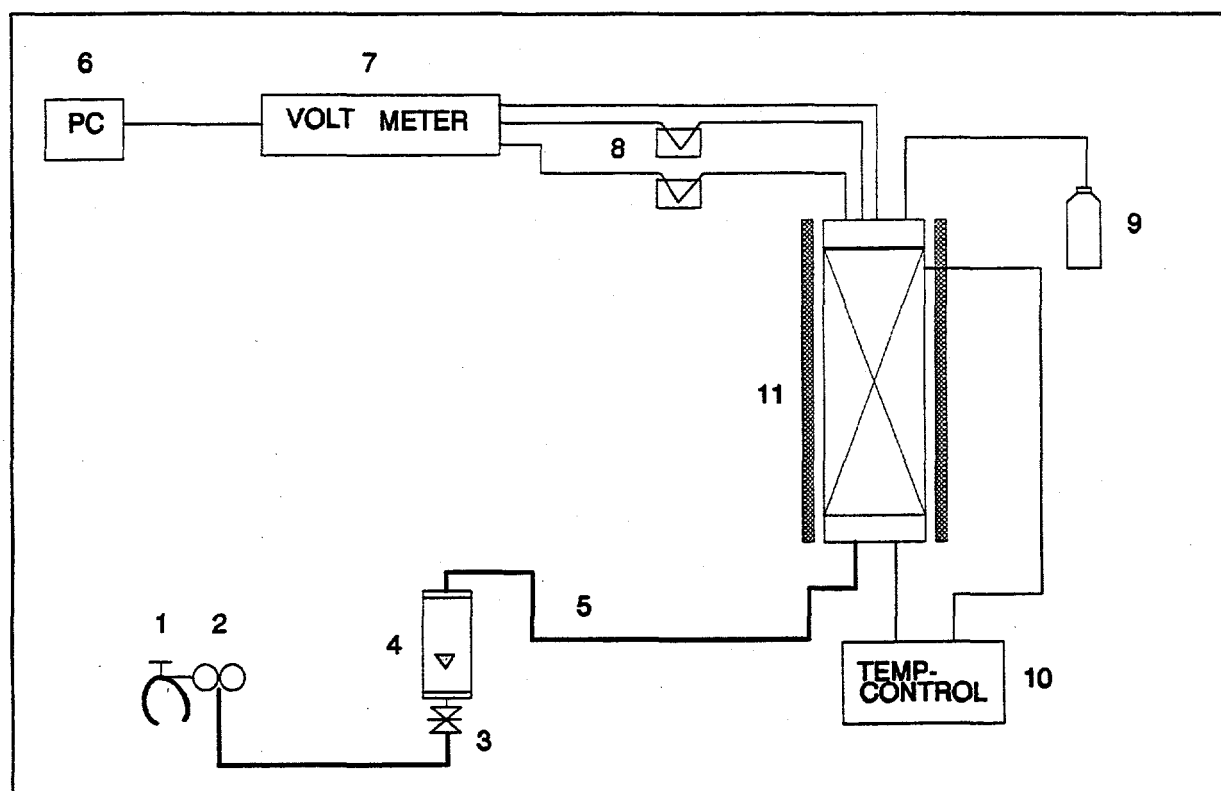


Figure A2 Flow diagram for the apparatus. Specifications for the different parts are given in the text.

1. Gas bottle valve, Argon gas
2. Reduction valve  
Hydro gas  
Medium : Ar  
Pressure area : 0-250 bar inlet  
0-15 bar outlet  
Connections : Female NPT, outlet

3. Needle control valve
4. Flowmeter  
SHO-RATE II, Brooks Instruments B.V  
Model : 1355/D2A4A1C5F00  
Connections : Female NPT, both outlet and inlet  
Medium : Ar<sub>(g)</sub>  
Temperature : ~ 20°C  
Pressure : ~ 1.01 bar  
Capacity : 1.16-11.60 ln/h
5. Stainless Steel tubing  
Dimension : (1/8)" outer diameter  
1.5 mm inner diameter
6. PC-Olivetti M24
7. Multimeter  
HP 3457A, Hewlett Packard
8. Ice point  
Temperature : 0°C
9. Bubble bottle  
Saturated mixture of CaCl<sub>2</sub>, CaCO<sub>3</sub> and NaCO<sub>3</sub>
10. Temperature control unit  
Eurotherm  
Model : 94
11. Furnace surrounded by a steel mantel with water cooling tubes.

## APPENDIX E Materials and Chemicals Used in the Experiments

Table A3 gives the producers, grade and the pretreatment of the chemicals used in the experiments. The producers, distributors, grade and the pretreatment of the materials are given in Table A4.

Table A3 Chemicals used in the experiments

Formula	Producer	Grade	Pretreatment
$\text{Na}_3\text{AlF}_6$	Kryolitselskabet Øresund, Greenland	"Natural, handpicked"	Grinded and dried at 200°C for 24 hours
$\text{NaF}$	Merck (Art.6449)	p.a.	
$\text{Al}$	Vigeland Metal Refinery A/S, Norway	> 99.99%	Cleaned by ultrasonic vibration, in acetone for 30 minutes
$\text{AlF}_3$	Nordzink, Norway	Technical	Sublimated at 1000°C at less than 2 torr, for 30 hours
$\text{Al}_2\text{O}_3$	Merck (Art. 1095 )	Wasserfrei	Fired at 1600°C for 4-hours

Table A4 Materials used in the experiments

Material	Producer	Distributor	Grade	Pretreatment
Carbon	The Carbon Graphite Group Inc, USA	Svensk Specialgrafit AB	780 GL	Cleaned by ultrasonic vibration, in ethanol for 30 minutes
TiB <sub>2</sub> /BN	BN Products LTD	BN Products LTD	HDS	Cleaned by ultrasonic vibration, in acetone for 30 minutes
Boron nitride	BN Products LTD	BN Products LTD	HBR	Cleaned by ultrasonic vibration in acetone for 20 minutes. Removing of water and binder B <sub>2</sub> O <sub>3</sub> by evaporation in vacuum at 900 °C
Inconel	Inco Alloys Limited	Harald Pihl, Sweden	Alloy 600	
Platinum	K.A. Rasmussen	K.A. Rasmussen	Thermocouple	
Pt-10%Rh				
Alumina ceramic	Haldenwanger, Technishe Keramik Germany	Falchenberg or Nerliens, Norway	99.7, Alsint	Fired at 1300°C for 4-hours
oxide ceramic			1800Z, Pythagoras	

## APPENDIX F Statistics

Regression analysis is one of the most widely used statistical techniques for analysing multifactor data. Its broad appeal results from the conceptually simple process of using one equation to express the relationship between a set of variables. The statistical methods used in this work will be given in detail in this appendix. This is because it will make it simpler to compare the results of this work with the result from other authors and in future work.

The principle of indicator variables used in regression analysis and an example of its use is given in Section F.1. In Sections F.2 and F.3, the Seebeck coefficients in Table 4.2 Section 4.1, is tested if they are equal and if second order terms should be included in the regression model. The statistics in Sections F.1, F.2 and F.3 are based on the theory of indicator variable, Montgomery and Peck (1982)<sup>1</sup>.

### F.1 INDICATOR VARIABLES

The variables employed in regression analysis are usually quantitative variables, that is the variables have a well-defined scale of measurement. Occasionally it is necessary to use qualitative or categorical variable as predictor variables in regression. A qualitative variable has no natural scale of measurement. It must be assigned a set of levels to a qualitative variable to account for the effect that the variable may have on the response. This is done by indicator variables. Sometimes indicator variable is called "dummy" variables, Montgomery and Peck (1982).

---

<sup>1</sup> D. C. Montgomery and E. A. Peck, *Introduction to Linear Regression Analysis*, (Wiley, New York, 1982)

The theory of indicator variables may be used to test whether two or more regression lines have a common slope or not. Indicator variables can also be used to test for second order corrections. A qualitative variable with  $a$  levels is represented by  $a-1$  indicator variables, each taking the values 0 and 1. If there are three regression lines to be tested, two indicator variables,  $X_2$  and  $X_3$ , will be required to incorporate the three levels of the lines into the model. The levels of the indicator variables are given in Table A5.

How to use the statistics with indicator variables to determine whether three regression lines have a common slope is demonstrated in Example A1.

Table A5 Levels of the indicator variables  $X_2$  and  $X_3$

$X_2$	$X_3$	
0	0	if the observation is from experiment A
1	0	if the observation is from experiment B
0	1	if the observation is from experiment C

**Example A1**      **Indicator Variables, test on common slope**

Six observations on tool life and lathe speed for tool types A, B and C are presented in Table A4 and the scattered diagram is shown in Figure A3. Inspection of this scattered diagram indicates that three different regression lines are required to adequately model these data, with the intercept depending on the type of tool used. Therefore the model given in Equation [A.7] will be fitted the data. The indicator variables will be given the same levels as in Table A5.

Table A6 Observations on tool life and lathe speed for tool types A, B and C

	$x_i$ (RPM)	$y_i$ (Hours)
Tool A	530	24.39
	610	18.73
	720	17.43
	840	14.54
	890	12.68
	980	13.44
Tool B	500	43.67
	590	40.01
	670	34.9
	810	30.56
	910	26.07
Tool C	1000	25.2
	500	19.39
	580	13.73
	690	12.43
	810	9.54
	860	7.68
	950	7.5

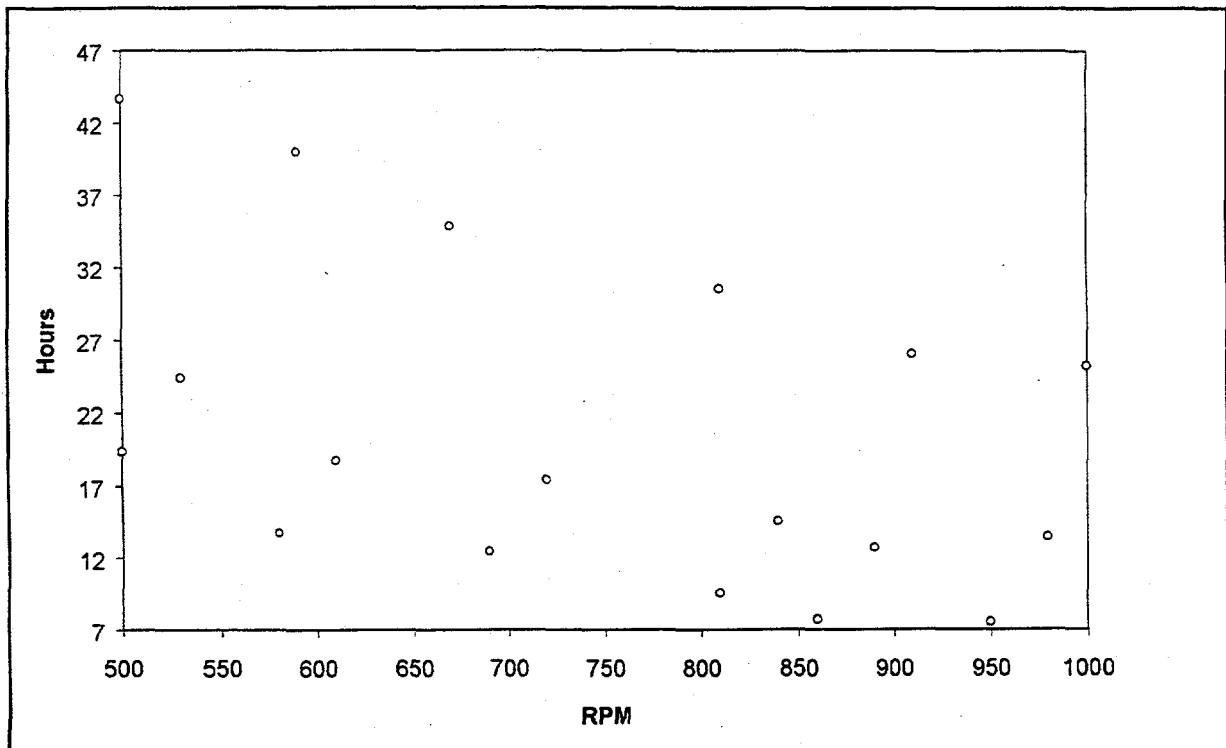


Figure A3 Plot of tool life versus lathe speed for tool types A, B and C

The regression model is:

$$y = \beta_0 + \beta_1 X_1 + \beta_2 X_2 + \beta_3 X_3 + \beta_4 X_1 X_2 + \beta_5 X_1 X_3 + \varepsilon \quad [A.7]$$

where  $y$  is the tool life,  $X$  is the lathe speed and  $\varepsilon$  is the statistical error or the difference between the observed value  $y$  and the straight line.

To interpret the parameters in this model, consider first tool type A, for which  $X_2=0$  and  $X_3 = 0$ . The regression model becomes:

$$\begin{aligned}
 y &= \beta_0 + \beta_1 X_1 + \beta_2(0) + \beta_3(0) + \beta_4 X_1(0) + \beta_5 X_1(0) + \varepsilon \\
 &= \beta_0 + \beta_1 X_1 + \varepsilon
 \end{aligned}
 \tag{A.8}$$

Thus the relationship between tool life and lathe speed for tool type A is a straight line with intercept  $\beta_0$  and slope  $\beta_1$ . For tool type B,  $X_2 = 1$  and  $X_3 = 0$  and:

$$\begin{aligned}
 y &= \beta_0 + \beta_1 X_1 + \beta_2(1) + \beta_4 X_1(1) + \varepsilon \\
 &= (\beta_0 + \beta_2) + (\beta_1 + \beta_4) X_1 + \varepsilon
 \end{aligned}
 \tag{A.9}$$

That is, for tool type B the relationship between tool life and lathe speed is a straight line with slope  $\beta_1 + \beta_4$  and intercept  $\beta_0 + \beta_2$ . For tool type C is  $X_2 = 0$  and  $X_3 = 1$ , then:

$$\begin{aligned}
 y &= \beta_0 + \beta_1 X_1 + \beta_3(1) + \beta_5 X_1(1) + \varepsilon \\
 &= (\beta_0 + \beta_3) + (\beta_1 + \beta_5) X_1 + \varepsilon
 \end{aligned}
 \tag{A.10}$$

Thus, the relationship between tool life and lathe speed for tool type C is a straight line with intercept  $\beta_0 + \beta_3$  and slope  $\beta_1 + \beta_5$ . The parameters  $\beta_3$  and  $\beta_5$  expresses the difference in intercept or the difference in heights, if the lines are parallel, among the three regression lines. The differences in the three slopes are expressed by  $\beta_4$  and  $\beta_5$ . If  $\beta_4$  and  $\beta_5$  are equal to zero, then the three experiments have the common slope  $\beta_1$ .



$$F_0 = \frac{SS_R(\beta_4, \beta_5 / \beta_0, \beta_1, \beta_2, \beta_3) / 2}{MS_E} \quad [A.11]$$

where:

$$\begin{aligned} SS_R(\beta_4, \beta_5 / \beta_0, \beta_1, \beta_2, \beta_3) &= SS_R(\beta_0, \beta_1, \beta_2, \beta_3, \beta_4, \beta_5) - SS_R(\beta_0, \beta_1, \beta_2, \beta_3) \\ &= 1990.9 - 1968.3 \\ &= 22.6 \end{aligned} \quad [A.12]$$

The observed value of  $F_0$  is equal to 4.9. Since  $F_{0.027, 2, 12} = F_0$ ,  $H_0$  should be accepted at a test level of 97.3 % or higher.

Table A7 Summary statistics for tool types A, B and C

<b>Model with <math>\beta_4</math> and <math>\beta_5</math></b>			
Source of Variation	Sum of Squares	Degrees of Freedom	Mean Square
Regression	1990.898	5	398.18
Error	27.67738	12	2.306
Coefficient	Estimate	Standard Error	
$\beta_0$	34.8834	3.063293	
$\beta_1$	-0.02365	0.003939	
$\beta_2$	27.15315	4.083687	
$\beta_3$	-4.85628	4.251184	
$\beta_4$	-0.0147	0.005282	
$\beta_5$	-0.00138	0.00557	
<b>Model without <math>\beta_4</math> and <math>\beta_5</math></b>			
Source of Variation	Sum of Squares	Degrees of Freedom	Mean Square
Regression	1968.2934	3	654.1
Error	50.28209	14	3.59
Coefficient	Estimate	Standard Error	
$\beta_0$	39.51648	2.215404	
$\beta_1$	-0.02973	0.002725	
$\beta_2$	16.08731	1.094927	
$\beta_3$	-6.04872	1.097214	

The statistics, to test for second order corrections are very similar to the statistics for testing whether three regression lines have a common slope or not. The regression model with a second order term is:

$$y = \beta_0 + \beta_1 X_1 + \beta_2 X_2 + \beta_3 X_3 + \beta_4 X_1 X_2 + \beta_5 X_1 X_3 + \beta_6 X_1^2 + \varepsilon \quad [A.13]$$

## F.2 TEST ON COMMON SLOPE IN EXPERIMENTS A, B AND C, TABLE 4.2

In Section 4.1 three experiments A, B and C, Table 4.2 were done under approximately the same conditions. The theory of indicator variables, described in Section F.1, will be used to test whether the three experiments have a common slope or not. The regression model is given in Equation [A.7] and the analyses of variance and other statistics for the model are given in Table A8.

The null hypothesis,  $H_0$ , is rejected if  $F_0 > F_{\alpha, 2, n-6}$ , where  $F_{\alpha, 2, n-6}$  is the  $\alpha$  percentage points of the  $F$  distribution with 2 and  $n-6$  degrees of freedom ( $n$ =experimental points). Since  $F_{0.029, 2, 635} = F_0 = 3.55$ ,  $H_0$  should be accepted on a test level of 97.1 % or higher.

The coefficient  $\beta_1$  in Table A6, in the model without  $\beta_4$  and  $\beta_5$ , gives the mean slope of the three curves.

Table A8 Summary statistics for the experiments A, B and C in Section 4.1, Table 4.2.

Model with $\beta_4$ and $\beta_5$			
Source of Variation	Sum of Squares	Degrees of Freedom	Mean Square
Regression	1009383	5	201876
Error	12782	635	20.1295
Coefficient	Estimate	Standard Error	
$\beta_0$	2.45498	0.8090	
$\beta_1$	-1.72336	0.037902	
$\beta_2$	8.692527	0.964573	
$\beta_3$	35.11968	0.844579	
$\beta_4$	-0.0561	0.047872	
$\beta_5$	-0.10171	0.040973	
Model without $\beta_4$ and $\beta_5$			
Source of Variation	Sum of Squares	Degrees of Freedom	Mean Square
Regression	1009240.4	3	336413
Error	12924	637	20.2895
Coefficient	Estimate	Standard Error	
$\beta_0$	3.887089	0.50950	
$\beta_1$	-1.80437	0.012967	
$\beta_2$	7.610315	0.563179	
$\beta_3$	33.74928	0.579619	

### F.3 TEST ON INDIVIDUAL REGRESSION COEFFICIENTS

For large values of  $\Delta T$ , the variation in potential with  $T$  can give second order corrections, and these must be taken into account, see Section 2.2. The experiments A, B and C in Section 4.1 have temperature differences up to 50-60°C, and will therefore have to be tested for second order corrections. The same model as in Section F.2 will be used with addition of second order terms. The regression model is given in Equation [A.13].

In Section F.2, it was shown that  $\beta_4$  and  $\beta_5$  were equal to zero. The regression model then reduces to:

$$y = \beta_0 + \beta_1 X_1 + \beta_2 X_2 + \beta_3 X_3 + \beta_6 X_1^2 + \varepsilon \quad [\text{A.14}]$$

The same levels of the indicator variables are used as in Section F.1. To interpret the parameters in this model, consider first experiment A, for which  $X_2 = 0$  and  $X_3 = 0$ . The regression model becomes:

$$\begin{aligned} y &= \beta_0 + \beta_1 X_1 + \beta_2(0) + \beta_3(0) + \beta_6 X_1^2 + \varepsilon \\ &= \beta_0 + \beta_1 X_1 + \beta_6 X_1^2 + \varepsilon \end{aligned} \quad [\text{A.15}]$$

Thus the relationship between cell potential and temperature difference for experiment A is a second order curve with intercept  $\beta_0$ , slope  $\beta_1$  and where  $\beta_6$  is a measure of the curvature. For experiment B,  $X_2 = 1$  and  $X_3 = 0$ , then:

$$\begin{aligned}
 y &= \beta_0 + \beta_1 X_1 + \beta_2(1) + \beta_6 X_1^2 + \varepsilon \\
 &= (\beta_0 + \beta_2) + \beta_1 X_1 + \beta_6 X_1^2 + \varepsilon
 \end{aligned}
 \tag{A.16}$$

That is, for experiment B the relationship between cell potential and temperature difference is a second order line with the slope  $\beta_1$  and curvature  $\beta_6$ , and with intercept  $\beta_0 + \beta_2$ . For experiment C,  $X_2 = 0$  and  $X_3 = 1$ , then:

$$\begin{aligned}
 y &= \beta_0 + \beta_1 X_1 + \beta_3(1) + \beta_6 X_1^2 + \varepsilon \\
 &= (\beta_0 + \beta_3) + \beta_1 X_1 + \beta_6 X_1^2 + \varepsilon
 \end{aligned}
 \tag{A.17}$$

Thus, the relationship between cell potential and temperature difference for experiment C is a second order line with intercept  $\beta_0 + \beta_3$ , slope  $\beta_1$  and curvature  $\beta_6$ . The parameters  $\beta_3$  and  $\beta_2$  express the difference in intercepts.

To test that the three regression lines have a common second order heat effect, but possibly different intercepts the hypotheses are:

$$H_0 : \beta_6 \neq 0 \text{ against } H_1 : \beta_6 = 0$$

The null hypothesis,  $H_0$ , will be rejected if  $F_0 < F_{\alpha, \gamma_1, \gamma_2}$ . Two regressions have to be done to test the hypotheses. The summary of the statistics for the regression where all terms are included is presented in Table A9. The second regression, where  $\beta_6$  is not included, is already given in Table A8.

To test the hypothesis that second order heat effects are significant, the statistics used are:

$$F_0 = \frac{SS_R(\beta_6 / \beta_0, \beta_1, \beta_2, \beta_3) / 1}{MS_E} \quad [A.18]$$

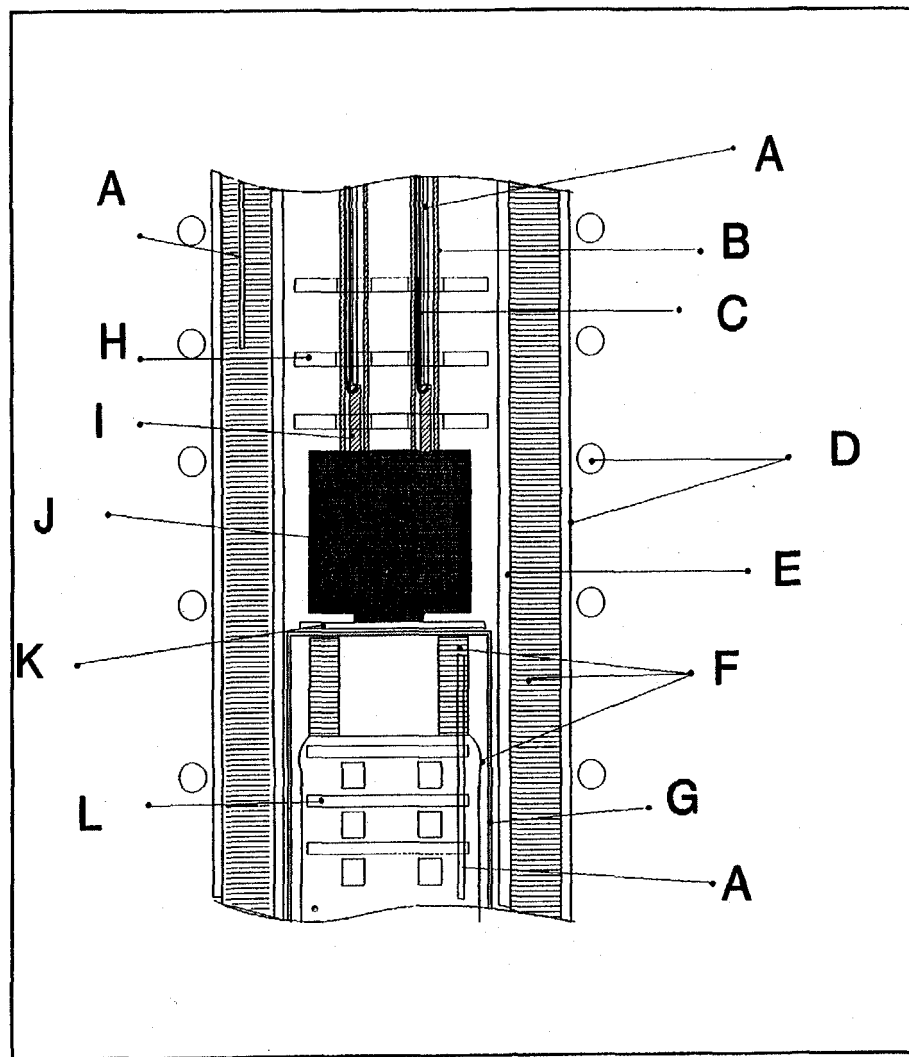
where:

$$\begin{aligned} SS_R(\beta_6 / \beta_0, \beta_1, \beta_2, \beta_3) &= SS_R(\beta_0, \beta_1, \beta_2, \beta_3, \beta_6) - SS_R(\beta_0, \beta_1, \beta_2, \beta_3) \\ &= 1009242 - 1009240.4 \\ &= 1.6 \end{aligned} \quad [A.19]$$

$MS_E$  is the error mean square and is equal to 20.32. Equation [A18] gives  $F_0$  equal to 0.079. Since  $F_{0.78, 1, 636} = F_0$ , the  $H_0$  hypothesis is rejected on a test level of 22% or higher. It can be concluded that experimental data do not allow for the inclusion of second order heat effects in the model.

Table A9 Summary of the statistics for the experiments A, B and C in Section 4.1, Table 4.2. Test for, second order heat effects.

Model with $\beta_6$			
Source of Variation	Sum of Squares	Degrees of freedom	Mean Square
Regression	1009242	4	252311
Error	12923	636	20.32
Coefficient	Estimate	Standard Error	
$\beta_0$	3.940374	0.544689	
$\beta_1$	-1.80455	0.012993	
$\beta_2$	7.595052	0.566254	
$\beta_3$	33.72215	0.588186	
$\beta_6$	-0.00011	0.000395	



- A: Type-S thermocouple, Platinum-10% rhodium versus platinum
- B: Alumina ceramic protection tube
- C: Molybdenum wire  $\varnothing 0.5$ , protected by an alumina ceramic tube and connected to the TiB<sub>2</sub>/BN-rod
- D: Steel mantle with water cooling tubes
- E: Oxide ceramic tube (Pythagoras-76 wt% Al<sub>2</sub>O<sub>3</sub>)
- F: Kanthal wires, heating elements
- G: Faraday shield in nickel connected to earth ground
- H: Upper radiation shields
- I: TiB<sub>2</sub>/BN-rod, electric connection to the aluminium electrode
- J: Graphite crucible
- K: Insulation between the graphite crucible and grounding
- L: Lower radiation shields and support

Figure 3.2 Sketch of the cross section of the tube furnace with inner arrangement

